Measurements of NO_X in Remote & Polluted Environments

Amy Foulds MChem (Hons)

Master of Science by Research

University of York

Chemistry

October 2015

ABSTRACT

A laser induced fluorescence instrument was tested for NO_x measurements. Laboratory tests at the University of York indicated that the instrument could be efficiently used for NO_2 measurements in a polluted atmosphere, with the installation of a gas phase titration system also showing promising results for NO characterisation. However, deployment at the Cape Verde Atmospheric Observatory for measurements in the remote marine boundary layer resulted in a significant over-estimation of NO_2 mixing ratios. The LIF instrument measured NO_2 levels that were around 8 times higher than those measured by a standard chemiluminescence analyser. The measurement inaccuracy was concluded to be a result of some kind of leak within the instrument. This meant that NO_2 in the laboratory would also have been detected, resulting in greatly enhanced mixing ratios than would have been expected. This led to the conclusion that, in its current configuration, the instrument would not be suitable for long-term NO_2 measurements in the remote boundary layer. This, along with consumable restrictions meant that the laser induced fluorescence was not used for NO measurements at the Cape Verde Atmospheric Observatory.

A photolytic chemiluminescence analyser was used to measure NO_x emissions from oil and gas rigs in the North Sea as part of the airborne "Oil and Gas" campaign in the summer of 2015. Substantial NO_x enhancements were observed during the campaign, with numerous exceedances of 10,000 pptv (10 ppbv). The direct integration method was used to derive NO_x emissions coming from a specific set of rigs in the North Sea. These were then scaled up to evaluate the NAEI estimates for the whole North Sea drilling region. This study found that the NO_x emissions from oil and gas rigs in the North Sea are poorly represented by the NAEI, with over 40,000 tons per year being unaccounted for. Such a substantial discrepancy highlights the need for regular assessment of inventory estimates, as these provide a basis for air quality directives and legislation, which in turn, are put in place to protect and improve local and regional air quality.

TABLE OF CONTENTS

LIST OF FIGURES

LIST OF TABLES

LIST OF EQUATIONS

ACKNOWLEDGEMENTS

I would like to thank my supervisor, Dr James Lee, for his continued guidance and encouragement throughout this project, and for taking the time to read several drafts of this thesis and giving me constructive feedback.

In addition, I would also like to thank Dr Piero di Carlo for putting his faith in me to look after his beloved LIF instrument both in York and in Cape Verde, whilst always replying promptly to my emails when the instrument decided to misbehave.

Many thanks also go to Dr Stéphanne Bauguitte, without whom I would not have felt confident enough to operate the BAe-146 NO_x instrument solo during the "Oil and Gas" flight campaign.

I would also like to thank everyone at the Wolfson Atmospheric Chemistry Laboratories – your constant humour and our regular Friday night pub sessions kept me positive throughout this project. I will miss you all greatly when I continue my research career in Bristol.

Thanks also go to all of my friends, particularly Emma and Meghan, who have been a great source of support and positivity to me. Finally, many thanks go to my Mum and Dad, without whose unwavering emotional support (and copious amounts of tea), this thesis would not have been possible. Thank you for being there.

AUTHOR'S DECLARATION

I, the candidate, hereby declare that all work presented here is my own, except where otherwise acknowledged, and has not been submitted in full or part for any other degree.

CHAPTER 1: INTRODUCTION

1.1 Motivation for this Study

Nitrogen oxides (NO_x = NO + NO_2) are trace species which have a central role in atmospheric chemistry. They are predominantly emitted via fossil fuel combustion processes, with one of the most significant sources being the road transport sector. Natural sources of NO_x include lightning and soil, though these are minimal in comparison.

NO_x emissions play a role in the formation of photochemical smog[1,2] and affect the oxidative capacity of the atmosphere, through their involvement in photochemical cycles which result in the formation of tropospheric ozone (O_3).[3,4,5] When photolysed, O_3 is a major source of the hydroxyl radical (OH), which controls the lifetime of many other atmospheric species, such as methane and carbon monoxide, through its ability as a powerful oxidising agent. Methane is a potent greenhouse gas, thus meaning that NO_x mixing ratios also have an indirect effect on the earth's radiative forcing. Nitrogen dioxide (NO_2) itself reacts with the OH radical, providing a sink for NO_x and having an additional impact on the polluted atmosphere.[6] This reaction also reduces the radical mixing ratios, therefore causing elevated mixing ratios of gases which would have ordinarily been removed from the atmosphere.

It is the rapid interconversion between nitric oxide (NO) and NO_2 which results in their direct part in the formation of tropospheric O_3, should their ambient mixing ratios be sufficiently high. Unperturbed, the interconversion of O_3, NO and NO_2 establish a photo-stationary state equilibrium whereby no net O_3 production or destruction occurs.[7] This equilibrium is represented by reactions (1) and (2) below, where NO reacts with O_3 to form NO_2. This is then photolysed back to NO by sunlight.

$$O_3 + NO \rightarrow NO_2 + O_2 \qquad (1)$$

$$NO_2 + h\nu \rightarrow NO + O(^3P) \qquad (\lambda < 420\ nm) \qquad (2)$$

$$O(^3P) + O_2 + M \rightarrow O_3 + M \qquad (3)$$

Reactions (1-3) result in no net formation of O_3, should there be no other species which could cause additional NO to NO_2 transformations. This is rarely the case, with peroxy radicals (RO_2) catalysing the interconversion between NO and NO_2.

RO_2 are predominantly found in clean or moderately polluted conditions, and are formed during the OH-initiated oxidation of hydrocarbons (R refers to any organic group):

$$RH + OH\ (+O_2) \rightarrow RO_2 + H_2O \quad (4)$$

The RO_2 radical then reacts with NO, producing an organic oxy radical (RO) and NO_2:

$$RO_2 + NO \rightarrow RO + NO_2 \quad (5)$$

The NO_2 is then photolysed, ultimately leading to the production of O_3. If the mixing ratios of NO_x are extremely low, the RO_2 radicals undergo recombination reactions, rather than reacting with NO. This consequently terminates the radical chain, meaning that O_3 destruction dominates under these conditions. However, at higher NO_x mixing ratios, the RO_2 radicals oxidise NO to NO_2. This then leads to net O_3 production, which has impacts on human health, as well as natural vegetation and crop yields.[8,9] The critical NO_x level at which this change from an O_3 destroying regime to an O_3 producing regime occurs is known as the O_3 compensation point, and typically lies between 5 and 100 pptv.[10]

The main daytime sink of NO_x is the formation of nitric acid (HNO_3), through the reaction of gaseous NO_2 and the OH radical. The nocturnal atmospheric chemistry of NO_x is dominated by an accumulation of the nitrate radical (NO_3) and its reservoir species, dinitrogen pentoxide (N_2O_5),[11] which results from reactions (6) and (7), shown below. With no photolysis occurring at night, NO_2 instead reacts with O_3 to generate the NO_3 radical. Reaction of NO_3 with NO_2 results in a chemical equilibrium with N_2O_5. The N_2O_5 can result in further acid deposition, through its subsequent reaction with atmospheric water vapour to form HNO_3.

$$NO_2 + O_3 \rightarrow NO_3 + O_2 \quad (6)$$

$$NO_3 + NO_2 \leftrightarrow N_2O_5 \quad (7)$$

The HNO_3 is scavenged by precipitation in the lower troposphere, resulting in wet deposition.[11] The NO, NO_2 and HNO_3 can also be taken up as gases or solid particles by plants and surfaces (dry deposition). It is by this deposition process that NO_x has detrimental effects on the environment, through the resultant acidification and eutrophication of ecosystems.[12] This cycle is completed through the recycling of HNO_3 back to NO_x. This can occur through the reaction of HNO_3 with the OH radical or by photolysis.

As well as having detrimental impacts on the environment, NO_x emissions are known to have significant effects on human health.[4] NO_2 in particular causes respiratory problems on both short and long-term scales. High mixing ratios of the species can cause inflammation of the airway, while long-term exposure may reduce lung capacity and cause enhanced susceptibility to allergens[13,14]

1.2 Global Distribution of NO_x

As discussed previously, the dominant source of NO_x emissions in the troposphere is the combustion of fossil fuels, with a high proportion coming from the road transport sector. NO_x mixing ratios are therefore highly variable across the globe, on both temporal and spatial scales, as a result of the non-uniform distribution of sources and sinks.[15]

The lifetime of NO_x in the lower troposphere is extremely short, in the order of a few hours.[16,17] This means that the highest mixing ratios are often observed in close proximity to the emissions sources, such as large cities with extensive road networks. NO_x mixing ratios measured in the boundary layer above such an area are typically on the scale of several tens ppbv.[4] For example, a study by Aruffo et al. (2014)[18] measured the mixing ratios of various species over the metropolitan area of London, with maximum NO_x mixing ratios of around 30 ppbv being detected downwind of the city.

In contrast, in the upper troposphere, NO_x emissions persist for several days.[16,17] Here, it can be transported to remote regions (where there are minimal local sources of NO_x) by reservoir species such as peroxyacetyl nitrate (PAN).[19] This species thermally decomposes at altitudes below 7 km, which subsequently releases NO_x into the remote troposphere. [19,20] Due to their location away from large emission sources, NO_x mixing ratios in remote regions are several orders of magnitude smaller than those measured in industrialised areas, rarely exceeding 200 pptv.[4] A good representation of the remote atmosphere is the Cape Verde Atmospheric Observatory (CVAO), which is used for long-term measurements of atmospheric species, such as NO_x and O_3. Various studies have taken place at this site, with typical mixing ratios of NO_x being well below 30 pptv.[10]

1.3 Instrumental Techniques for the Measurement of NO_x

The measurement of NO_x is extremely challenging for a number of reasons. The first of which is the fact that there is a large dynamic range of mixing ratios which are spread non-uniformly around the earth, as discussed in section 1.2. NO_x mixing ratios also change on a timescale of hours, with any primary emissions being converted into other species extremely quickly.[1] This highlights another challenge associated with NO_x measurements: selective detection. Species such as HNO_3 and PAN can easily decompose into NO_2, thus meaning that interferences from these species are often detected.

1.3.1 NO_2 Measurement Techniques

Differential Optical Absorption Spectroscopy (DOAS)

Many spectroscopic methods have been developed for the measurement of NO_2, which exploit the broad absorbance spectrum of NO_2 in the ultraviolet and visible regions of the electromagnetic spectrum.[21] An example of such a technique for NO_2 measurements is DOAS[22], which is based on the use of a beam of white light of a specific wavelength which is "folded" by an array of retro-reflectors. The absorption bands associated with the returning light beam are used to determine which molecules are present at any point in the beam path. The amount of the absorber (i.e. the amount of a particular species) along the light path is then determined through the application of Lambert's law, which relates the amount of light absorbed to the distance it travels through an absorbing medium (for example, air).

Cavity Enhanced Absorption Spectroscopy (CEAS)

Another technique which has also been applied to NO_2 measurements is CEAS.[23,24] Where DOAS is applied to smaller molecules through tuning to narrow lines of the absorption spectra, CEAS is more applicable to larger molecules with broader spectra through the use of a broadband source. This means that it can be used to observe several species simultaneously. CEAS is therefore essentially a multi-pass variant of the DOAS technique.

Cavity Ring Down Spectroscopy (CRDS)

This is another spectroscopic technique which has been widely used for NO_2 measurements.[25,26] This method works by "trapping" a single frequency laser in a cavity which is defined by several high reflectivity mirrors, thus causing the intensity of laser light to build up. The laser light is tuned across very narrow individual lines of a spectra. This makes it possible to measure a particular molecule, by selecting a laser frequency which is tuned to specific absorption lines associated with that molecule. When the laser is turned off, the light pulse decays, undergoing thousands of reflections between the mirrors. This then eventually emerges through one of the mirrors, with the instrument measuring how long it takes for the light to decay to 1/e of its original intensity (also known as the "ring-down time"). The ring-down time decreases when the absorbing species is introduced into the cavity and can therefore be used to determine the mixing ratio of said species in the air sample.

Cavity Attenuated Phase Shift Spectroscopy (CAPS)

This also works in a similar way to CRDS in that photons are injected into and "trapped" in a mirror-defined cavity. The photons are then reflected between the mirrors and slowly leak out of the cavity, travelling to the detector. The wave form resulting from the coupling of the square or sine wave modulated light source and the cavity is slightly shifted from the original waveform, and it is this which is measured by the detector. The technique is used to measure the mixing ratio of a molecule which absorbs in the same wavelength band as the light within the cavity. For example, Kebabian et al. (2005)[27] used a 430 nm light emitting diode (LED); a light source with an absorption wavelength specific to NO_2. Absorbance of the light by the molecule in question (for example, NO_2), adds another loss term into the instrument, causing a phase shift that is proportional to its mixing ratio.

Tunable Diode Laser Absorption Spectroscopy (TDLAS)

The TDLAS technique uses a laser diode which is tuned to a wavelength for the measurement of a specific species and has been used for the measurement of tropospheric NO_2 on various occasions.[28,29] As with other spectroscopic techniques, TDLAS uses the Beer-Lambert law to directly relate the absorption of light by a chemical species to its mixing ratio. The method

works by passing laser light though the gas in the sample cell, towards the detector. The light is absorbed if the species in question is present. The size of the absorption peak can be accurately measured and subsequently used to determine the mixing ratio of a species in the air sample. As with CRDS, TDLAS is particularly useful for gaseous molecules with narrow, strong and distinct absorption bands. These molecules are quantified by tuning the laser diode over a small wavelength range, thus making it possible to identify the absorption bands and attribute them to a particular species.

Laser Induced Fluorescence (LIF)

Although all of the spectroscopic techniques discussed can be specific to NO_2, the LIF technique combines this with a much higher sensitivity, as well as providing a direct, in-situ, fast response technique for NO_2 detection.[21] A variant of this technique, fluorescence assay by gas expansion (FAGE) was used for NO_2 quantification by George and O'Brien (1991)[30], using a frequency doubled Nd:YAG laser. This resulted in a detection limit of 500 pptv averaged over one minute at an SNR (signal to noise ratio) of one. Fong and Brune (1997)[31] found that this detection limit could be improved to 300 pptv through the use of a tunable dye laser and multi-pass alignment. More recent developments of the technique have shown consistently high levels of sensitivity. Thornton et al. (2000)[22] for example, used a two-wavelength excitation instrument, resulting in a detection limit of 15 pptv averaged over ten seconds at an SNR of two. A YAG Q-switched inter-cavity doubled laser was used for NO_2 quantification by Dari-Salisburgo et al. (2009).[32] This instrument had an extremely low detection limit of 10 pptv averaged over one minute, and was used in a number of ground-based and aircraft campaigns,[33,34,35,36] thus giving assurance that this technique could accurately quantify NO_2 mixing ratios in a range of atmospheric environments. The LIF technique itself works by selectively exciting NO_2 molecules through one of their molecular transitions, using a narrow-band laser. In most cases, the transition used in LIF is between the ground $^2A_1$ electronic state and the excited $^2B_2$ electronic state of NO_2. When NO_2 absorbs a photon in the visible region for this transition, it becomes electronically excited, becoming NO_2*. On relaxation back to its ground state, NO_2* emits red-shifted fluorescence, which is proportional to the mixing ratio of NO_2 in the air sample.

Thermal Dissociation-Laser Induced Fluorescence (TD-LIF)

The LIF technique has been developed further for in-situ measurements of other reactive nitrogen (NO_y) species, namely alkyl nitrates (hereafter referred to as "ANs"), peroxy nitrates (hereafter referred to as "PNs") and HNO_3. This has been done by combining two analytical techniques, thermal dissociation and laser induced fluorescence.[37] Most NO_y species thermally dissociate to produce NO_2 and a radical species (x):

$$XNO_2 + \text{heat} \rightarrow x + NO_2 \qquad (8)$$

The NO_2 is measured directly by laser induced fluorescence, as discussed previously. The organic nitrates and HNO_3 channels of the instrument are heated to their respective dissociation temperatures to form NO_2, which is then measured by laser induced fluorescence. The temperatures required for complete dissociation of PNs, ANs and HNO_3 are 200°C, 400°C and 650°C, respectively. A similar instrument was used by Di Carlo et al. (2013)[38] for simultaneous NO_2, PN, AN and HNO_3 measurements. The instrument was found to be sensitive and fast enough with a time resolution of 0.1 seconds) to provide accurate NO_2 and organic nitrate measurements, with detection limits of 9.8, 18.4, 28.1 and 49.7 pptv for NO_2 detection by the NO_2 cell, PN cell, AN cell and HNO_3 cell, respectively.

1.3.2 NO Measurement Techniques

Chemiluminescence

Aside from spectroscopic methods, the most widely-used and commercially available technique for NO_x detection is based on the gas-phase chemiluminescent reaction of NO and O_3.[39,40]

$$NO + O_3 \rightarrow NO_2^* + O_2 \qquad (9)$$

$$NO_2^* \rightarrow NO_2 + h\nu \qquad (10)$$

NO reacts with O_3 to produce the electronically excited NO_2* molecule (reaction (9)). The excited NO_2 molecule fluoresces at wavelengths in the visible and near-infrared regions of the electromagnetic spectrum (i.e. wavelengths longer than 600 nm).[41] A cooled

photomuliplier tube (PMT) detects the photons released during fluorescence. The sample is kept under low pressure in order to maximise the fluorescence lifetime of the NO_2*. The intensity of the signal is proportional to the mixing ratio of NO, when the O_3 is in excess, thus meaning that this technique provides a direct measurement of NO. This method can also be applied to indirect NO_2 measurements, by converting it to NO prior to chemiluminescence detection. This signal then represents the mixing ratio of total NO_x in the air sample. Generally, instruments which use the O_3 chemiluminescence technique therefore have two operating modes, one which measures NO directly, and one which measures total NO_x. The difference between these two signals can then be reported as the ambient mixing ratio of NO_2.

NO_2 Converters

Many commercial instruments use a heated molybdenum (Mo) catalyst to reduce the NO_2 to NO.[40,42] Although this method has proved to be highly successful in terms of NO_2 to NO conversion efficiencies (often converting around 90% of the NO_2 to NO),[41] one of its biggest downfalls is the fact that the conversion is not specific to NO_2. Other reactive nitrogen species, such as PAN and HNO_3 may also decompose to produce NO on contact with the heated Mo catalyst. [40,43,44,45] This consequently means that, rather than solely being due to NO_2, it is more likely that the subtraction of the NO signal from the total NO_x signal will be representative of the summed mixing ratio of all nitrogen species which have been reduced to NO.

A variation of this instrumentation involves a photolytic, rather than a catalytic converter. This method exploits the fact that, in the presence of UV radiation (at wavelengths shorter than 420 nm), NO_2 readily photo-dissociates to form NO.[10] Photolytic converters can therefore be used to convert NO_2 to NO specifically, over a narrow wavelength band (thus minimising interferences from species like PAN and HNO_3). A number of different types of photolytic converters have been tested for NO_2 quantification, including metal halide and high pressure xenon lamps. Although these have shown conversion efficiencies of up to 70%,[46,47] they required a huge amount of power for continuous operation, meaning there was scope to improve the conversion efficiencies and to develop a photolytic converter which was more economical to use. Such converters came in the form of LEDs (light-emitting diodes). These have longer lifetimes and lower power requirements compared to the metal

halide and xenon lamps,[42] and provide consistently high conversion efficiencies of around 90%[41] (compared to 70% using metal halide or xenon lamps).The use of LEDs in the near-UV region, which produce radiation of wavelengths 385 to 405 nm, are known to be particularly efficient at specifically converting NO_2.[10] with recent work demonstrating a particularly high affinity for NO_2 conversion using 395 nm "blue light" LEDs (also known as blue light converters, or "BLCs").[48] LEDs have proved to be invaluable in chemiluminescence-based NO_x measurements, and are now widely used in both ground-based and airborne research campaigns.[10,18,38,49] However, they are not without interferences. The wavelength of many of these converters coincides with the photolysis wavelength of other ambient nitrogen-containing species, such as chlorine nitrate ($ClONO_2$), bromine nitrate ($BrONO_2$) and nitrous acid (HONO).[48] There are also many atmospheric species which thermally decompose to produce NO_2 at the operating temperatures of the converters. A recent study reported a significant interference from the thermal decomposition of PAN in a BLC-equipped chemiluminescence analyser.[50] This study also used model estimates to postulate that the decomposition of other NO_2-containing species (such as peroxynitric acid (HO_2NO_2)) may also be leading to the over-reporting of NO_2 mixing ratios by chemiluminescence analysers, via positive interferences in the BLC.

Although the specificity problem has been substantially minimised through the use of photolytic converters in chemiluminescence instruments, the main downfall of the technique is its inability to directly measure NO_2. The only way that the NO_2 can be observed is if it is first converted into NO, as discussed earlier in the chapter. This means that the apparent NO_2 signal is still likely to suffer from interferences, thus affecting the accuracy of the measurements. This is where direct NO_2 measurement techniques, such as laser induced fluorescence, have a big advantage over the chemiluminescence method. These two techniques will be discussed in greater detail in chapter 2.

1.4 Aims and Objectives of the Study

One of the main aims of the study was to assess a TD-LIF instrument for NO measurements in a remote atmospheric environment. The instrument was first tested for ambient NO_2 measurements alongside a P instrument in York, with further experiments being undertaken to characterise the instrument for NO_x measurements. On completion of these experiments, the LIF was deployed at the CVAO in order to assess its ability to measure the low NO_2 mixing

ratios observed at this remote site, which is widely representative of the marine boundary layer. Observations from the laboratory tests in York would then be used to configure the LIF for NO measurements at the observatory.

Another objective of the study was to measure NO_x in a polluted environment, through participation in the UK-based airborne "Oil and Gas" aircraft campaign, in collaboration with the Facility for Airborne Atmospheric Measurements (FAAM) in Cranfield. The survey flights of the campaign took place over the active oil and gas drilling areas of the North Sea, with a view to measuring the atmospheric emissions from the rigs. As a point source of NO_x in the National Atmospheric Emissions Inventory (NAEI – this will be described in detail in chapter 4), it was hoped that observations regarding oil and gas rig emissions could be used to assess the accuracy of inventory estimates. This could then also have long-term impacts, particularly in terms of air quality legislation in the UK.

CHAPTER 2: EXPERIMENTAL

2.1 Introduction to the TD-LIF Instrument

The TD-LIF instrument used during this research project was originally developed at the CETEMPS Department of Physical and Chemical Sciences at the University of L'Aquila for ground-based measurements of NO_2.[32] It was a very similar instrument to that initially developed by Day et al. in 2002.[37] The instrument has four channels, which enables direct measurement of NO_2 via laser induced fluorescence. The remaining three channels are heated for the simultaneous detection of the sum of total peroxy nitrates (ΣPNs), the sum of total alkyl nitrates (ΣANs) and HNO_3, via thermal dissociation.

2.1.1 Instrument Components

Light Source

Although similar to the original TD-LIF instrument, one key difference is the light source used. The instrument used in this work uses a Q-switched, pulsed Nd:YAG laser, which emits light at 532 nm. The laser has a maximum power of 3.8 W, with a 15 kHz repetition rate and a pulse width of 30 ns. The energy per pulse (in units of Joules per pulse) can be calculated by dividing the laser power by the repetition rate, that is:

$$\text{Energy per pulse} = \frac{\text{Laser power (W)}}{\text{Repetition rate (Hz)}} = \frac{3.8}{15{,}000} = 2.53 \text{ x } 10^{-4} \text{ J/pulse} \qquad \textit{Equation 2.1}$$

The units of laser power and repetition rate can be converted into Joules/second and seconds, respectively (1 W = 1 Joule/second and 1 Hz = 1 second), hence why the resultant energy is given in units of Joules/pulse. As can be seen in **Equation 2.1**, the energy of each laser pulse is extremely low, which makes the laser suitable for the use in the laser-induced fluorescence measurement technique. The laser pulses have sufficient energy to solely act as an excitation source for the NO_2 molecules, without dissociating other species present in

the sampled ambient air. This could affect the accuracy of the NO_2 data, producing molecules which are able to quench the fluorescence, thus meaning that it is essential to minimise the dissociation through the use of a low powered laser.

High reflectivity mirrors are also installed between each cell, which direct the laser beam towards the next detection cell. The laser must be well aligned, ensuring that as much of the laser light passes through each of the detection cells. This will mean that the maximum number of fluorescence photons are detected, thus resulting in as accurate a measurement as possible. To monitor the laser power during calibrations and measurements, photodiodes are located before the entrance of each detection cell.

NO_2 Spectroscopy

Spectroscopic techniques such as laser-induced fluorescence are used for NO_2 measurements, due to the nature of the absorption cross-section of NO_2 itself.

The majority of the cross-section lies in the visible region, with a maximum observed at approximately 420 nm.[25] The reason behind this lies in the interaction between the ground state and first excited state of NO_2. The upper vibrational levels of the ground state configuration of NO_2 ($X\ ^2A_1$) are strongly coupled to the first excited state configuration ($A\ ^2B_2$) via Herzberg-Teller interactions.[51] As a result, there are an extremely high number of energy levels in the ultraviolet-visible region of the electromagnetic spectrum, thus also meaning that the transitions between these energy levels are optically active. It is these interactions which provide a basis for the nature of the absorption cross-section of NO_2.

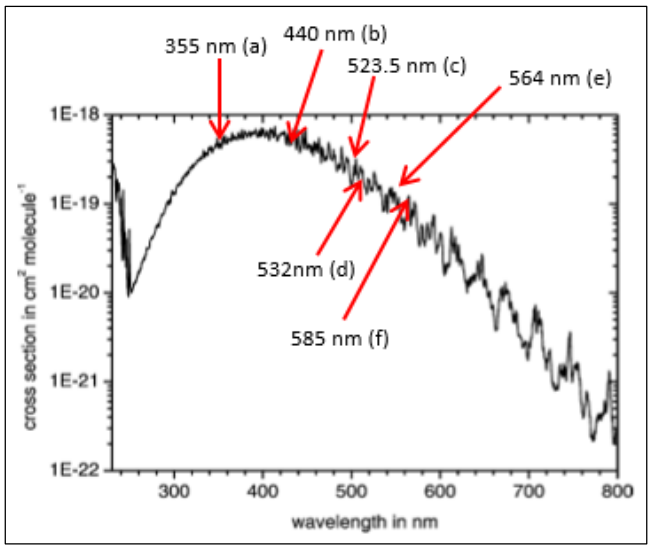

Figure 2.1: Absorption cross section of NO_2 at 300K and 760 Torr. Letters (a) to (f) represent the excitation wavelength used in various LIF instruments. (a) Bradshaw et al. (1999)[52], (b) Matsumi et al. (2001)[33], (c) Matsumoto et al. (2003)[21], (d) George and O'Brien (1991)[30] and this thesis, (e) Fong and Brune (1997)[31] and (f) Perkins et al. (1999)[53]

As the majority of the cross-section is in the visible region (400 to 700 nm), it means that the radiation wavelength used to excite the NO_2 molecule can be chosen based on the particular instrument in question, some of which are shown in **Figure 2.1.** In order to understand why these wavelengths were selected, it is first necessary to get a clear idea as to what an absorption cross-section actually is. The definition of an absorption cross-section is "the effective area of the molecule that a photon needs to traverse in order to be absorbed. The larger the absorption cross-section, the easier it is to photo-excite the molecule." As can be seen in **Figure 2.1**, the corresponding absorption cross-sections at the excitation wavelengths used are large, thus increasing the likelihood of absorption of the radiation. As previously mentioned, the light source in the instrument used during this project is an Nd:YAG laser which emits UV radiation at 532 nm. This wavelength corresponds to the second harmonic of the Nd:YAG laser and, as can be seen on **Figure 2.1**, has been used in other instruments for the detection of NO_2, [21,30] due to the absorption cross-section of NO_2 being relatively large at this wavelength. Another benefit of using 532 nm is that there are no other gas-phase absorbers at this wavelength, aside from O_3.[54,55] The Rayleigh scattering cross-section of air is also modest at this wavelength,[56,57] which assists in reducing the background signal of the instrument. A single pass configuration is used in the instrument. This is similar to that used by Matsumoto et al.,[21] whose study found that using such a configuration can dramatically reduce the instrument's limit of detection. Using a single pass configuration and a single wavelength, powerful laser consequently means that the laser would be simpler to align,

whilst also providing laser light powerful enough to supply all 4 detection cells for the in-situ measurement of NO_2, PNs, ANs and HNO_3.

Excitation of NO_2 at 532 nm results in fluorescence at wavelengths longer than 630 nm, allowing for optical filtering of the laser radiation. This was also observed by Matsumoto et al.,[21] who used an Nd:YAG laser with the same excitation wavelength. This feature of the laser also means that it possible to deduce that the only origin of the fluorescence is the NO_2 present, Although O_3 also absorbs UV radiation at 532 nm, it does not fluoresce at wavelengths longer than 630 nm, thus meaning it is impossible for the fluorescence signal to be due to O_3.

Detection Cells

The four detection cells in the instrument comprise of a central cubic structure, with two cylindrical arms on opposite faces of said cube. The internal assembly of the cells has many features which are in place to reduce the background signal. These arms hold a sequence of baffles, which reduce scattering of the laser light inside the cell, whilst also minimising the amount of external solar light that reaches the central cubic part of the detection cell. A schematic illustrating the assembly of one of these detection cells is shown in **Figure 2.2**.

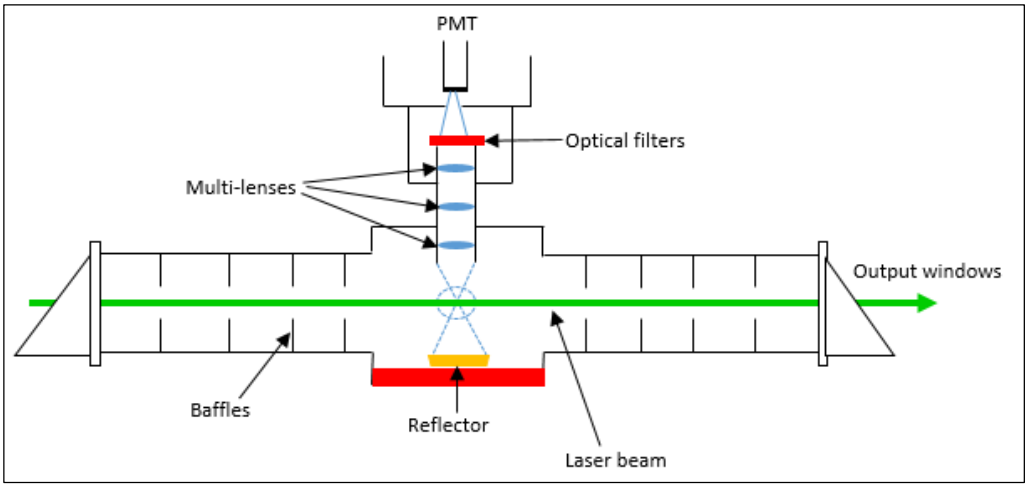

Figure 2.2: Schematic of a LIF detection cell

The walls of the cell, along with the arms and baffles are coated with a low fluorescent optical black paint, which also acts to minimise any scattering within the cell. The cells are also designed to maximise the fluorescence signal measured.

An aluminium-coated concave mirror is mounted below the centre of each detection cell, which directs the laser beam towards the PMT detector. This, along with two lenses, which are placed before the PMT, act to maximise the photon collection efficiency of the instrument. In order to minimise the amount of Raman or Rayleigh scattering, there are a number of low fluorescence optical filters. These work by separating the fluorescent and non-fluorescent photons (which can be thought of as the "background" – see later). These filters are non-fluorescent and are specifically chosen, as they need to transmit over the range of wavelengths at which NO_2 fluoresces. As a result, the fact that the filters are non-fluorescent means it is possible to deduce that there is no fluorescence coming from the filters, solely the NO_2 molecules. There are two long-pass filters, which cut out wavelengths of 620 and 640 nm (to reject any Raman-scattered radiation), whilst transmitting more than 85% above 640 nm. In addition to these, there are also two filters which reject any Rayleigh-scattered radiation at 532 nm, also demonstrating a very high transmission (>95% above 640 nm). These lenses and filters are therefore in place to optimize the fluorescence detection and minimise any non-fluorescent photons that reach the detector.

Sampling and Inlet System

The common inlet consists of a PFA tube, which samples ambient air at a flow rate of approximately 8.5 L/min. Once the air reaches the instrument, the flow is split into four channels. The first of these channels is another PFA tube, which is kept at ambient temperature to measure ambient mixing ratios of NO_2 in the detection cell in closest proximity to the light source (i.e. the NO_2 cell). The other three channels comprise of U-shaped quartz tubes, which are heated to different temperatures using a heated 132 W wire, and connect the inlets to the respective detection cells. The temperatures are specifically chosen to correspond to the thermal dissociation temperatures of RO_2NO_2 species (200°C), $RONO_2$ species (400°C) and HNO_3 (550°C). At the exit of each of these quartz tube, there is a pinhole which acts to dramatically reduce the pressure from ambient to around 50 Torr. This means that the residence time of the sample air in the tubes is reduced, minimising any recombination reactions which could occur. The sample air then travels through another PFA

tube to a stainless steel tube in the centre of the detection cell, bringing with it another pressure drop, this time to around 4 Torr.

Vacuum System

The pressure within the detection cells needs to be maintained at 3-4 Torr, at a flow rate of 6 standard litres per minute (slpm). A pump system, which includes a roots blower coupled to a rotary vane pump, maintains these required pressure and flow conditions. Low pressure conditions are required in order to minimise the collisional quenching (which contributes to the background signal observed), whilst also maximising the fluorescence lifetime for the delayed time-gating detection. This is the standard detection method used in LIF instrumentation.[5,21] In this method, the PMT detectors are not turned on until around 0.25 nanoseconds (μs) after the laser pulse. After this time delay, at the end of the laser pulse, the fluorescence is measured for around 5 μs (this is referred to as the "time gate window"). This procedure is shown in **Figure 2.3**. Low pressure is critical in this method, as this ensures that the lifetime of the fluorescence exceeds the laser pulse, thus allowing it to be detected.[32]

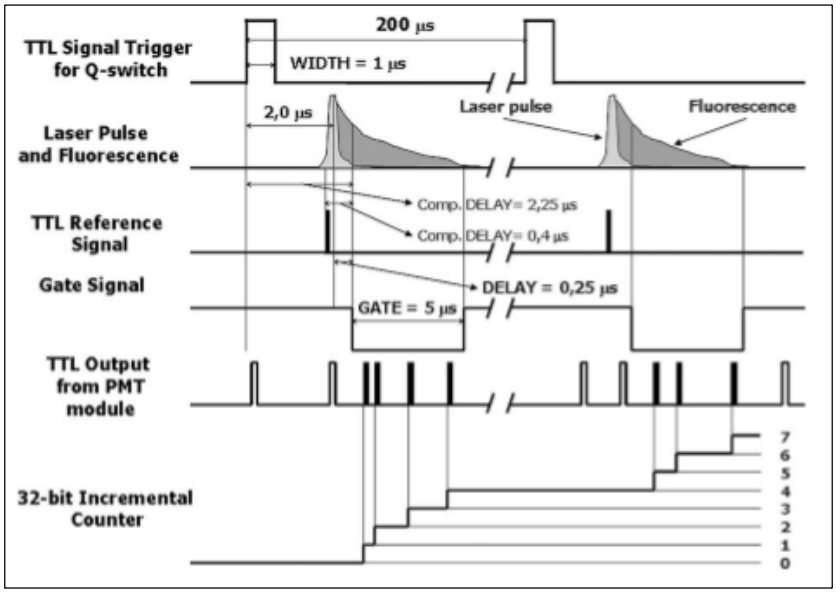

Figure 2.3: Time gating detection method used of LIF detection of NO_2 (Figure taken from Dari Salisburgo et al. (2009)[ref])

2.1.2 Instrument Parameters

Sensitivity

The instrument sensitivity has a great influence on the quality of the data, meaning it is therefore important to discuss the factors which affect it.[58] The overall equation which gives the sensitivity of LIF (α), in units of counts per second per ppbv, is given below.

$$\alpha = \frac{S_F C}{n_{NO2}} = l_{CF} \frac{\sigma(\nu) P(\nu)}{a_q} \int \Omega(\nu, V_F)\, T(\nu)\, \eta(\nu)\, \varepsilon(\nu)\ \partial\nu \qquad \textit{Equation 2.2}$$

Where:

- ν = frequency of incident radiation (photon s^{-1})
- S_F = fluorescence signal (photons s^{-1})
- C = collection efficiency
- n_{NO2} = mixing ratio of NO_2 (ppbv)
- l_{CF} = effective path length where fluorescence takes place (cm)
- $\sigma(\nu)$ = absorption cross section (cm^2 $molecule^{-1}$)
- $P(\nu)$ = photons flux (photons s^{-1})
- a_q = quenching factor (cm^3)
- V_F = volume of fluorescence (cm^3)
- $\Omega(\nu, V_F)$ = fraction of photons emitted into volume of fluorescence
- $\eta(\nu)$ = quantum efficiency of PMT
- $\varepsilon(\nu)$ = normalized fluorescence spectrum of the molecule

During work with the instrument, the sensitivities of the NO_2, PN, AN and HNO_3 channels were found to be stable at 173, 83, 46 and 18 counts per second per ppbv (c/s/ppbv). This decline in sensitivity from the NO_2 to the HNO_3 cell can be explained using **Equation 2.2**, with a gradual decrease in laser power playing a key role in this. However, it should be noted that it is not possible to quantify all terms in this equation, hence illustrating a need for an actual calibration. The sensitivity of the instrument is a function of the collection efficiency and the fluorescence photons. The collection efficiency is dependent on the quality of the optics which are used to collect the fluorescence signal, along with the quality of the PMT, which is used to detect the fluorescence photons.

The amount of fluorescence photons that reach the detector (i.e. the degree of fluorescence observed) is affected by a number of competitive processes. Another way that the excited NO_2 molecules can lose energy is through collisional quenching with other molecules, namely nitrogen and oxygen molecules. The sensitivity of the instrument is therefore improved in a number of ways. The first is to increase the number of fluorescence photons by reducing the instrument background. Methods of reducing the background signal were discussed in section 2.1.1, with low pressure operation and the use of baffles and optical filters being some of the key examples. Increasing the laser power also increases the amount of fluorescence photons. Referring back to the decline in sensitivity observed from the NO_2 to the HNO_3 cell, this can be put down to the laser power gradually weakening at it travels through the instrument. As the sensitivity is a function of fluorescence photons, which depend partly on the power of the laser, the more powerful the laser, the higher the sensitivity will be (in conjunction with other factors discussed above).

Background signal

The background signal can have significant impacts on instrumental performance, particularly through its contribution to the instrumental sensitivity (see later). In order to keep the background down to a minimum, it is important to consider where the signal actually comes from.

The background signal comprises of a number of terms:

$$B = B_{Chamber} + B_{P-scatter} + B_{solar} + B_{PMT} + B_{interference} \qquad \textit{Equation 2.3}$$

Where:

$B_{Chamber}$ = optical scatter from surfaces inside the detection cell

$B_{P\text{-}scatter}$ = sum of pressure dependent Raman, Rayleigh and Mie scattering

B_{solar} = solar-induced background

B_{PMT} = dark current of the photomultiplier tube

$B_{interference}$ = any time-dependent signal, such as fluorescence or scattering from other atmospheric gases or aerosols

As discussed previously, the design of the detection cells plays a key role in the reduction of the background signal. The low fluorescent paint coating the arms and baffles of the detection cell, as well as the baffles themselves, reduces the amount of scattered laser light (i.e. the "$B_{chamber}$" term). The baffles also act to minimise the amount of solar light that intrudes into the detection cell, thus reducing the "B_{solar}" term. The optical filters within the detection cell reduce the "$B_{P\text{-}scatter}$" term by cutting off radiation wavelengths which correspond to that resulting from Raman and Rayleigh scattering.

The "$B_{P\text{-}scatter}$" term is also minimised through the use of the vacuum system, which reduces collisional quenching, by keeping the pressure low (between 3 and 4 Torr). This low pressure has a key role in the delayed time gating detection, which also reduces the amount of Raman, Rayleigh and Mie scattering that occurs within the instrument. Photons emitted as a result of Raman or Rayleigh scattering have a similar lifetime to the laser pulse. As a result of this,

these photons are not detected when using the time-gating method, so do not affect the fluorescence counts.

Limit of Detection

The limit of detection of the LIF instrument is dictated by the signal to noise ratio (SNR), which in turn, is dependent on both the sensitivity (α, which is calculated using **Equation 2.2**) and the background (B, which is calculated using **Equation 2.3**).

The mixing ratio is then determined through the division of the fluorescence signal by the calibration factor (see **Equation 2.8**).

It is assumed that the statistics of the photon counts is Poissonian and that the same amount of time is spent on measuring the background as is spent on measuring the fluorescence signal. With these assumed conditions, the SNR can be calculated using **Equation 2.4**, where "X_t" refers to the fluorescence signal detected at time "t" and "B_t" refers to the background signal.

$$\mathrm{SNR} = \frac{X_t}{\sqrt{X_t + 2Bt}} \qquad \textit{Equation 2.4}$$

At the limit of detection, the fluorescence signal, X_{min}, is considered to be much lower than the background signal, B. As a result of this, **Equation 2.4** is then rearranged to become:

$$X_{\min} = \mathrm{SNR}\sqrt{\frac{2B}{t}} \qquad \textit{Equation 2.5}$$

The detection limit is then calculated using **Equation 2.6**:

$$n_{NO2}^{\min} = \frac{\mathrm{SNR}}{\alpha}\sqrt{\frac{2B}{t}} \qquad \textit{Equation 2.6}$$

The detection limits (1s, SNR = 2) for NO_2, PNs, ANs and HNO_3 are 9.8, 18.5, 28.1 and 49.7 pptv, respectively.[38] It should be noted however, that these limits of detection correspond to calibrations which were carried out in a laboratory, thus sampling laboratory air. Therefore, for calibrations and measurements in remote atmospheric environments, such as Cape Verde, it is vital that any interferences and leaks within the instrument are minimised, as these could cause significant interferences.

Calibration and Background Procedures

LIF is not an absolute technique, and the instrument used in this work does not have an automated calibration or background measurement system in place.

Calibrations of the instrument are done by first overflowing the lines and detection cells with zero air by opening the zero air valve. This is done in order to ensure that the instrument is no longer measuring ambient air, thus providing a background measurement. The background signal has a number of sources, which are given in **Equation 2.3**. In this work, the zero air was supplied from a BTCA-172 cylinder containing synthetic air (5 ppmv, certified by BOC for less than 1 ppmv NO_x), filtered with a Sofnafil/activated charcoal trap.

The instrument is then calibrated by standard addition of a known mixing ratio of NO_2 from a standard cylinder (5 ppmv, NIST traceable), which is diluted in zero air. The flows of both the NO_2 and the zero air are controlled using internal mass flow controllers (0 – 20 standard cubic centimetres per minute (sccm) and 0 – 20,000 sccm, respectively). Both of these flows are manually selected in order to give a calibration mixing ratio of NO_2. Flows generally used for calibrations during this work were 50 sccm NO_2 in 8000 sccm zero air. This gives a calibration NO_2 mixing ratio of approximately 35.8 ppbv. This calibration mixing ratio is calculated by multiplying the mixing ratio in the cylinder by the dilution factor (i.e. the dilution of NO_2 within the total gas flow), that is:

$$\mathrm{NO_2\ (ppbv)} = (5.00\ x\ 10^{-6})\ ppmv\ x\ \frac{\xi_{NO2}}{\xi_{zero} + \xi_{NO2}} \qquad \textit{Equation 2.7}$$

Where:

ξNO_2 = NO_2 flow (sccm)

ξ zero = zero air flow (sccm)

The instrument software works by taking a known amount of NO_2 (i.e. the calibration mixing ratio) and dividing this by the counts observed during the calibration. This then gives the instrument sensitivity.

The mixing ratio observed is then determined through the division of the fluorescence signal, X (counts per second) by the calibration factor, α (counts per second per ppbv):

$$n_{NO2}^{obs} = \frac{x}{\alpha}$$ *Equation 2.8*

The NO_y channels of the instrument were not calibrated during this work, as these were done by Di Carlo et al. in 2013, prior to the airborne "Role of Night-time Chemistry in Controlling the Oxidising Capacity of the Atmosphere" (RONOCO) campaign.[38]

2.1.3 Detection of Organic Nitrates and Nitric Acid

As mentioned earlier in the chapter, the PN, AN and HNO_3 channels are heated to dissociate the aforementioned compounds into NO_2. This results in the indirect formation and measurement of NO_2. Each of these channels therefore measure ambient NO_2, as well as NO_2 which is produced from the thermal decomposition of the respective compounds. The instrument is therefore also able to simultaneously detect the dissociated compounds. Mixing ratios of these species are determined by subtracting the NO_2 produced in the cooler cell, from that produced in the warmer cell. For example, the PN mixing ratio is calculated by subtracting the NO_2 produced in the PN cell (heated to 200°C), from that in the NO_2 cell (ambient temperature). **Figure 2.4** is a schematic of the instrument layout. The LIF instrument measures NO_2, PNs, ANs and HNO_3 at a resolution of 10 Hz. Each channel has a flow rate of 1.5 slpm, giving a total flow rate through the instrument of 6.0 slpm.

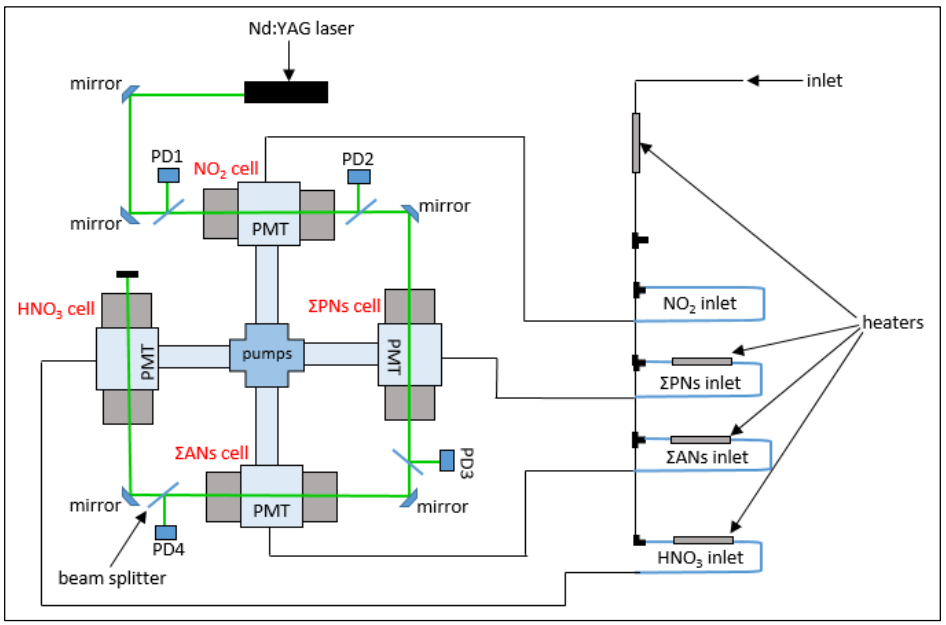

Figure 2.4: Simplified schematic of the LIF instrument

2.1.4 Error Analysis

It is important to ensure that the data obtained from the instrument is as accurate and reliable as possible. This therefore means that the uncertainties and errors associated with the instrument and the data need to be considered.

As the calibration of the instrument determines the sensitivities of each of the instrument channels, the procedure needs to be done as accurately as possible. The accuracy is dependent on the uncertainty associated with the mixing ratio of NO_2 in the standard cylinder. Cylinders of between 2 and 10 ppmv NO_2 are typically used (the cylinder used during this research project was certified to contain 5 ppmv NO_2) and have an uncertainty of between 1 and 3%.

The accuracy of the calibration also depends on the uncertainty of the mass flow controllers used for the air and NO_2 flows. This uncertainty therefore depends on the flow rate of the air and NO_2. The mass flow controller used for the air flow has uncertainties of between 3.4 and 1%, when the flow rate is 1500 and 5,000 sccm, respectively. The mass flow controller used for the NO_2 calibration gas has uncertainties of between 100 and 1%, when the flow rate is 0.2 and 20 sccm, respectively. It should also be noted that there is a relative error in the sensitivity itself, of approximately 3%. In its current configuration, the accuracy of the channels of the LIF instrument is considered to be 10, 22, 34 and 46% for the NO_2, PN, AN and HNO_3 channels, respectively.[38]

As discussed previously, the total mixing ratios of PNs, ANs and HNO_3 are determined through the subtraction of the NO_2 produced in the cooler cell, from that produced in the warmer cell. This means that the limit of detection of each of the channels depends on the signal, along with the uncertainties associated with the channels in question. This is expressed in **Equation 2.9** below, referring to signals from adjacent channels "A" and "B" and their associated uncertainties.

$$(\mathrm{B} - \mathrm{A}) \pm \left(\sigma_{\mathrm{A}}^2 + \sigma_{\mathrm{B}}^2\right) \qquad \textit{Equation 2.9}$$

There are also some potential interferences which have errors, although are very small and easily quantifiable, associated with them. These interferences include the reduction of NO_2 by O_3 at higher temperatures and the complexation of NO_2 to produce PNs or HNO_3. The total error associated with all three of these interferences summed together, is less than 5%. The

most likely interference, however, is the heterogeneous conversion of NO_2-containing compounds (e.g. N_2O_5) to NO_2 in the sample lines or the oxidation of NO to NO_2. However, this interference is minimised by simply increasing the sample flow rate.

2.1.5 General Laboratory Testing of the LIF

General Instrumental Operation

Once the instrument was turned on, parameters needed to be set before it could be used for laboratory testing. The laser power of the instrument was gradually dialled up to full power, at a wavelength of 532 nm, thus providing a suitably long time period for the diodes and thus, the laser, to heat up and reach full power. This is an extremely important factor for optimal instrumental performance, due to the spectroscopic nature of the technique.

On stabilisation of the laser at full power, the instrument was calibrated using the procedure given in section 2.1.2. Flows used for the calibrations in the lab were 50 sccm NO_2 in 8000 sccm zero air, which resulted in a calibration mixing ratio of 35.8 ppbv. Background checks were also conducted, using the method described in section 2.1.2. After conducting several calibrations and background checks, the sensitivities and zero signals were found to be stable at the values given in **Table 2.1**.

Table 2.1: LIF sensitivity and background counts

Instrument Channel	Background signal (counts)	Channel Sensitivity (c/s/ppbv)
NO_2	78.0	178
PN	83.3	83.1
AN	64.3	46.0
HNO_3	130	18.3

These calibrations and background were conducted on a regular basis, in order to monitor any changes in sensitivities of the individual channels. If the values deviated too much from the values given above, the likely cause was misalignment of the laser. In such cases, the laser power was reduced to 30%, meaning it was then safe to open the instrument and adjust the mirrors on the relevant detection cells, in order to re-align the laser.

Zero Air Supply Testing

It is important to have a good source of zero NO_x, as this makes it possible to assess interferences on both the LIF and other instruments used for NO_x measurements. The instrument was therefore used to evaluate the quality of different zero air supplies in the laboratory (i.e. rather than to test the performance of the instrument itself). The first potential source of zero air tested was a pure air generator (with a Sofnafil/activated charcoal trap), which was used for all background air measurements required by the various instruments in the laboratories. The second supply was a BTCA cylinder (5 ppmv, certified by BOC). The air coming from this cylinder was also scrubbed with a Sofnafil/activated charcoal trap (as with the pure air generator). These supplies were connected to the zero air inlet on the LIF, with the instrument then left running for a period of approximately 10 minutes in order to monitor the background counts on the NO_2 channel.

The results of the zero air supply test are illustrated in **Figure 2.5**. NO_2 mixing ratios from both sources never got above zero, with very little difference observed between them. The negative NO_2 mixing ratios observed are due to a small bias associated with either the background measurements or in the calibration factor (see section 2.1.2), as these parameters are used to derive the NO_2 mixing ratio. However, the uncertainty of the mixing ratio retrieval is sufficiently large that the negative values are within the measurements.

The results of this test led to the conclusion that the gas cylinder was not required for background measurements of the LIF whilst in York, the supply from the pure air generator was good enough. Another purpose of these tests was to evaluate the BTCA cylinder as a zero air supply for the use of the LIF in Cape Verde. The remote nature of the site would mean that the cylinder would be the only feasible source of zero air for the instrument, thus meaning it had to contain next to no NO_2. The results from this test therefore also provided evidence that the cylinder would be a suitable supply for the deployment of the instrument

in Cape Verde. With extremely low mixing ratios of NO_2 being expected at the site, this background mixing ratio should not have a significant effect on the instrument sensitivity.

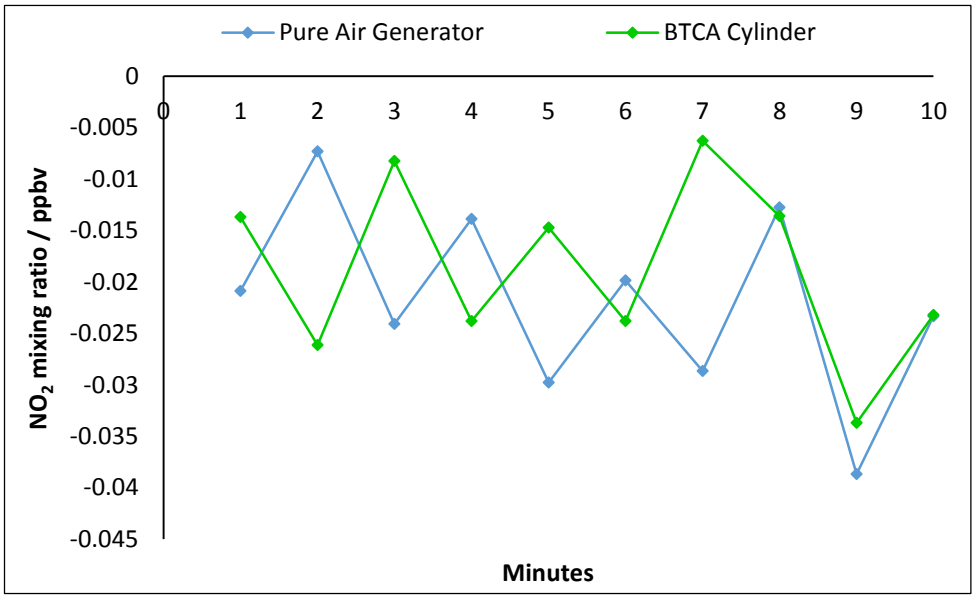

Figure 2.5: Evaluation of zero air supplies for the LIF instrument

Ambient Measurements and Comparisons with a Chemiluminescence Instrument

Inlets of the LIF and a photolytic chemiluminescence (P-CL) instrument[10] were placed outside in order to measure ambient mixing ratios of NO_2 at the University of York campus in Heslington, York (see **Figure 2.6**).

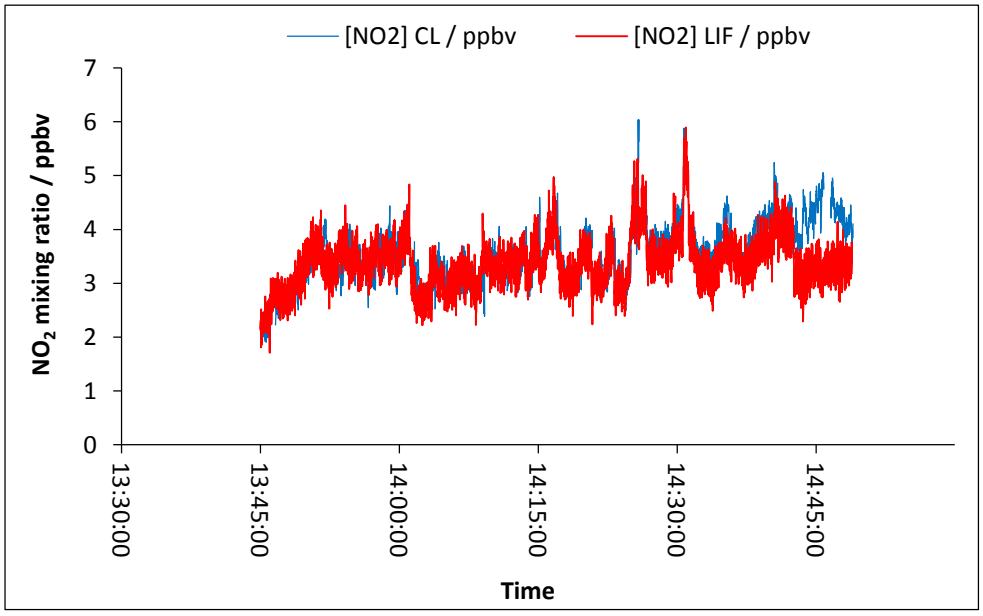

Figure 2.6: LIF and P-CL measurements of NO_2 in Heslington

A direct comparison between the two instruments would also give an indication as to how reliable their measurements are. As can be seen in **Figure 2.6**, both instruments measured very similar NO_2 mixing ratios over the time period studied. Chemiluminescence is a standard technique for atmospheric NO_x measurements. It has been used in a number of ground-based and airborne studies to provide reliable data.[59,60,61] Therefore, the comparability of the LIF and P-CL data provided some assurance that the NO_2 mixing ratios measured by the LIF could be trusted to be an accurate representation of the surrounding atmosphere.

The LIF was then used to measure ambient mixing ratios of NO_2 at the University of York campus in Heslington, York over two days in October 2014 (**Figure 2.7**). Three of the four channels were used to measure NO_2 at this stage (i.e. not heated), in order to directly to compare the channels in terms of nominal NO_2 mixing ratios and trends observed. The HNO_3 channel was not used due to problems encountered with the cell assembly and consequential sensitivity issues.

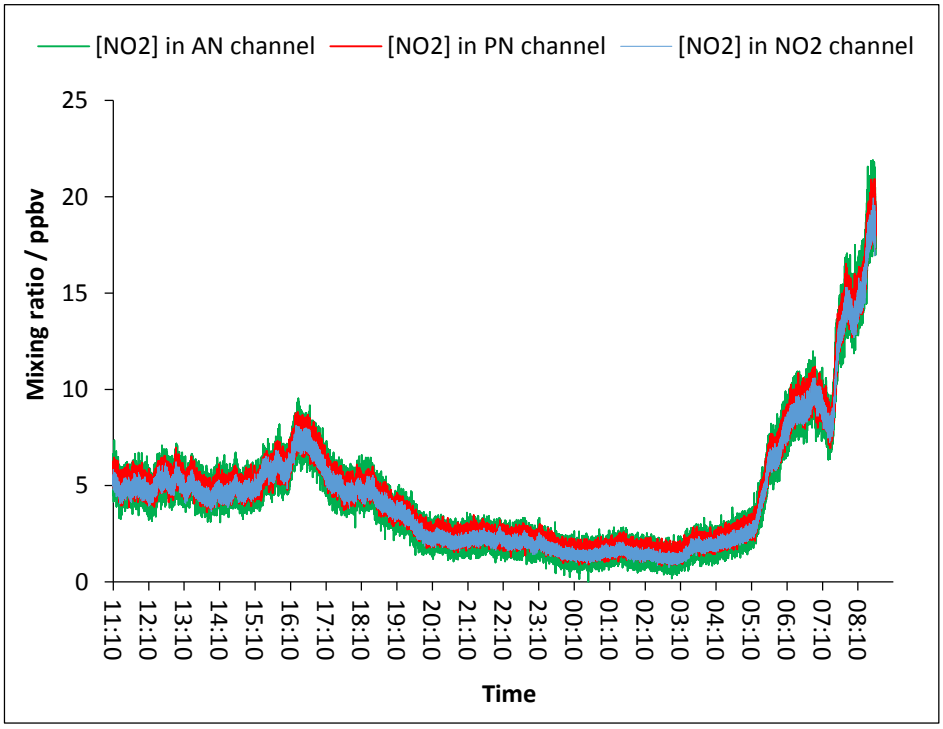

Figure 2.7: LIF measurements of NO_2 in Heslington, York, taken between 15th and 16th October 2014

All of the channels were found to be comparable with each other, with each measuring very similar NO_2 mixing ratios and trends. The mixing ratios show an upward trend from around 05:10, reaching a maximum at around 08:30. The reasoning behind this increase can be put down to the fact that this time period coincides with the morning rush-hour.

In the UK as a whole, the main contribution of NO_x emissions comes from the road transport sector, with regular exceedances of the hourly and annual limits set by the EU (200 µg/m^3 and 40 µg/m^3, respectively).[62] The proportion of NO_x which is being emitted in the form of NO_2 has also been increasing over the past few years,[63,64,65] particularly in areas which are close to the source (i.e. close to roads). These increases coincide with the increase in the number of newer diesel vehicles in the national fleet. These vehicles contain oxidation catalysts, which convert NO to NO_2, thus resulting in an increase in direct emissions of NO_2.

On a more local scale, diesel vehicles in and around York are again responsible for the majority of direct NO_2 emissions. A report was published by the City of York Council in 2011, which provided details on the NO_2 emissions on the main road through Fulford, York (less than 2 miles from the university campus).[66] The report found that, although they made up a smaller proportion of the vehicle fleet, diesel-fuelled vehicles were responsible for approximately three times the NO_2 emissions than petrol vehicles (12.4% compared to 3.6%). The high volume of buses travelling in and around York were also believed to be responsible for a high proportion (32%) of local NO_2 emissions in 2011, despite only making up approximately 2% of the total vehicle fleet. With regular bus services travelling through the university campus, it is therefore likely that these, along with other diesel vehicles, are the sources of these high NO_2 levels in the early morning.

The NO_2 mixing ratios measured in Heslington were then compared to those measured in Fishergate, York, over the same time period.[67] These two data-sets are shown in **Figure 2.8**.

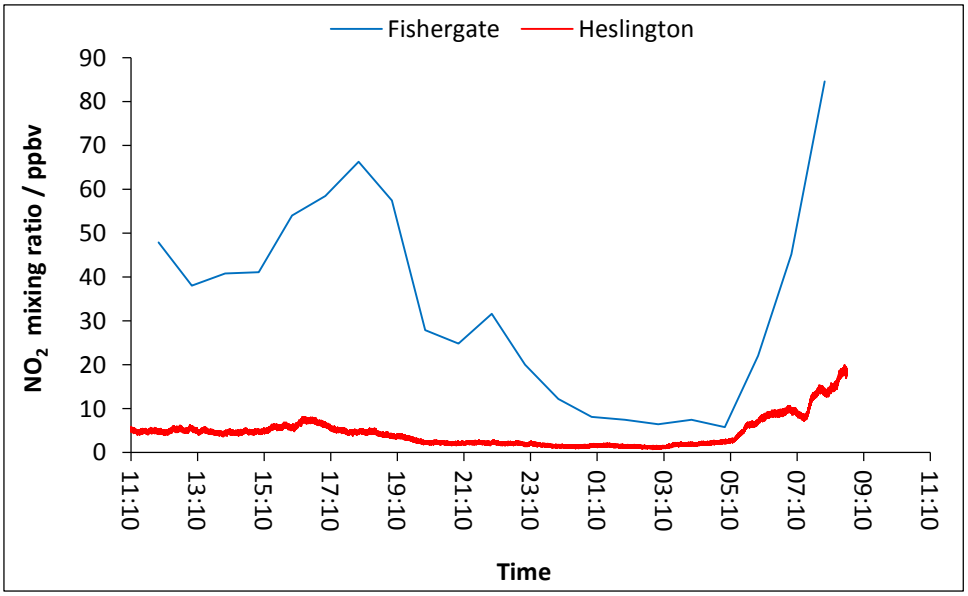

Figure 2.8: NO_2 measurements in Fishergate and Heslington, taken between 15th and 16th October 2014)

The NO_2 mixing ratios measured in Fishergate show similar trends to those measured in Heslington (**Figure 2.7**) with elevations observed during the morning and evening rush-hour periods. However, looking at **Figure 2.8**, a large difference in NO_2 mixing ratios in the two areas is evident. Levels in Fishergate are consistently much higher than those seen in Heslington. For example, at 18:00, the NO_2 mixing ratios in Heslington were around 5 ppbv. However, the NO_2 mixing ratio in Fishergate at this time was over ten times higher, approaching 70 ppbv. This can be explained by the fact that Fishergate is situated in the centre of York, thus meaning that it regularly witnesses high volumes of traffic, travelling into and out of the city. Heslington, however, is a suburban village, with much lower traffic counts compared to the city centre. As discussed previously, the dominant NO_2 source in York (and in the UK as a whole) is the transport sector. This therefore means that the observations surrounding NO_2 mixing ratios in Fishergate can be attributed to the abundant road traffic emissions in the surrounding area.

2.1.6 Characterisation for NO Measurements

The measurement of NO is just as important as the measurement of NO_2, as the two species quickly and easily convert. This means that they are able to catalyse many reaction cycles. One of the most important reaction cycles which is initiated by the oxidation of NO to NO_2 involves O_3. If the mixing ratios of NO_x are too low, RO_2 radicals react with each other, rather than with NO, terminating the radical chain. In these conditions, therefore, O_3 destruction dominates. However, at higher NO_x mixing ratios, the RO_2 radicals oxidise NO to NO_2, which then leads to net O_3 production via the photochemical cycle represented by reactions (1) to (3) (see section 1.1). It is therefore important to consider both the NO and NO_2 mixing ratios, as these can dictate whether O_3 production or destruction processes will dominate in a particular atmospheric environment.

The LIF was originally designed to measure NO_2, PNs, ANs and HNO_3, through thermal dissociation (see section 2.1.3). However, the aim of these experiments was to try to measure NO by titration. This involved the use of only the NO_2 and PN channels, which were selected based on their high sensitivities. The NO_2 channel was used to measure ambient NO_2 mixing ratios. The PN channel was used to measure NO. This was done by installing a gas phase titration (GPT) system, i.e. a supply of NO and O_3, into the apparatus. On addition of sufficient O_3 into the system, the NO_2 and PN channel signals should diverge, with the difference in

signal being due to the production of converted NO_2 (i.e. that produced through the reaction of O_3 and NO). With the O_3 being in excess, this would mean that the mixing ratio of converted NO_2 could then be considered to be equivalent to the mixing ratio of NO. A schematic of the set-up can be seen in **Figure 2.9**. As seen on the schematic, an NO standard cylinder (5 ppmv) provided the NO supply, with a multi-gas calibrator (Monitor Europe model S6100) acting as the O_3 source. Due to flow rate constraints of the multi-gas calibrator, both the AN and HNO_3 channels were capped, giving a total flow rate of 3 slpm during NO characterisation experiments. Mass flow controllers were also put in place to alter the dilution factors of the two species during subsequent laboratory experiments. The ultimate objective of these experiments was to characterise the LIF for NO measurements. This was done using a range of instrumental configurations and reaction conditions, which were used to find the optimal conditions needed for the highest conversion efficiency possible. The set-up giving the highest conversion efficiencies would then be used to measure NO on deployment of the instrument at the CVAO.

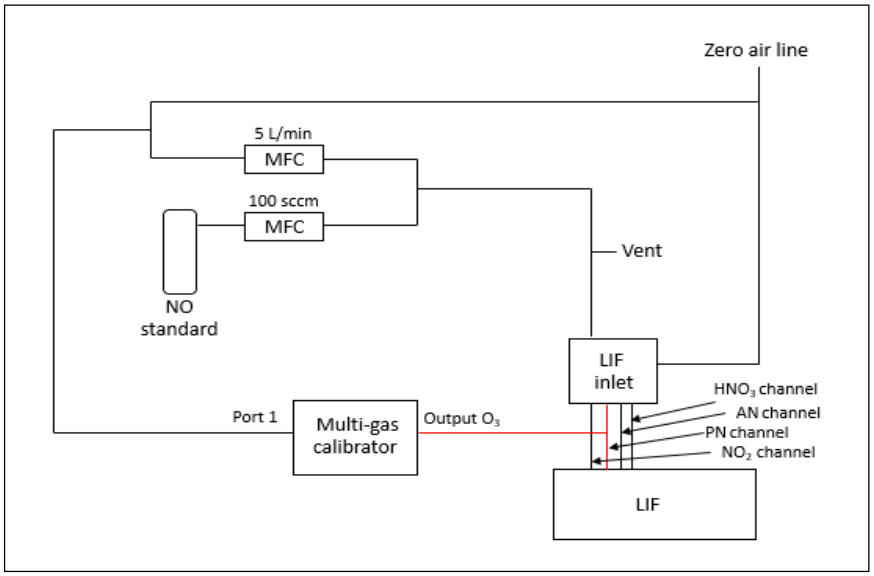

Figure 2.9: Schematic of the LIF configuration for NO characterisation (the GPT channel is shown in red)

Calculation of Conversion Efficiency

In order to characterise the LIF instrument for NO measurements, an essential parameter to monitor is the conversion efficiency (i.e. how much of the NO is converted to NO_2 through titration with O_3). In order to calculate this, the following must be done for each data-set.

- Allow the PN channel signal (i.e. the converted NO_2 signal) to stabilise
- Take the average of the converted NO_2 data
- Calculate the mixing ratio of NO that is being used during the test in question. The 5 ppmv cylinder is diluted to the mixing ratio required in each test. In order to determine this diluted mixing ratio, **Equation 2.10** below is used.

$$\frac{\text{NO flow (sccm)}}{\text{zero air+NO flow (sccm)}} + \text{cylinder mixing ratio (ppmv)} \qquad \textbf{Equation 2.10}$$

Dividing the averaged converted NO_2 by the calculated NO mixing ratio then derives the proportion of NO_2 which has been successfully converted into NO.

Determination of O_3 Mixing Ratio Required for Conversion

In order to make efficient NO measurements, it was first necessary to determine the lowest mixing ratio of O_3 required for the GPT. The NO cylinder was diluted in zero air to 50 ppbv, with different O_3 mixing ratios being added to the system by manually changing the O_3 output of the multi-gas calibrator. The mixing ratios of O_3 used were 600, 700, 900, 1500, 3000, 6000, 10,000 and 20,000 ppbv. **Figure 2.10** shows the results of said experiment. The conversion efficiency reaches a peak conversion efficiency as 10,000 ppbv of O_3 is added.

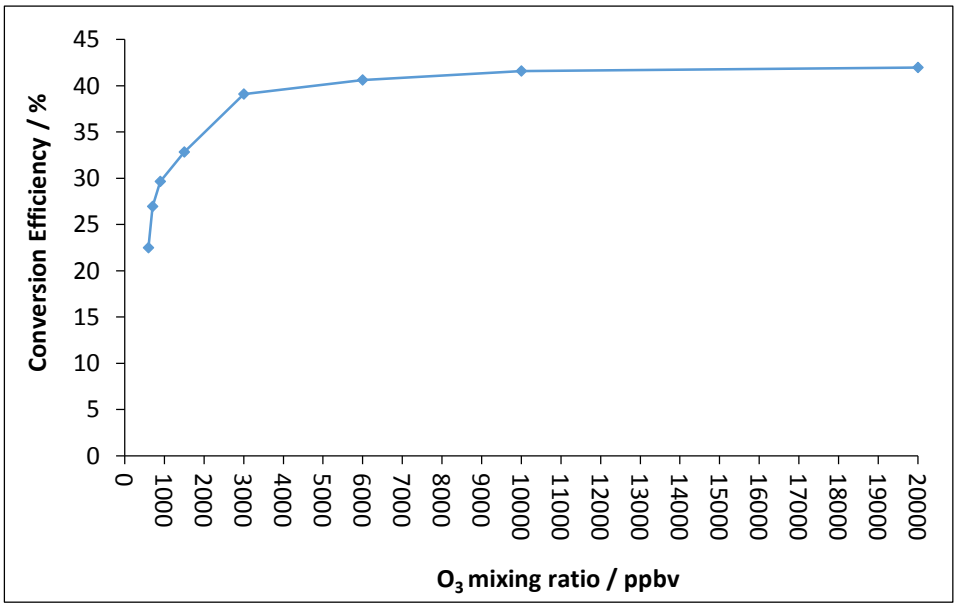

Figure 2.10: Determination of the O_3 mixing ratio required for gas phase titration

Although the conversion efficiency was slightly higher using 20,000 ppbv (41.59% and 41.98%, respectively), this was not considered a great enough improvement with such a large increase in O_3 mixing ratio. It was therefore decided that an O_3 mixing ratio no higher than 10,000 ppbv would be used in further experiments. As can be seen in **Figure 2.10**, the conversion efficiency did not exceed 42%, i.e. less than half of the NO_2 was converted. The most likely explanation for this is the limited mixing time for the NO and O_3 within the instrument channel, i.e. the reaction chamber was not large enough to ensure that all of the NO reacted with O_3 to produce NO_2 before detection, hence resulting in reduced conversion efficiencies.

Monitoring the Conversion at Different NO Mixing Ratios

As the mixing ratio of O_3 required for titration had been determined, it was then necessary to vary the mixing ratio of NO. This would mean that it would be possible to assess the consistency of the conversion efficiency, thus giving an indication of the applicability for NO measurements in Cape Verde.

The NO mixing ratios were varied between 60 and 40 ppbv at 5 ppbv intervals, with each individual test using a different O_3 mixing ratio (10,000, 7500, 6000 and 5000 ppbv). The O_3 mixing ratio was changed in order to confirm or refute the initial mixing ratio required for efficient GPT.

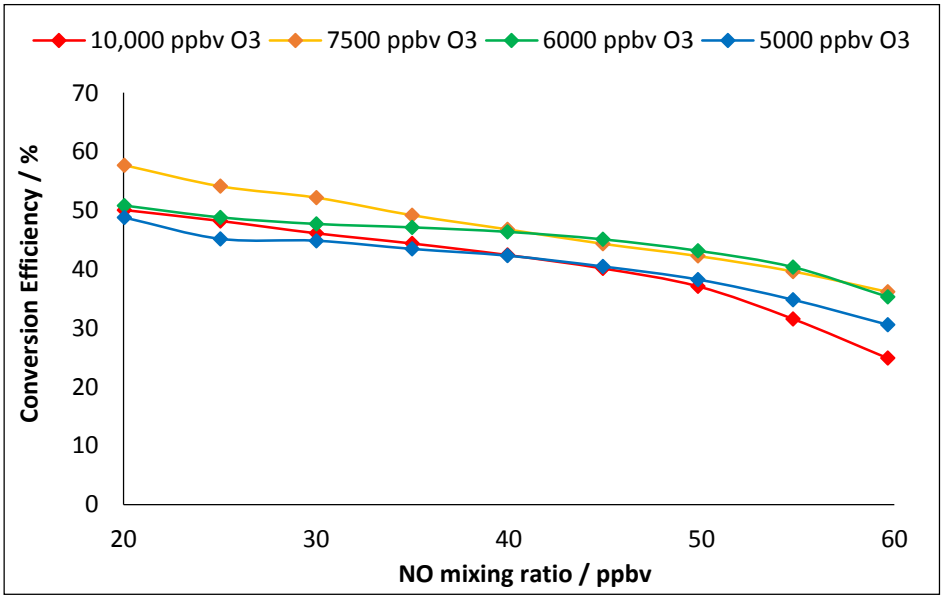

Figure 2.11: Assessing the effect of changing NO mixing ratios on the conversion efficiency of the LIF instrument

From these experiments, a maximum conversion efficiency of 57.8% was found, using 7500 ppbv O_3 and 20 ppbv NO (**Figure 2.11**). However, a decrease in conversion efficiency was observed as the NO mixing ratio was increased. This could be explained by the fact that there is smaller proportion of NO available to react with the constant supply of O_3, meaning that less converted NO_2 is produced, thus resulting in an overall lower conversion efficiency.

Increasing Reaction Time: Alterations in Tube Diameter

As discussed previously, the mixing time of NO and O_3 needs to be maximised, as this would likely increase the amount of converted NO_2 produced, thus improving the conversion efficiency. One way of doing this would be to increase the reaction volume. In order to test this hypothesis, two lengths of ½ inch PFA tubing (10 and 30 cm) were added to the PN channel. **Table 2.2** displays the results of these tests. With the addition of the 30 cm piece of tubing increasing the conversion efficiency by around 5%, the O_3 mixing ratio was changed to look at the impact this had on the conversion. As **Table 2.2** shows, a maximum conversion efficiency of 90.9% was found using 30 cm of tubing and 10,000 ppbv of O_3.

Table 2.2: The effect of increasing the reaction volume using ½ inch tubing

Reaction Tube Length / cm	Residence Time /s	Mixing Ratio of O_3 / ppbv	Conversion Efficiency / %
10	0.157	7500	84.3
30	0.471	7500	89.8
30	0.471	10,000	90.9

In order to see if 90.9% conversion could be improved upon, the mixing time was increased further, by an extra 3 inches to the reaction volume. Prior to starting any experiments using the trap, the background signals of both the NO_2 and PN channels were first measured for approximately 10 minutes. The 10 minute averaged values were then subtracted from the data obtained during subsequent experiments.

The trap was then tested over a range of NO mixing ratios, which were varied between 30 and 100 ppbv, at 10 ppbv intervals. Each mixing ratio was tested for a period of 15 minutes and the results can be seen in **Figure 2.12**.

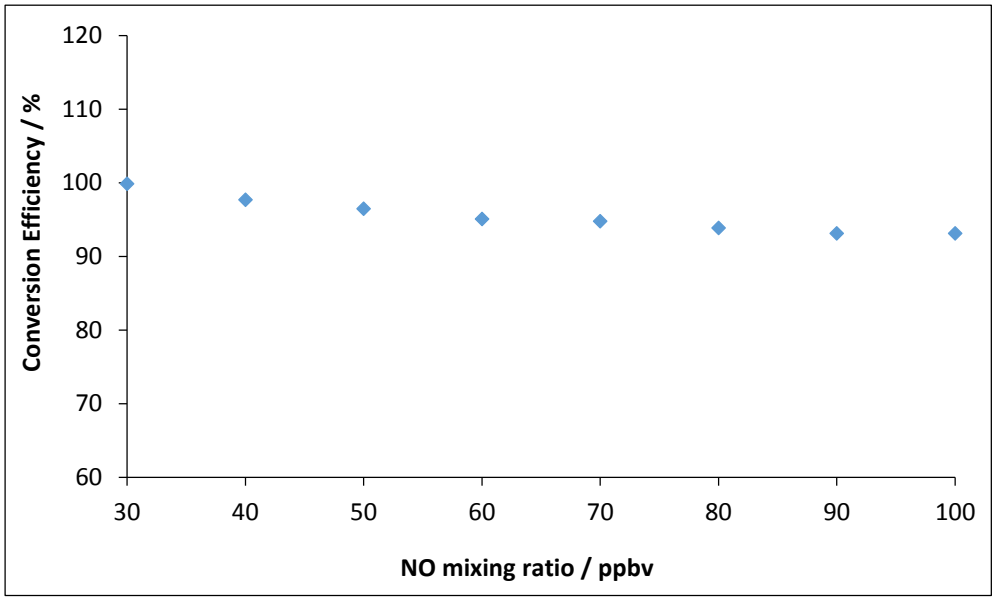

Figure 2.12: Evaluating the effect of increased reaction volume at different NO mixing ratios

The results from these experiments confirmed the adding the 3 inch diameter reaction volume improved the conversion efficiency greatly, thus emphasising the key role that the NO and O_3 mixing time has on the performance of the LIF for NO characterisation.

Alteration of O_3 Source: Mercury Lamp

A spectral calibration lamp (model 6035, manufactured by "Oriel Instruments", a "Newport Corporation" brand), was tested as an alternative O_3 source for NO characterisation of the LIF. The lamp works by producing narrow, intense lines from the excitation of argon gas and mercury vapour, operating at 13 to 23 milliamps (mA). This would be a more practical option than the multi-gas calibrator, due to the much reduced space and weight requirements, particularly for transportation and deployment in Cape Verde. The lamp in question emitted UV light at a wavelength which leads to photolysis of molecular oxygen (185 nm). The oxygen molecules then react with the dissociated oxygen atoms, thus producing O_3. The lamp was inserted into an empty reaction vessel, which was then covered in a layer of black insulation, to minimise exposure to the harmful UV radiation. Due to the fact that the lamp was in the preliminary stages of testing, its suitability as an O_3 source was as yet unknown. The seal of the lamp was therefore only temporary.

Once the lamp was installed into the PN channel of the instrument, a background signal of around 3 ppbv was observed prior to the lamp being turned on. The poor seal of the lamp was believed to be the reason behind this. The background of the instrument was run for approximately 5 minutes prior to each test, with the averaged value then being subtracted from the measured converted NO_2 (i.e. the PN channel signal).

An initial test was conducted to assess the efficiency of the lamp in the GPT process. The power of the lamp was dialled up to its maximum, with the NO cylinder being diluted to 5, 10 and 20 ppbv using the multi-gas calibrator. The results of these tests can be seen in **Table 2.3**.

Table 2.3: Testing the mercury lamp at various NO mixing ratios

Mixing Ratio of NO / ppbv	Conversion Efficiency / %
20	35.9
40	46.3
60	48.6

During these tests, the signal from the PN channel signal (i.e. the channel containing the mercury lamp) showed a substantial amount of fluctuation. As a background signal had been observed on initial implementation of the lamp, these fluctuations were considered to be a result of the instability of the lamp (namely the rudimentary seal with the reaction vessel). In order to see if this was indeed the case, the background signal of the PN channel was measured without the lamp in-line. This gave values at or around zero. When the lamp was re-incorporated into the channel, the background signal went back up to 3 ppbv, thus confirming that the lamp was behind the poor background signal. The decision was then made to test the lamp further, with other alterations to the instrument configuration, in order to test the lamp under a range of reaction conditions.

Testing the Mercury Lamp: Increasing the Reaction Tube Length

The reaction tube length was increased in an attempt to improve the initial conversion efficiency achieved using the mercury lamp (48.6% - see **Table 2.3**). A range of lengths of ¼ inch PFA tubing (20, 30, 50, 100 and 150 cm) were added to the instrument, with each tube being tested using three different NO mixing ratios: 20, 10 and 5 ppbv. The corresponding residence times were calculated for each length of tubing, using pre-calculated values of the tubing volume and the flow rate (3 slpm). The mercury lamp at maximum power was used as the O_3 source. Results of the experiments can be seen in **Table 2.4**.

Table 2.4: Testing the mercury lamp with various reaction tube lengths

Tube Length / cm	Residence Time / s	Conversion Efficiency (5pppbv NO) / %	Conversion Efficiency (10 ppbv NO) / %	Conversion Efficiency (20 ppbv NO) / %
20	0.0503	11.1	29.7	36.1
30	0.0754	13.0	30.5	38.0
50	0.126	52.7	48.2	43.0
100	0.251	11.6	31.4	38.8
120	0.302	N/A	22.0	34.7

The tests highlighted the issue of the background signal coming from the lamp, particularly when longer reaction tubes were used. This is the reason why "N/A" is seen at 5 ppbv for tube 5, where the background was found to be higher than the average converted NO_2 mixing ratio (which was around 6-7 ppbv). The data was therefore not considered to be reliable, which significantly outweighed its practicality in terms of working in the field. A more permanent, secure seal would be required for future use in this type of experiment.

NO Characterisation: Concluding Remarks

After conducting these experiments, it could be concluded that the conditions required for maximum (> 90%) conversion were the use of the multi-gas calibrator as the O_3 source, with the addition of 3 inch diameter reaction volume in the PN channel. Although more practical

in terms of field work, the mercury lamp was not deemed suitable for NO characterisation in its current configuration. The lowest O_3 mixing ratio required for efficient conversion was found to be 10,000 ppbv, thus meaning that this, along with the aforementioned apparatus, would be used to measure NO in Cape Verde.

2.2 Introduction to the Airborne P-CL Instrument

The instrument used for airborne NO_x measurements during the 2015 "Oil and Gas" campaign is a P-CL instrument designed by "Air Quality Design Inc." (Colorado USA). The instrument detects NO directly from the chemiluminescence resulting from the reaction of NO and O_3. NO_2 is then quantified using the same instrument, by first photolytically converting NO_2 to NO using blue light LED diodes centred at 385 nm[10] followed by chemiluminescence.

The instrument is fitted into a rack, which can then be installed in the BAe-146-301 research aircraft used for the airborne measurements. It is then possible to sample and measure air in-situ during flights around a particular area of interest. Typically, the aircraft flights at a speed of 200 knots (100 m/s), thus meaning that it is possible to obtain measurements with high spatial resolution, if the both the sampling and analysis of the air are conducted using a sufficiently high time resolution (typically 1 Hz).

2.2.1 Instrument Components

The instrument has five components; a two-channel chemiluminescence analyser, a two-channel ozoniser, a calibration control box, an inlet panel and a data acquisition instrument. A schematic of the instrument configuration can be seen in **Figure 2.13** below.

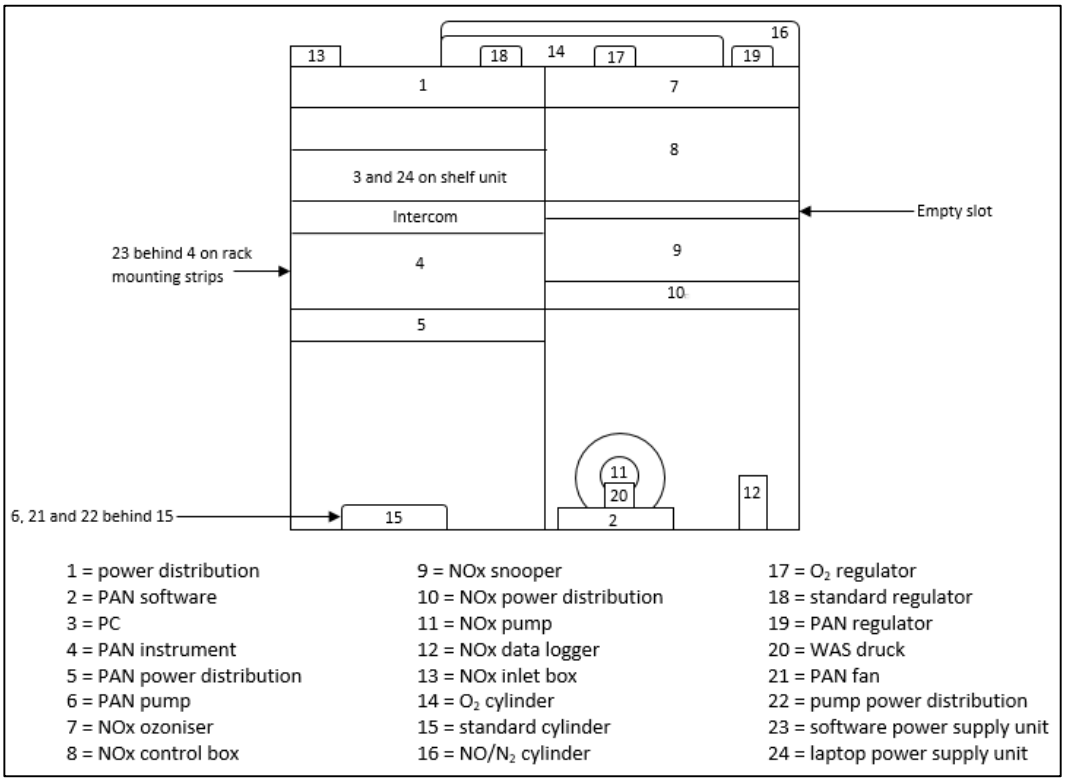

Figure 2.13: Box schematic of P-CL instrument

Figure 2.14 overleaf is a detailed flow schematic of the P-CL instrument. This gives a great amount of detail regarding the constituent parts of the instrument, and they are all connected to each other to enable the measurement of NO and NO_2.

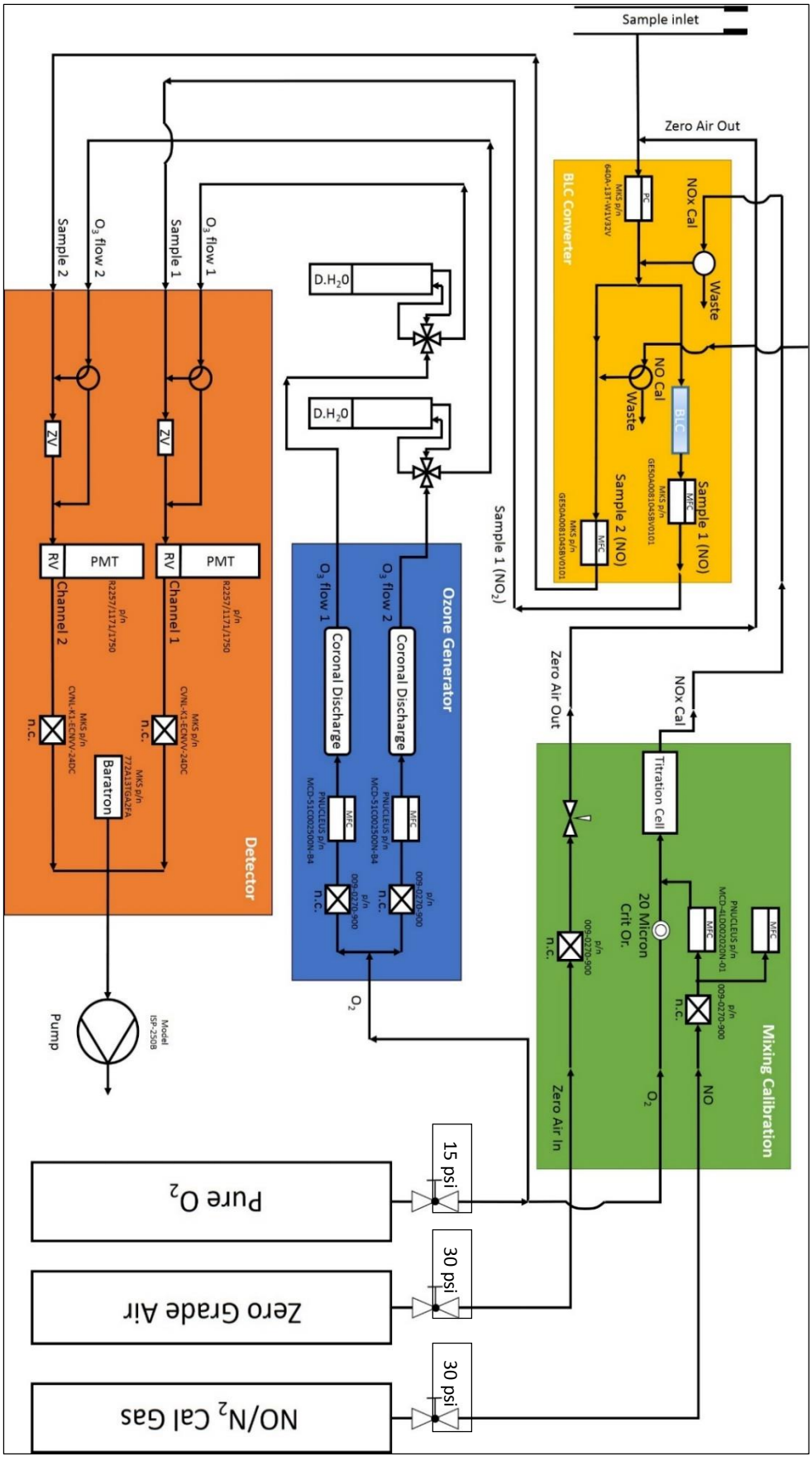

Figure 2.14: Flow diagram of P-CL instrument (courtesy of Stephanne Bauguitte, Facility of Airborne Atmospheric Measurements, Cranfield, UK)

NO_x Inlet Box

The inlet box (13 on **Figure 2.13**) houses the calibration valve for NO and NO_2. The zero valve is used for zero air displacement calibrations, as well as testing for artefacts in the zero air supply. There is also a pressure controller in the inlet box (manufactured by "MKS", model 640A), which is used to regulate the pressure as the aircraft changes altitude during the flights.

The inlet box also contains the two mass flow controllers in the instrument (manufactured by MKS, model GE50A); one for the NO channel and one for the NO_2 channel. The NO_2 and NO_y converters are housed in the inlet box. The NO_2 converter is a photolytic BLC (manufactured by "Droplet Measurement Technologies Inc." (Boulder, Colorado, USA)), centred at 395 nm. The assembly of the inlet box is displayed in **Figure 2.15**.

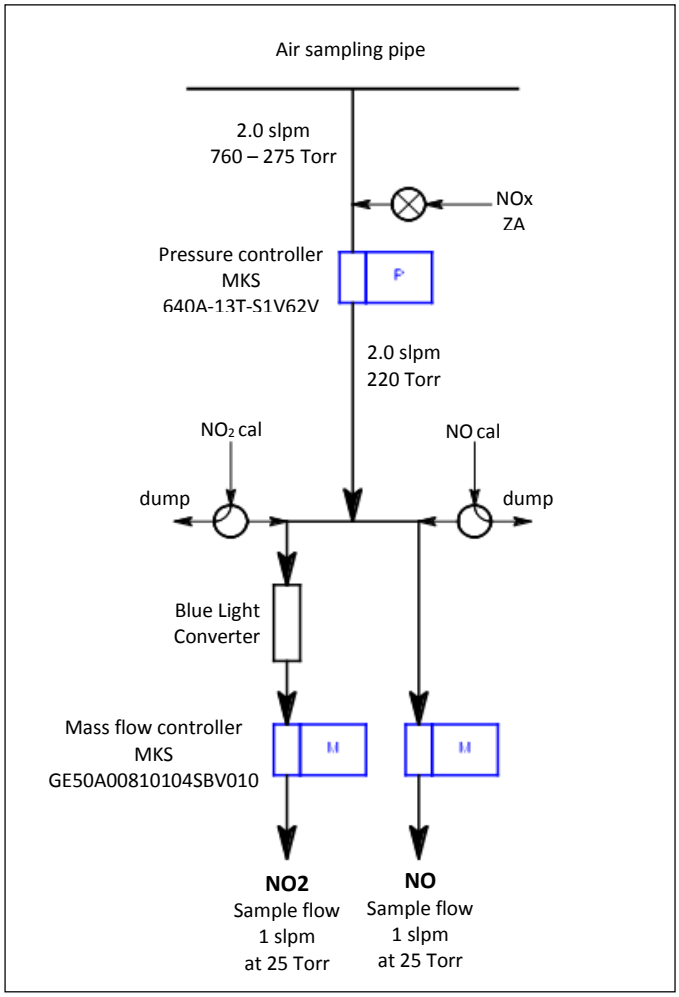

Figure 2.15: Flow diagram of P-CL inlet box

NO_x Calibration Box and Calibration Procedure

This part of the aircraft rack (8 on **Figure 2.13**), contains the mass flow controller for the NO calibration gas. One of the main components situated in the control box is the GPT cell. The cell comprises of an aluminium block containing a Teflon tube. A small amount of air and calibration gas then flows through this cell and, when illuminated by a pen-ray lamp (which is also situated within the aluminium block), the NO calibration gas is titrated with the O_3 (see "Ozoniser" section for more information) to produce NO_2. The lamp itself is turned on, thus starting the NO_2 channel calibrations (it is left off for the NO channel calibrations).

The instrument is calibrated using the method of standard addition, whereby a small flow of the NO calibration gas (5 sccm) is added to the flow of ambient sample gas (1000 sccm) in both instrument channels. The mixing ratio of the NO calibration gas used is 5 ppmv. However, the cylinder mixing ratio is diluted at the inlet. This mixing ratio of NO at the inlet is calculated by multiplying the mixing ratio in the cylinder by the flow dilution (i.e. 5/1000). On doing this, the inlet mixing ratio was calculated to be 25,000 pptv (25 ppbv). The calibration procedure consists of two cycles. The first cycle calibrates for the sensitivity of the NO channel, by flowing NO gas in nitrogen. The second and final cycle calibrates the sensitivity of the NO_2 channel, using the NO calibration gas with the added O_3. This then gives a known mixing ratio of NO_2. The instrument measured the background signal using a duty cycle of a 15 second long zero measurement, every two minutes. However, the zeros could be manually paused for a certain time period, if necessary.

This standard addition calibration method requires a low and stable background of NO and NO_2. As a result, pre- and post-flight calibrations required a NO_x trap to be connected to the inlet. These calibrations were done around 90 and 30 minutes before take-off, and repeated prior to instrument shut-down. If the calibrations results were outside 15% of the nominal sensitivities, these were changed to the calibration results. It was important to do this, as it was these numbers which were then used to calculate the flight data. The trap was then removed and the inlet line attached to the instrument. This also meant that any in-flight calibrations could only be done on a straight run above the boundary layer (typically between 8,000 and 10,000 ft). If only a "quick" calibration (i.e. only the NO sensitivities of both channels) was done, a straight and level run was not required. It did, however, require a stable background, so was typically done above the boundary layer.

NO Detector

This contains the cooling housing for the PMT detectors (9 on **Figure 2.13**). The PMTs are cooled to -25°C using a thermoelectric refrigerated chamber. This chamber leads to a reduction in the anode dark current through the cooling of the photocathode. This improves the SNR of the instrument. The pre-reaction and reaction volume are also located in this part of the instrument. The pre-chamber system involves the addition of O_3 upstream of the main reactor, and this provides the instrument's zero (or background) reading. This is discussed further in section 2.2.2.

Also housed in this box are the pulse amplifier/discriminator, as well as the pressure sensor and power supplies for the snooper instrument. This part of the instrument also controls the high voltage applied to the PMT detectors, the zero and vacuum valves, through the use of switches, which have three settings: on, off and automatic.

Ozoniser

The ozoniser, which is housed in the control box, generates O_3 using a corona discharge tube (manufactured by "Ozone Services"). This piece of apparatus operates by splitting oxygen molecules into two oxygen atoms using an electric discharge. These unstable oxygen molecules then react with other oxygen molecules, thus forming O_3.

Data Acquisition System

This part of the instrument consists of a USB port accessible data acquisition board (LabJack), a connection panel that contains the instrument connections, and a laptop computer. "DaqFactory" software is used for the running of the instrument, with the LabJack data acquisition card also being controlled by said software.

Photolytic Converter

The instrument is able to quantify ambient NO_2 mixing ratios if it is first pre-converted to NO. This takes place in the second instrument channel, whereby NO_2 is photolytically reduced to NO using UV-LED converters (or BLCs). The efficiencies of these converters have been found to exceed those of others (namely metal halide and xenon lamps). They showed maximum NO_2 to NO conversion efficiencies of around 90%, compared to the 70% achieved using metal halide or xenon lamps.[41,46] These converters are centred at a wavelength of 395 nm, which is known to have a specific affinity for NO_2 to NO conversion.[48] The subsequent chemiluminescence from the reaction of this NO and O_3 is then used to quantify the NO_2 mixing ratio.

Photolytic converters have been shown to have a significant advantage over the use of heated molybdenum converters. These work by reducing NO_2 to NO. However, although relatively cheap, they are known to experience interferences from NO_y species (e.g. organic and particulate nitrates, HNO_3), reducing these, as well as NO_2, to NO.[40,42]

There are a number of different types of photolytic converters, namely metal halide lamps, xenon arc lamps and LEDs. Studies have provided evidence that light-emitting diodes have distinct benefits over the use of metal halide and high pressure xenon arc lamps. These include lower power requirements and longer operational lifetimes, whilst also providing a higher NO_2 conversion efficiency than the aforementioned lamps.[42]

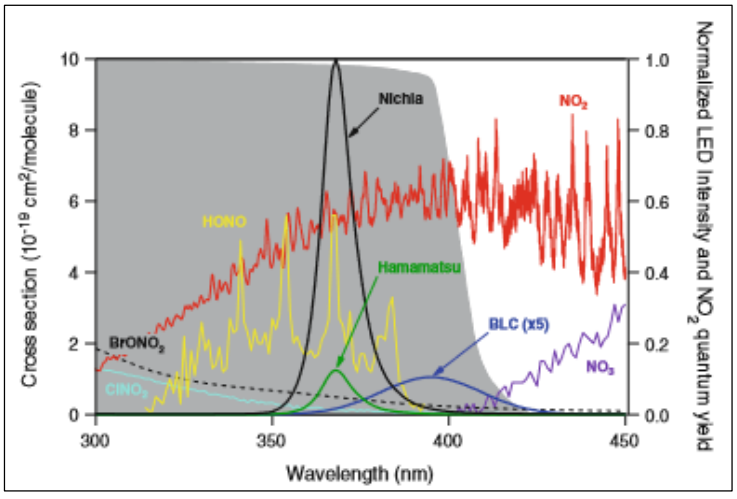

Figure 2.16: Emission spectra of 18W Nichia (black) and 0.5W Hamamatsu (green) LED converter centred at 365 nm, and a BLC spectrum (blue) centred at 395 nm – BLC spectrum has been multiplied by a factor of 5 for clarity. The absorption cross section of NO_2 (red), NO_2 quantum yield (shaded grey) and other chemical species are also depicted. (Figure taken from Pollack et al. (2010)[48])

The BLC in the instrument used during this research project is similar to that used in a study by Pollack et al.,[48] which compared three different types of LED. The BLC used by Pollack et al. consisted of two 395 nm LED modules at each end of the photolysis, thus producing emission in the same wavelength interval as the BLC used in this thesis. As seen in **Figure 2.15**, the BLC, centred at 395 nm, has a distinct advantage. As well as showing good overlap with the NO_2 absorption cross section, the wavelength emitted from the BLC exhibits a very poor amount of overlap with the absorption cross section of HONO. The affinity of 395 nm for NO_2 photolytic conversion to HNO_3 thus provides a great amount of analyte selectivity within the channel, due to the low probability of other species, such as HONO, being photolyzed. This provides the reasoning behind the use of a BLC in the airborne chemiluminescence instrument.

The total NO_x is therefore quantified simply through addition of the direct NO measurement from the first channel, and the indirect NO_2 measurement in the second instrument channel. NO and NO_x measurements are therefore synchronous, as a result of the dual channel configuration. This is a key requirement for the instrument, particularly in terms its use for airborne measurements, which require it to measure at a resolution of 1 Hz.

2.2.2 Instrument Parameters

NO Mixing Ratios and Sensitivities

The measurement of the NO mixing ratio is direct, as this corresponds to the signal observed when the LEDs in the BLC are turned off. It is calculated using **Equation 2.11**:

$$[\mathrm{NO}] = \frac{(\mathrm{NO_{meas}} - \mathrm{NO_{zeroint}})}{\mathrm{NO\_NO_{sensint}}} \qquad \textit{Equation 2.11}$$

Where:

NO_{meas} = counts recorded by PMT while in measure mode

$NO_{zeroint}$ = interpolated value of averaged counts recorded while in pre-chamber mode

$NO_{sensint}$ = interpolated value of the sensitivity

The sensitivity of the NO channel is determined using **Equation 2.12**:

$$\mathrm{NO\_NO_{sensint}} = \frac{(\mathrm{NO} - \mathrm{NO_{measint}})}{\mathrm{NO\_NO_{calconc}}} \qquad \textit{Equation 2.12}$$

Where:

$NO_{measint}$ = interpolated value of the measure-mode counts

$NO_{calconc}$ = mixing ratio of the NO calibration

NO_2 Mixing Ratios and Sensitivities

The mixing ratio of NO_2 is calculated in a similar way to NO, using **Equation 2.13**:

$$[\mathrm{NO_2}] = \frac{(\mathrm{NO2_{meas}} - \mathrm{NO2_{zeroint}})}{\mathrm{NO2\_NO2_{sensint}}} \qquad \textit{Equation 2.13}$$

Where:

$NO2_{meas}$ = counts recorded by PMT while in measure mode

$NO2_{zeroint}$ = interpolated value of average counts measured in the zero mode

$NO2\_NO2_{sensint}$ = interpolated NO_2 sensitivity for the instrument

The NO_2 channel sensitivity is calculated using **Equation 2.14**:

$$\mathrm{NO2}_{\mathrm{NO2_{sens}}} = \frac{(\mathrm{NO2_{cal}} - \mathrm{NO2_{measint}})}{\mathrm{NO2\_NO2_{calconc}}} \qquad \textit{Equation 2.14}$$

Where:

$NO2_{cal}$ = average of counts from the instrument in calibration mode

$NO2_{measint}$ = interpolated value of the measure-mode counts

$NO2\_NO2_{calconc}$ = mixing ratio of the NO_2 calibration

"Zero" Instrument Modes

The instrument has two "zero" modes. The first mode uses the pre-chamber to react the O_3 with NO before reaching the PMT detector. This means that all chemiluminescence occurs here and a background signal of the PMT is measured. The signal resulting from the addition of O_3 in the prechamber accounts for any interferences (namely, the reaction of O_3 with hydrocarbons and the reaction chamber walls),[41] thus giving the instrument's zero (or background) reading. This is a result of the reaction of NO and O_3 being faster than most of these interference reactions. Then, during measure mode, the O_3 is added to the main reaction chamber. The difference in signal between said measure mode and the zero mode (when O_3 is added to the pre-reaction volume) corresponds to the NO mixing ratio in the sample air. It is the chemiluminescence resulting from the gas-phase titration (i.e. the reaction of NO and O_3) which is then observed by the PMT.

The other zero mode is when zero air is added to the sample lines, thus giving an indication of the artefact associated with each instrument channel. This mode is particularly important when looking at the errors associated with the instrument, and is discussed further in section 2.2.3.

2.2.3 Error Analysis

It is important to carry out error analysis associated with the instrument, as this allows assessment of the reliability of the data obtained during the flights. This involves looking at both the accuracy and precision of the data.

Accuracy

The accuracy of the observations is affected by a number of uncertainties. The first of which is in the calibration procedure. The total accuracy of the calibration depends on the errors associated with three instrumental features; the sample and calibration gas MFCs, the mixing ratio of the NO standard and the NO_2 conversion efficiency.

It is vital that during calibrations, the mixing ratio of NO standard gas that is added to the system is measured with as high an accuracy as possible. This consequently depends on the accuracy of the sample and calibration gas mass flow controllers. These have an associated accuracy of 1% each, and are calibrated before, during and after any research campaign using a digital flow meter. This ensures that they are measuring flows as accurately as possible, thus minimising the error associated with the mass flow controllers. It is also important to check the mixing ratio of the reference gas against the manufacturer's stated mixing ratio. This is done using the ACTRIS protocols (see http://www.actris.eu/ for details).

The mixing ratio of the NO standard is known to an accuracy of ±1% (British Oxygen Company (BOC), certified to the UK National Physical Laboratory). The NO/N_2 mix should be stable for 5 years (certified by BOC). The oxygen cylinder has a high purity level of N2.6. This means that it has a guaranteed minimum purity of 99.6% and maximum impurity level of 0.4%, certified by BOC.

There is also an error associated with the NO_2 conversion efficiency that the instrument measures. This is particularly important for the NO_2 mixing ratios that are measured during the calibration. This error is only small, at 1%, but must be considered as an important component in the determination of the instrument's total error (see later).

As a very efficient quencher of both the excited state of NO_2 and reactions that produce the background signal, water vapour can significantly affect the sensitivity of the instrument through alterations of the background signal. During the flights, changing altitudes leads to

coincident changes in ambient humidity. This would lead to significant instrumental interferences, thus affecting the accuracy and reliability of the data. This issue is minimised by humidifying the ozonisers. This ensures controlled conditions whilst also meaning that the background signal, and hence, the sensitivity of the instrument is not affected by water vapour during the flights.

The NO-O_3 reaction upstream of the reaction chamber also has uncertainties associated with it. The reaction can affect the mixing ratio of NO that is measured by the NO channel, thus meaning that it is required to correct for the NO titration. This is done using a system specific correction algorithm, whereby the NO sensitivity measured over several calibration cycles is plotted against the coincident measured O_3 mixing ratio.

As well as these systematic errors, it is also important to consider the instrument artefact. This defined as "the apparent signal measured while the instrument is sampling zero air", and is quantified for both channels by looking at the mixing ratios measured when the zero air is added to the sample lines. An example of the artefact data is shown in **Figure 2.17**.

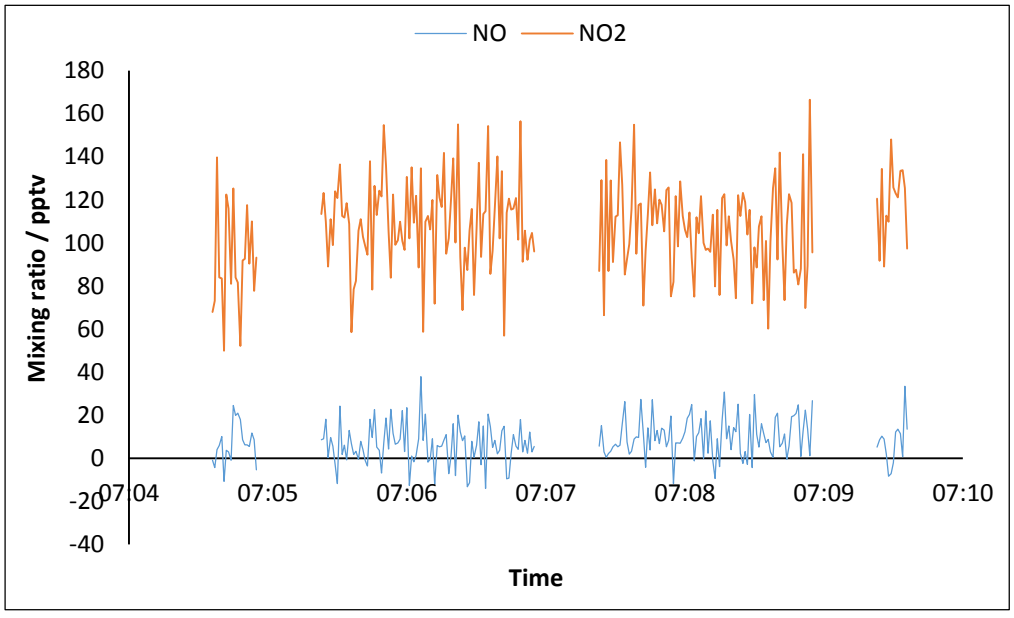

Figure 2.17: Sample artefact data from the P-CL instrument

The average artefact of the NO and NO_2 channel is approximately 8 pptv and 107 pptv, respectively. At such low mixing ratios, these artefacts can be considered insignificant when looking at NO_x levels in the ppbv range, such as those observed in the oil and gas flight plumes. However, the artefact does need to be taken into account when measuring the low level NO_x, such as during background data analysis. These artefacts would then be more

comparable to the low NO_x mixing ratios measured in the background air (see section 4.3), hence meaning they would be a far more prominent aspect of the error analysis associated with this low level data.

Precision

The precision of the measurements made by the instrument is assessed by looking at the variation in NO and NO_2 mixing ratios when the NO_x trap is attached to the inlet, i.e. when the instrument is theoretically sampling "NO_x -free" air.

The data in the NO channel has a 2σ precision of 25.3 pptv, at a resolution of 1 Hz. The 2σ precision of the data in the NO_2 channel at the same resolution is 53.2 pptv. On averaging the data to a 10 second resolution, the 2σ precision of the NO and NO_2 channel is estimated to be 18.8 and 32.3 pptv, respectively. This observed enhancement in precision is a result of the coincidental improvement of the SNR that occurs when data is averaged up in such a way.

Total Error

The total error associated with the instrument and its measurements takes both the accuracy and precision errors into account. It is calculated by taking the root sum of squares of these errors. The total error is calculated at a range of mixing ratios, accounting for the range of atmospheric conditions which the instrument may be exposed to during airborne measurements.

The total accuracy error (i.e. the error associated with the instrument calibration) is calculated as being 4%. This comprises of; 1% error on the two mass flow controllers, 1% error on the NO standard mixing ratio and 1% error on the NO_2 conversion efficiency. For ease of comparison, the error is given in fractional form. This error is independent of the mixing ratio measured, so remains constant when the mixing ratio is altered. The total precision error is calculated by dividing the calculated precision by the mixing ratio in question and is again given as a fractional error.

Table 2.5: Total errors associated with 1 Hz NO data on the P-CL instrument (2σ precision: 25.3 pptv)

NO Mixing Ratio / pptv	Accuracy Error	Precision Error	Total Error
5000	0.04	0.00506	0.0403
2000	0.04	0.0127	0.0420
1000	0.04	0.0253	0.0473
500	0.04	0.0506	0.0645
100	0.04	0.253	0.256

Table 2.6: Total errors associated with 1 Hz NO_2 data on the P-CL instrument (2σ precision: 53.2 pptv)

NO_2 Mixing Ratio / pptv	Accuracy Error	Precision Error	Total Error
5000	0.04	0.0106	0.0414
2000	0.04	0.0266	0.0480
1000	0.04	0.0532	0.0666
500	0.04	0.106	0.114
100	0.04	0.532	0.533

Table 2.7: Total errors associated with 10 second NO data on the P-CL instrument (2σ precision: 18.8 pptv)

NO Mixing Ratio / pptv	Accuracy Error	Precision Error	Total Error
5000	0.04	0.00376	0.0402
2000	0.04	0.00939	0.0411
1000	0.04	0.019	0.0442
500	0.04	0.0376	0.0549
100	0.04	0.188	0.192

Table 2.8: Total errors associated with 10 second NO_2 data on the P-CL instrument (2σ precision: 32.3 pptv)

NO_2 Mixing Ratio / pptv	Accuracy Error	Precision Error	Total Error
5000	0.04	0.00646	0.0405
2000	0.04	0.0162	0.0431
1000	0.04	0.0323	0.0514
500	0.04	0.0646	0.0760
100	0.04	0.323	0.326

As can be seen in **Tables 2.5-2.8**, the precision error only becomes a more significant part of the total error at extremely low mixing ratios. The instrument was exposed to relatively high mixing ratios during the "Oil and Gas" flight campaign. This means that the precision error should not be considered as the main source of error when assessing the reliability of the data from these campaigns. It is the accuracy of the instrument calibration which makes a greater contribution to the overall uncertainty of the NO_x data.

2.2.4 Laboratory Testing of the Airborne P-CL Instrument

Conversion efficiency: the influence of ambient pressure

The P-CL instrument's use in airborne campaigns means that it is exposed to rapid and sometimes dramatic changes in ambient conditions, such as pressure, that come with changes in altitude. If the pressure is not controlled, the conversion efficiency of the instrument is affected. The residence time of the NO_x instrument is a function of pressure. A laboratory experiment was undertaken to evaluate the efficiency of the internal blue light converter at a range of pressures. The pressure was changed manually, ranging from 220 to 720 Torr, and the results of said experiment can be seen in **Table 2.9** and **Figure 2.18** below.

Table 2.9: Monitoring the conversion efficiency of the P-CL instrument with respect to pressure changes

Pressure / Torr	Residence time / s	Conversion efficiency / %
220	0.295	45
300	0.403	53.4
400	0.537	63.3
500	0.671	68.5
600	0.805	74.4
700	0.939	77
720	0.966	77.2

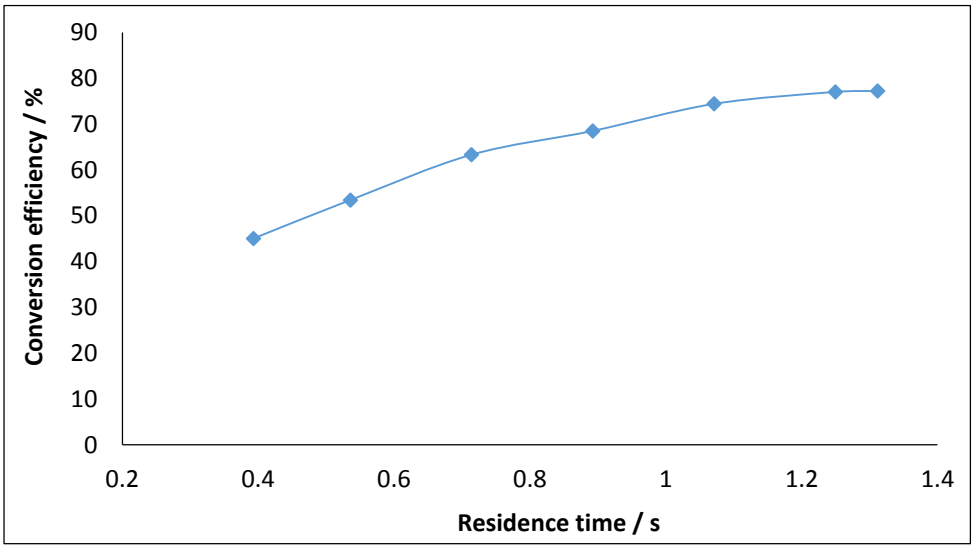

Figure 2.18: Monitoring the conversion efficiency of the P-CL instrument with respect to pressure changes

With a variation of approximately 30% across a range of pressures, the experiment confirmed the fact that the conversion efficiency changes with residence time (and hence pressure). This highlighted the importance of control the pressure at which the instrument operates.

Airborne measurements are taken at high resolution, typically 1 Hz (or 1 second), in order to match the timescale of atmospheric changes that take place. In order for the P-CL instrument to do this, the minimum residence time required is 1 second. As can be seen in **Table 2.9**, at the lowest pressure tested (220 Torr), the corresponding residence time was around 0.3 seconds. This means that a pressure of 220 Torr would be high enough to provide measurements with a resolution of 1 Hz.

During the flights, the photolysis pressure was kept constant using an internal pressure controller, at approximately 220 Torr. This is done to minimise the effects illustrated in **Figure 2.18**, thus ensuring that the conversion efficiency and the instrument as a whole, would not be affected. Altitude and pressure data obtained during test flight B903 are illustrated in **Figure 2.19** below indicating the stability of the instrument's internal pressure over a wide range of altitudes.

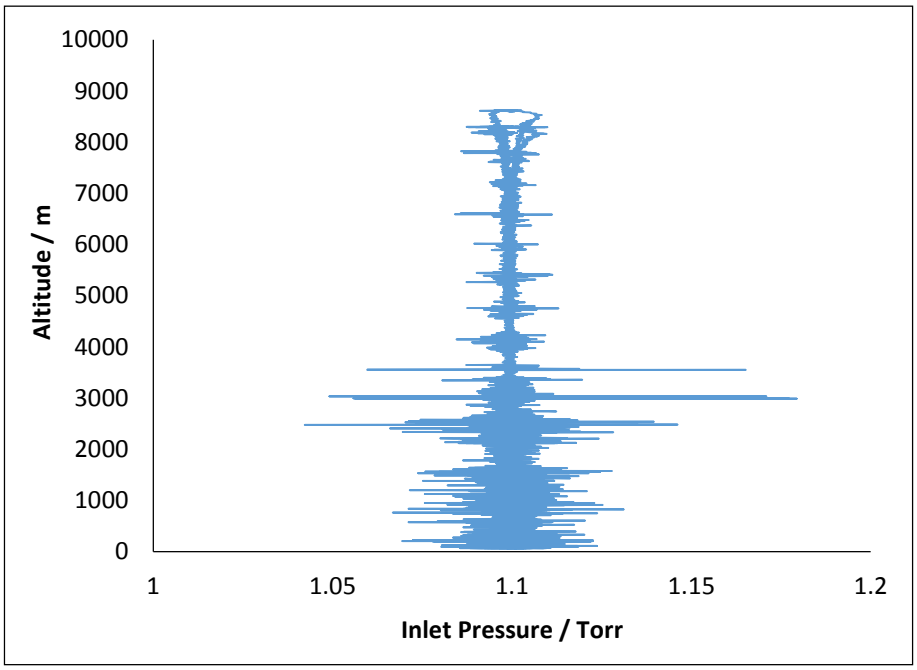

Figure 2.19: Variation of inlet pressure of the P-CL instrument with changes in altitude (test flight B903)

CHAPTER 3: MEASUREMENT OF NO_x IN THE REMOTE ATMOSPHERE – TD-LIF DEPLOYMENT AT THE CVAO

3.1 NO_x Measurements in the Remote Atmosphere

NO_x emissions in the remote boundary layer, such as the North Atlantic Ocean are very low, due to their location away from large emission sources (e.g. vehicular combustion and biomass burning). This consequently means that there are very few local emissions of NO_x in these areas.

The amount of NO_x directly transported to remote regions is also very low. Any primary NO_x is reacted away on a timescale of a few hours. This occurs through the oxidation of NO_2 by the hydroxyl radical, and the hydrolysis of N_2O_5 onto aerosol surfaces.[68,69] Instead, it is produced via the thermal decomposition of compounds such as PAN. PAN is a secondary pollutant which is produced in regions of high NO_x and volatile organic compound (VOC) mixing ratios. Its stability in the mid-troposphere means that it is capable of long-range transport, acting as a NO_x reservoir in the process. However, PAN thermally decomposes at altitudes below 7 km, releasing NO_x into the remote atmosphere.[19,20]

Regions such Cape Verde are extremely sensitive to any slight changes in atmospheric conditions, particularly in terms of O_3 production. This is a result of the measured mixing ratios of NO_x often being extremely close to what is known as the O_3 compensation point. This is the level of NO_x at which there is a switch from net destruction to net production of O_3. It is widely believed that this is found between 5 and 100 pptv NO_x,[10] with the actual compensation point depending on the time of year, the location in the troposphere and the mixing ratios of tropospheric O_3 and water vapour. The measurement of NO_x at the CVAO is well documented, with consistent of NO_x mixing ratios which lie within this crucial NO_x range.[10,70] As a result of this, only minimal increases in NO_x mixing ratios in remote areas like Cape Verde could lead to a significant amount of O_3 production in the marine boundary layer, and in turn, have wide-reaching impacts on the global background atmosphere.[71]

3.2 Site Description

The CVAO is located on the island of São Vicente in the Cape Verde archipelago, off the west coast of Africa. The site is part of the World Meteorological Organisation Global Atmosphere Watch (WMO-GAW) long-term monitoring network, which measures a comprehensive range of atmospheric species across the globe. (See http://www.wmo.int/pages/prog/arep/gaw/gaw_home_en.html for more information.)

The main objective of the measurements at the site is to improve understanding of the interactions which take place between the ocean and the air, through the monitoring of trends of important atmospheric species. The CVAO is situated in the North Atlantic Ocean, meaning that the majority of air masses observed at the site are well-processed within the marine boundary layer, with minimal influence from local pollution sources. The location of the site also means that a number of air masses of various origins are observed, with the atmospheric chemistry taking place in the surrounding marine atmosphere being significantly influenced by long-range transport.[70] There are four main areas of air mass origin: the Atlantic Ocean, continental Africa, coastal Africa and Europe. The influence of these air masses varies depending on the time of year, with continental Africa being the most dominant air mass in winter months and air masses of Atlantic or coastal African origin having the most influence during the spring and summer months.[10]

3.3 Objectives of Deployment

As discussed in chapter 1, existing standard NO_2 measurement techniques only measure NO_2 indirectly, by first converting it to NO. A common way of doing this is to use heated molybdenum catalysts, which reduce NO_2 to NO. However, there have been noted interferences from other NO_y species, which also thermally decompose to produce NO_2.[40,44] Photolytic converters have been shown to minimise these interferences, using narrow wavelength bands of radiation to specifically convert NO_2 to NO.[10,41,48] However, Reed et al. (2015)[50] recently investigated interferences in photolytic NO_2 measurements, using a BLC-equipped chemiluminescence instrument. A notable increase in NO_2 mixing ratio was reported in the photolysis cell in the presence of PAN, thus indicating that the decomposition of PAN could also be a potentially significant source of interference for photolytic

chemiluminescence instruments. Earlier studies had also noted an interference from PAN with photolytic converters.[42,72]

These interferences are likely to lead to an over-estimation of NO_2 mixing ratios, with the apparent "NO_2" signal actually representing a range of other reactive nitrogen species in the surrounding atmosphere. The use of direct NO_2 measurement techniques alleviates this issue, by exploiting spectroscopic features which are specific to NO_2. The laser induced fluorescence technique for example, is now a well-documented method for direct NO_2 quantification[32,34,37,38] and has been developed to ensure minimal interferences from other atmospheric species are observed. (See sections 1.3 and 2.1)

The TD-LIF instrument used in this study has provided reliable NO_2 measurements in a number of field campaigns.[18,32,38] However, prior to this study, the instrument had not been used to measure NO_2 in the remote boundary layer. A key requirement of the instrumentation used for atmospheric measurements is that it is able to perform just as well in remote locations, as well as in regions which experience high pollutant mixing ratios. The TD-LIF instrument was deployed at the CVAO in January 2015, in order to assess the performance of the instrument in terms of remote NO_2 measurements. The NO_2 data from the TD-LIF would then be compared to the steady state NO_2 mixing ratio, along with data from a chemiluminescence instrument, which takes long-term measurements of NO_2 (and NO) at the observatory. A detailed description of this instrument can be found in a paper by Lee et al. (2009).[10] This instrument measures higher NO_2 mixing ratios than expected at the CVAO. This means that there is scope for improving the reliability and accuracy of long-term measurements at the site, with the deployment of the TD-LIF being an attempt to do so. Configuration of the TD-LIF for NO measurements also took place, using the experimental set-up and reaction conditions that gave the maximum conversion efficiency in laboratory tests conducted in York.

3.4 NO-NO_2-O_3 Photo-stationary state

As discussed in chapter 1, the cycle involving NO, NO_2 and O_3 generally results in no net chemistry occurring, with the three species reaching a photo-stationary state after only a few minutes.[7] It is possible to predict the photo-stationary state mixing ratios of any one of these three species by using **Equation 3.1**.

$$\frac{[NO] \text{ x } [O_3]}{[NO_2]} = \frac{J_2}{k_1}$$ ***Equation 3.1***

Where:

J_2 = rate of NO_2 photolysis (1 x 10^{-2} s^{-1})*

k_1 = rate coefficient for the reaction of NO with O_3 (1.90 x 10^{-4} molecules cm^{-3} s^{-1})[73]

[NO] = number density of NO (molecules cm^{-3})

$[O_3]$ = number density of O_3 (molecules cm^{-3})

$[NO_2]$ = number density of NO_2 (molecules cm^{-3})

*measured by a spectral radiometer[74]

At the CVAO, there is a chemiluminescence NO_x analyser which is used to take long-term measurements of NO and NO_2. A steady state calculation can be done to determine the mixing ratio of NO_2 expected at the CVAO, which will give an indication as to how accurately the chemiluminescence analyser is measuring NO_2. This is done by looking at **Equation 3.1** in more detail.

The photo-stationary state equation is rearranged in terms of the NO_2 mixing ratio.

$$[NO_2] = \frac{k_1 \text{ x } [O_3] \text{x } [NO]}{J_2}$$ ***Equation 3.2***

The mixing ratios of NO and O_3 used in subsequent calculations refer to those measured at CVAO in January 2007, at 33.4 and 4.5 pptv, with respect to O_3 and NO.[10]

The NO and O_3 mixing ratios were converted to number densities, and could be substituted into **Equation 3.2**, along with the kinetic constants, to derive the NO_2 number density.

$$[NO_2] = \frac{(1.90 \text{ x } 10^{-14} \text{ molecules cm}^{-3}\text{s}^{-1}) \text{ x } (8.23 \text{ x } 10^{11} \text{ molecules cm}^{-3}) \text{ x } (1.11 \text{ x } 10^{8} \text{ molecules cm}^{-3})}{1 \text{ x } 10^{-2} \text{ s}^{-1}}$$

$$= 1.74 \text{ x } 10^{8} \text{ molecules cm}^{-3}$$ ***Equation 3.3***

In order to convert the NO_2 number density back into a mixing ratio (for direct comparisons with 2015 measurements of the same units), the number of air molecules in 1 cm^3 of air must be calculated. This is done using a form of the ideal gas equation.

$$PV = Nk_BT \qquad \textit{Equation 3.4}$$

Where:

P = pressure (Pa)

V = volume (m^3)

N = number of molecules

k_B = Boltzmann constant (1.381 x 10^{-23} J K^{-1})

T = temperature (K)

Equation 3.4 is then rearranged in terms of the number of molecules (i.e. "N").

$$N = \frac{PV}{k_BT} = \frac{(10^5 \text{ Pa}) \text{ x } (10^{-6} \text{ m}^3)}{(1.381 \text{ x } 10^{-23} \text{ J K}^{-1}) \text{x } (298 \text{ K})} = 2.43 \text{ x } 10^{19} \text{ air molecules} \qquad \textit{Equation 3.5}$$

In order to calculate an NO_2 mixing ratio, in pptv, the number density of NO_2 is divided by the number of air molecules in 1 cm^3 of air and multiplied by 1 trillion (1 x 10^{12}).

$$NO_2 \text{ mixing ratio} = \frac{1.74 \text{ x } 10^8 \text{ molecules cm}^{-3} \text{ NO}_2}{2.43 \text{ x } 10^{19} \text{ molecules cm}^{-3} \text{ air}} \text{ x } (1 \text{ x } 10^{12})$$

$$= 7.16 \text{ pptv} \qquad \textit{Equation 3.6}$$

This means that the theoretical average daytime NO_2 mixing ratio at the CVAO in January 2007 is 7.6 pptv. The mean daytime NO_2 mixing ratio measured by the chemiluminescence instrument, however, is approximately 6 times higher than this, at 42.4 pptv.[10] This finding in itself is unsurprising, as several studies have reported a significant imbalance between the measured NO_2 and that expected from steady state calculations, particularly in low- NO_x environments.[75,76,77]

This has led to a number of hypotheses regarding the cause of this "gap" between theoretical and measured NO_2 mixing ratios in the remote environment. One suggestion is that there is some sort of "mystery", unmeasured oxidant which is reacting with NO to create NO_2.[78] Hosaynali Beygi et al. (2001)[76] found that the NO_2/NO ratio in the southern Atlantic Ocean was around a factor of seven higher that what would be predicted by the Leighton relationship (i.e. the steady state calculation).

The supporting measurements of other atmospheric species such as O_3, carbon monoxide and RO_2 radicals, proved to by typical of the surrounding atmosphere. The authors therefore attributed the discrepancy to an unknown oxidant, which selectively converts NO to NO_2.

Another postulation surrounding the over-estimation of NO_2 measurements in remote environments is that there are species in the atmosphere which, although only being present in trace quantities, are reacting with NO to produce NO_2. Several studies have suggested that the species in question are halogen oxides.[79] For example, Bauguitte et al. (2012),[75] reported a significant discrepancy between observed and calculated NO_2/NO ratios. However, the reaction of the halogen oxides with NO was shown to have an impact on the NO_2/NO ratios. When the halogen oxides were included in the steady state calculations, the agreement with the observations vastly improved. This suggested that the halogen oxides were reacting with NO to produce NO_2, thus resulting in increased the NO_2/NO ratios that were previously unaccounted for in the steady state calculation.

The LIF instrument was deployed at the CVAO to provide a direct, interference free method of NO_2 detection in order to confirm the high NO_2 observed with the chemluminescence instrument. This would also provide an insight into its suitability for NO_2 measurements in a remote atmospheric environment.

3.5 Results and Discussion

3.5.1 NO_2 Measurements at CVAO: January 2015

The raw 1 Hz NO_2 data was converted into a mixing ratio using the background counts and sensitivities associated with the instrument channel. (See section 2.1.1 for the procedure.) These values were likely to change over the course of the campaign for a number of reasons, an important factor to consider when looking at the worked up NO_2 mixing ratios from the instrument.

The NO_2 data (using the NO_2 channel only) from the LIF instrument measured during the deployment is shown in **Figure 3.1**, along with the NO_2 mixing ratios as measured by the chemiluminescence analyser at the site. The chemiluminescence instrument was only operating intermittently during the time of the campaign, hence why its time series is much shorter in comparison that of the LIF.

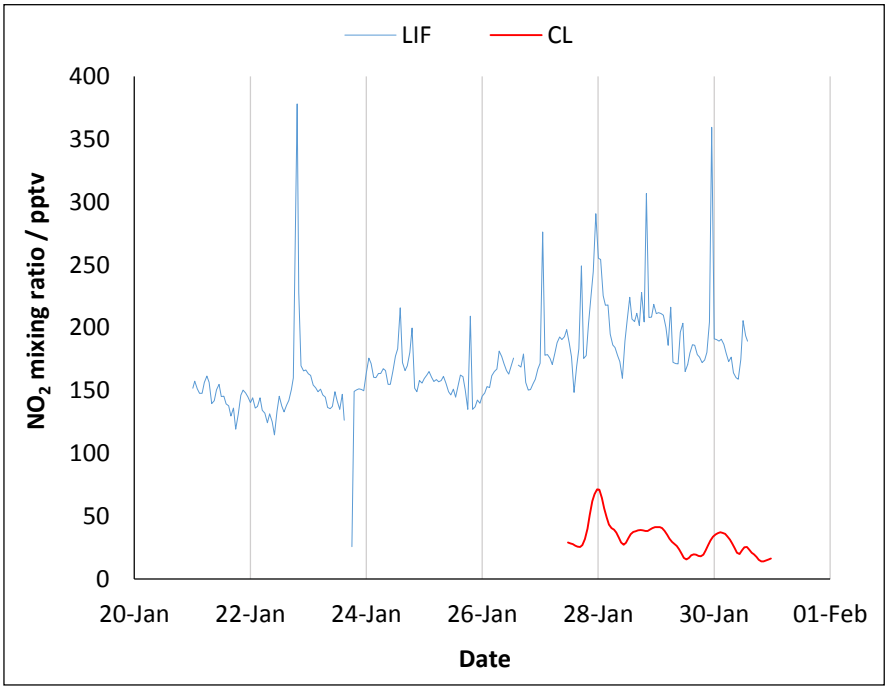

Figure 3.1: LIF and CL measurements of NO_2 at CVAO in January 2015 (LIF = laser induced fluorescence instrument, CL = chemiluminescence instrument. The vertical gridlines correspond to midnight of each day)

Table 3.1: Average NO_2 mixing ratios measured at CVAO in January 2007 and January 2015[a]

	Average Daytime NO_2 (pptv)	Average Night time NO_2 (pptv)
LIF	167.6	179.9
CL	25.7	40.5
CL (2007)[10]	42.4	35.8

[a]Daytime data refers to data between 11:00 and 15:00, and night time data refers to data between 20:00 and 04:00

As can be seen in **Table 3.1**, the average daytime and night-time NO_2 mixing ratios measured by the TD-LIF were both found to be nearly 7.5 and 4.5 times higher than the measurements taken by the chemiluminescence analyser, respectively. The substantial "gap" between the LIF and chemiluminescence instrument can be clearly seen on **Figure 3.1**, showing a significant over-estimation of NO_2 by the LIF instrument. This over-estimation can be confirmed through comparison of CVAO NO_2 data measured by the chemiluminescence instrument in January 2007 (also shown in **Table 3.1**).[10] The average daytime mixing ratio of NO_2 was found to be 42.4 pptv, which is only approximately 20 pptv higher than that which was measured in the same month of 2015. This illustrates that the chemiluminescence data in 2015 is consistent with other years. The daytime NO_2 measurements from both the LIF and chemiluminescence instruments are much higher than the expected steady state mixing ratio of 7.6 pptv. As discussed previously, this is a common observation for NO_2 measurements in the remote troposphere, even for the standard measurement techniques, such as chemiluminescence. However, at nearly 20 times higher than the steady state mixing ratio, and nearly 8 times higher than the chemiluminescence data, the NO_2 mixing ratios measured by the LIF instrument are extremely unlikely to be truly representative of the air sampled at the CVAO.

3.5.2 Instrument Performance

Before one can give a possible explanation behind this poor performance of the TD-LIF, it is first important to refer back to the instrument's performance prior to deployment at the

CVAO. The instrument was run in the laboratory at the University of York in order to run various experiments, and to assess the performance of the instrument in a polluted atmospheric environment. Whilst there, several calibrations per day were conducted, in order to get a stable background and sensitivity for all of the instrument channels. The sensitivity of the NO_2 channel stabilised at approximately 180 c/s/ppbv (the sensitivities of the other three instrument channels can be seen in section 2.1.5) Confidence in the instrument's data was provided by the comparison to the AQD chemiluminescence NO_x analyser in the same laboratory, which showed very similar mixing ratios that were representative of the surrounding area. (see section 2.1.5).

The TD-LIF was then deployed at the CVAO and the calibrations were conducted in exactly the same manner as in York, running several per day to ensure stable calibration data. However, a clear decline in the NO_2 channel sensitivity was observed, dropping from by 80 c/s/ppbv from 180 down to 100 c/s/ppbv. Looking at **Figure 3.1** and **Table 3.1**, one can see that the chemiuminescence analyser and the TD-LIF data are not comparable, with the only noticeable difference being the sensitivity of the instrument. However, the sensitivity is dependent on a number of factors, meaning that it is not sufficient to directly link it to the poor performance of the instrument. As discussed in section 2.1.2 the sensitivity is a function of the collection efficiency. This depends on both the quality of the optics in the instrument and on the quality of the PMT detector. The optics play a crucial role as these collect the fluorescence photons, i.e. the fluorescence signal. The laser alignment therefore has to be as good as possible, as this determines how much of the laser light passes through each detection cell. However, such a large over-estimation of the NO_2 mixing ratios by the LIF are unlikely to be due solely to the mis-alignment of the laser, particularly due to the fact that the data measured came from the first detection cell of the instrument (i.e. the NO_2 cell). As described and illustrated in section 2.1.1, this cell is in the closest proximity to the light source, with only two reflective mirrors between the two instrument components, thus meaning the laser power entering the would have been near-optimal. Therefore, slight mis-alignment of the laser would only be likely to result in a minimal over-estimation of NO_2 by the detection cell.

The high mixing ratios of NO_2 observed by the LIF must have therefore been due to a leak within the system. Looking at the configuration of the instrument, the components most likely to be prone to leaks would be the connection between the inlet line and the inlet box and the connection between the NO_2 inlet and the LIF instrument itself. Should either of

these experience leaks, the NO_2 detected by the instrument would be representative of not only the ambient air, but also the air within the laboratory. Although such leaks could not be found during the deployment, these could provide an explanation as to why such elevated NO_2 mixing ratios were measured by the instrument.

NO Measurements

The LIF instrument was set up for NO measurements at the CVAO using the GPT configuration described in section 2.1.6. A standard synthetic air cylinder (BTCA cylinder, 5 ppmv, certified by BOC) was used as a constant supply of air for the O_3 source, i.e. the multi-gas calibrator. Although only running at a pressure of around 2 bar for the NO measurements, the cylinder was also used as the zero air supply for the instrument calibrations. These calibrations were critical to the operation of the instrument and required zero air at a pressure of 4 bar, in order to completely flush all instrument channels. As discussed earlier in the chapter, the comparison of NO_2 data from the LIF and the chemiluminescence instrument indicated a substantial over-estimation of NO_2 mixing ratios by the LIF, which was believed to be due to some kind of leak within the instrument. This would have impacted on any other measurements made by the instrument. Therefore, for the sake of conserving the synthetic air cylinder for the instrument calibrations, it was considered more viable to use the instrument solely for NO_2 measurements, whilst the cause of the instrument's poor sensitivity was determined.

Concluding Remarks

The TD-LIF instrument showed promising results when used to measure NO_2 levels in a polluted atmospheric environment (i.e. at the University of York). However, over-estimation of NO_2 levels at the remote monitoring site of the CVAO was observed, with average mixing ratios being orders of magnitude higher than both the chemiluminescence analyser and the expected steady state mixing ratio. This has led to the conclusion that the sensitivity of the instrument is likely to have been over-estimated. It is thought that there may have been some disruption to the instrument's configuration, or leaks within the system, which has caused the decline in sensitivity. This means that it would not be a viable instrument for long-term NO_2 measurements at the CVAO in its current configuration.

CHAPTER 4: AIRBORNE NO_x MEASUREMENTS IN A POLLUTED ATMOSPHERE – THE "OIL & GAS" CAMPAIGN (SUMMER 2015)

4.1 Atmospheric Emissions from Oil and Gas Rigs

The oil and gas industry supplies the UK with more than 70% of its total primary energy, with oil meeting 97% of the country's transport sector demand and gas being a key fuel for heating and electricity generation.[80] The industry also has substantial economic benefits, supporting over 400,000 jobs and being the country's largest industrial investor, paying around £4.7 billion in production tax in 2013/14.[80]

However, the processes involved in the industry, namely extraction, stabilisation and export of hydrocarbons have substantial atmospheric emissions associated with them. The continued operation of the offshore oil and gas platforms also release gases through activities such as combustion, gas flaring and tank loading. The gases emitted by these processes are given in **Table 4.1**.

Table 4.1: Gases emitted by oil and gas platforms

Processes	Gases released
Fuel combustion and gas flaring	• Carbon dioxide (CO_2) • Carbon monoxide (CO) • Methane (CH_4) • Nitrogen oxides (NO_x) • Sulphur oxides (SO_x) • Nitrous oxide (N_2O)
Tank loading	• Volatile organic compounds (VOCs) • Methane (CH_4)
Refrigeration and firefighting	• Chlorofluorocarbons (CFCs)

As can be seen in **Table 4.1**, the oil and gas platforms release a range of gases into the surrounding atmosphere. According to Oil and Gas UK, the largest emission from the platforms in the UK is CO_2, with a 2014 document by the industry reporting the production of around 14 million tonnes of CO_2 in 2013.[81]

Many oil and gas platforms, particularly in the North Sea, are often manned, hence meaning that they require a large amount of power generation through fuel combustion. As **Table 4.1** shows, this process leads to the production and subsequent release of a number of gases, including NO_x. In order to allow them to operate continuously, these rigs often require support vessels which also produce NO_x through fuel combustion. As result, although the NO_x produced by the platforms is relatively small when compared to CO_2 (45,000 tonnes produced in 2013)[81], their operation involves continuous processes that can potentially emit substantial amounts of NO_x into an environment which is otherwise relatively clean.

Although the oil and gas industry is known to have many benefits in terms of meeting the UK's energy demands and economy, these substantial atmospheric emissions could have a number of impacts on the environment on a regional, even global scale. The emission of potent greenhouse gases, such as CO_2 and CH_4 through fuel combustion contributes to global warming, due to their stability in the atmosphere and subsequent long atmospheric lifetimes (5-200 and 12 years, respectively).[82] The reaction between VOCs and NO_x also has implications for tropospheric O_3 formation. This has knock-on effects for the oxidative capacity of the atmosphere through the role of O_3 as a precursor for OH radical formation,[8] and as a strong oxidising agent in itself. The OH radical is one of the most powerful oxidising agent in the atmosphere, controlling the lifetime of many potent greenhouse gases such as methane,[83,84] meaning that tropospheric O_3 also has an indirect impact on the earth's radiative balance. As well as the atmosphere, tropospheric O_3 also has adverse impacts on human health, vegetation and crop yield through oxidative damage it causes.[9] The acidic gases, NO_x and SO_x, can also cause damage to ecosystems through acidification and eutrophication.[11,12]

4.1.1 Oil and Gas Emissions in the North Sea

The North Sea oil and gas fields now constitute the world's most active drilling region, with around 173 rigs drilling. The sheer scale of the oil and gas industry, particularly in the North Sea is shown in **Figure 4.1**, which shows the number of operational rigs around the UK. The majority of rigs in the southern sector of the North Sea are gas rigs, whilst most in the northern sector are oil rigs.

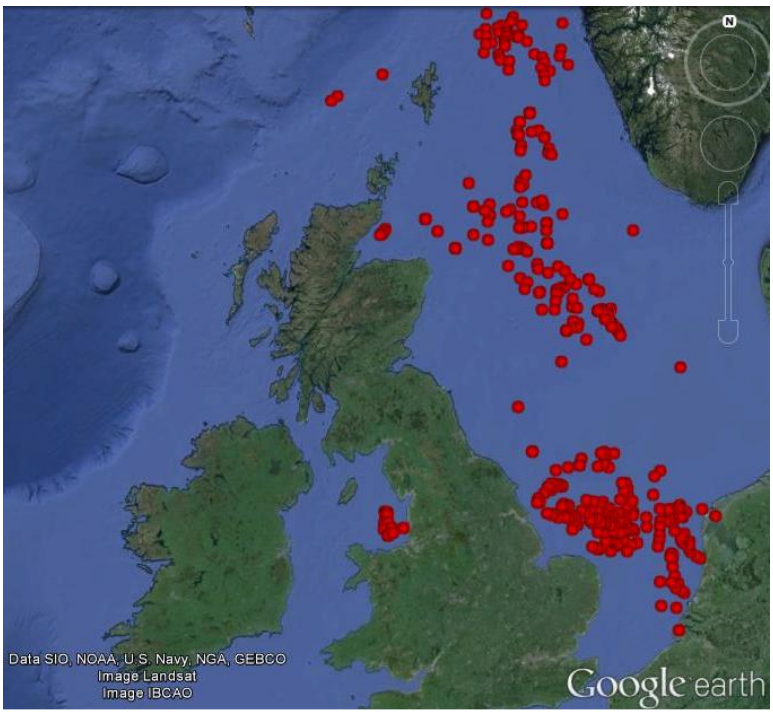

Figure 4.1: Operational oil and gas platforms around the UK. Each symbol represents a platform

The oil drilled from the North Sea rigs is a mixture of hydrocarbons, comprising liquid petroleum and natural gas, which originate from the extensive petroleum reservoirs beneath the sea bed. This high activity means that the North Sea is a hive of emissions, which results in there being a huge amount of potential for wide-reaching atmospheric impacts. For example, the production of NO_x in the North Sea could lead to surplus ground-level ozone formation in places such as Scandanavia, through its transportation by long-lived reservoir species (e.g. PAN) on a regional scale.

As a result, legislation is in place, which has a tight control of offshore chemical discharges and atmospheric emissions. Examples of such legislation are the "Carbon Reduction Commitment" (CRC), the "EU Emissions Trading Scheme" and the "Prevention and Control

of Pollution" (PPC). It is therefore essential that emissions inventories are as accurate as possible, as these provide estimates for current and likely future emissions from particular sources.

4.2 Oil and Gas Rig Emissions in the North Sea: the "Oil and Gas" Campaign

During the summer of 2015, a series of survey flights took place over operational oil and gas fields in the North Sea, on the UK's FAAM BAe-146 research aircraft. A range of measurements were made during the campaign, which are listed in **Table 4.2**. The airborne photolytic chemiluminescence analyser, described in section 2.2, was used to measure NO_x emissions during the flights. The aim of the campaign was to fly downwind of active oil fields, taking measurements in the plumes from oil and gas rigs. The direct integration method would then be used for one of these flights, which would target specific rigs and calculate the average emissions produced by each rig, in tons per year, which would then be compared to the respective estimates from the NAEI.

The NAEI comprises the Greenhouse Gas Inventory (GHGI) and the Air Quality Pollutant Inventory (AQPI). The inventory is maintained by Ricardo-AEA and is funded by Department of Energy and Climate Change (DECC), the Department for Environment, Food and Rural Affairs (DEFRA), the Scottish and Welsh governments, along with the Department of Environment in Northern Ireland. The NAEI estimates annual emissions of a number of air pollutants, most of which date back to 1970. In order to compile these inventories, information from a wide range of sources is collected. These sources can range in scale, from individual point sources such as power plants, to national energy statistics. Inventory data is used in a number of applications which rely on them being as accurate as possible. The estimates provide information about the sources and trends in emissions of greenhouse gases and other air pollutants, which can have adverse effects on human health and the natural environment. This, in turn means that the appropriate air quality reduction policies can be implemented. The data can be used to track the UK's progress towards international legislation targets for both regional air pollution and climate change. This would then bring the importance of improving the local, national and global environment to light.

Although several species were measured during the campaign, this thesis chapter will focus solely on NO_x emissions from the rigs, as these are point sources within the NAEI, thus meaning that the measurements taken in plumes from individual rigs can be used to assess the accuracy of these estimates.

Table 4.2: Instruments and measurements made on the BAe 146 (FAAM) aircraft during the "Oil and Gas" campaign

Species / parameter	Method / instrument details	Averaging time	Precision, accuracy	Affiliation, reference
Position, winds, u, v, w	INS, GPS, 5-port turbulence probe	0.1 s	0.01 $\Delta P/P_S$	• FAAM • Peterson and Renfrew (2009)[85]
Humidity (Dew point Temperature)	Hygrometer, General Eastern 1011b	0.25 s	± 0.5 - ± 3 K dependent on dew point and ambient conditions	• FAAM • Ström et al. (1994)[86]
Temperature	Rosemount Aerospace Ltd. sensor 102 AL	0.05 s	± 0.3K	• FAAM, • Lenschow (1986)[87]
CO	VUV resonance / fluorescence, Aerolaser 5002	1 s	1 ppbv, 3%	• FAAM. • Gerbig et al. (1999)[88]
O_3	UV absorption, TEI 49C	4 s	1 ppbv, ±5%	• FAAM • Wilson and Birks (2006)[89]
CO_2, CH_4	Cavity enhanced absorption spectrometer, Los Gatos Research Inc	1 s	2.5 ppbv for CH_4 and 0.5 ppmv for CO_2	• FAAM / University of Manchester, • O'Shea et al. (2013)[90]
NO, NO_2	Chemiluminescence with photolytic conversion for NO_2, Air Quality Design Inc.	10 s	5 pptv for NO and 15 pptv for NO_2 (10 s averaging)	• FAAM / University of York • Lee et al. (2009)[10]
NMHCs (Whole air samples (WAS)): (C^1-C^7 NMHCs (alkanes, alkenes, aromatics); small o-VOCs (acetone, methanol, acetaldehyde, ethanol); DMS	GC-FID (flame ionization detector), Perkin Elmer	30 s fill time for WAS	Species dependent, typically 5 pptv	• University of York • Hopkins et al. (2003)[91]
Cloud physics	CDP (Cloud Droplet Probe)	1 s		• FAAM • Rosenberg et al., (2012)[92]

4.2.1 Flight Tracks

Flights took place in both the northern and southern sectors of the North Sea. Both of these sectors are home to a high density of operational platforms, (see **Figure 4.1**). This therefore means that flying in these active areas would provide a great deal of insight into the atmospheric impacts of oil and gas platforms in the North Sea.

Southern Sector of the North Sea: Flights B907, B908, B910 and B912

Four survey flights took place over the southern sector of the North Sea, each of which involved conducting cross wind legs downwind of the oil fields at 152 metres. These legs were then repeated, this time at an altitude of 305 metres. These were done in order to establish the vertical extent of the emission plumes resulting from the oil platforms in this sector of the North Sea. The route of the four flights are shown in **Figures 4.2-4.5**. The plots are coloured by altitude, which was measured throughout the duration of the flights using the aircraft radar altimeter.

Flight B907: 13th May 2015

Figure 4.2: Route flown during flight B907

Flight B908: 20th May 2015

Testing of the newly turbulence probe took place during this flight, which are represented by the high altitude flight loops on **Figure 4.3** below.

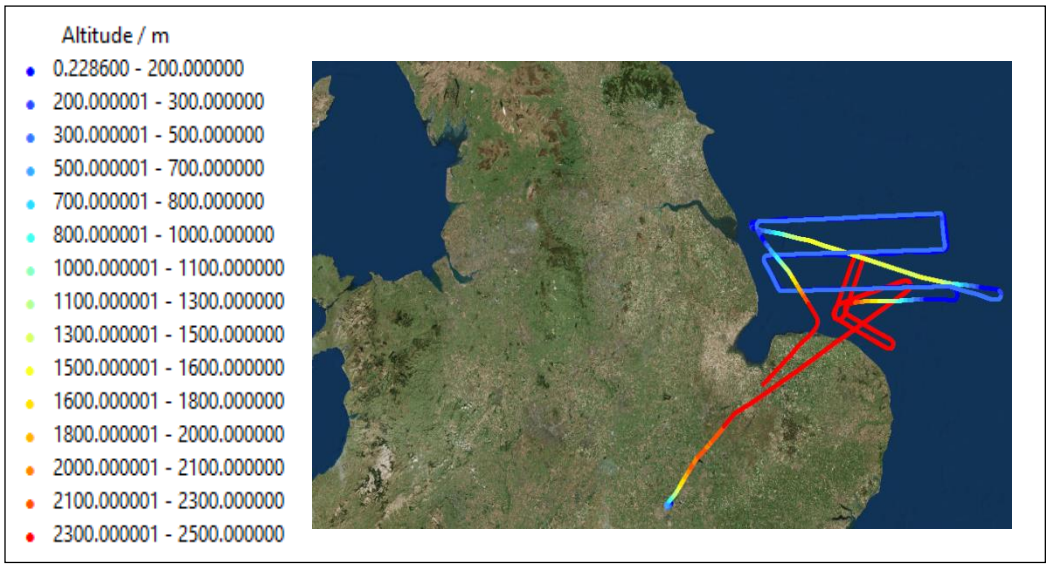

Figure 4.3: Route flown during flight B908

Flight B910: 26th May 2015

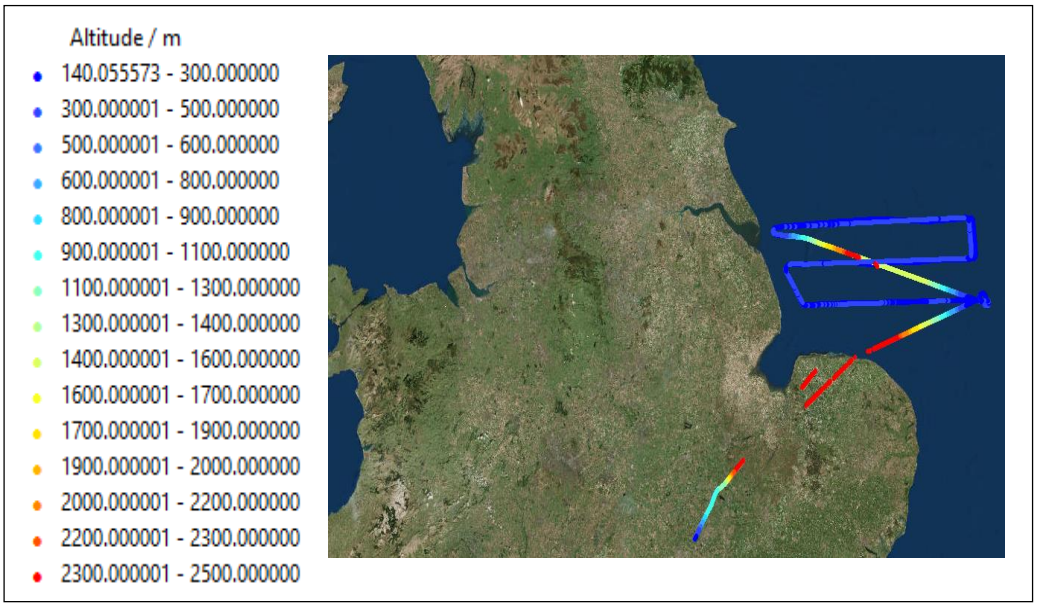

Figure 4.4: Route flown during flight B910

Flight B912: 9th June 2015

During this flight, a circuit around the Vale of Pickering was conducted, in order to collaborate with ground-based measurements over the same time period. This is represented by the low altitude circuit to the north of the Humber estuary, illustrated in **Figure 4.5** below.

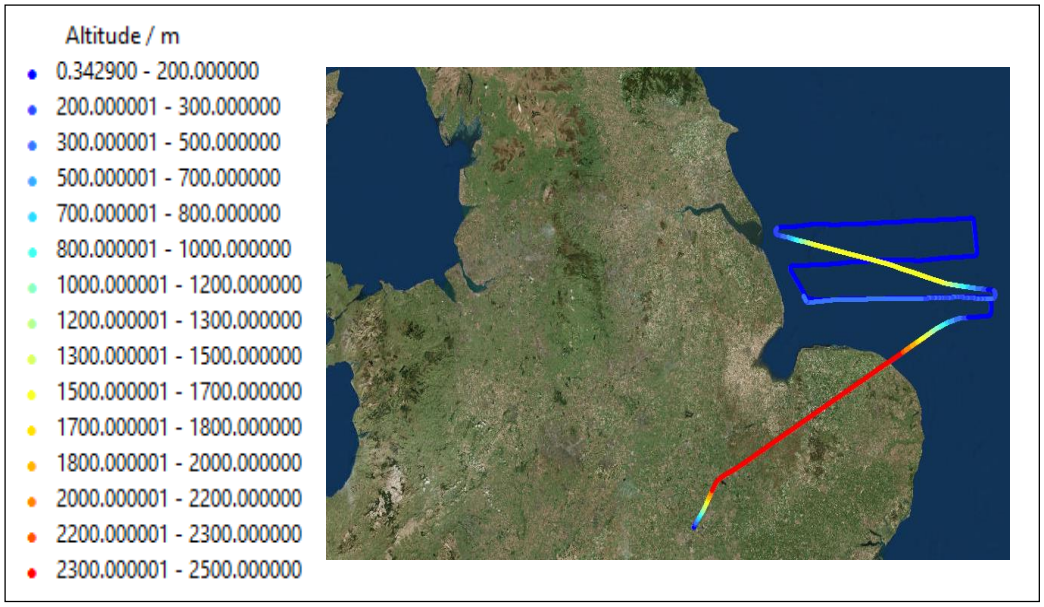

Figure 4.5: Route flown during flight B912

Northern Sector of the North Sea: Flights B913 and B918

Two survey flights around the northern sector of the North Sea. As with the southern sector flights, cross wind legs were conducted at different altitudes, downwind of the rigs in the area.

Flight B913: 23rd June 2015

During this flight, cross wind legs were conducted at an altitude of 152.4 metres, followed by 304.8 metres, as with the southern sector flights. It also included a circuit over the vale of Pickering, in order to coincide with ground-based measurements.

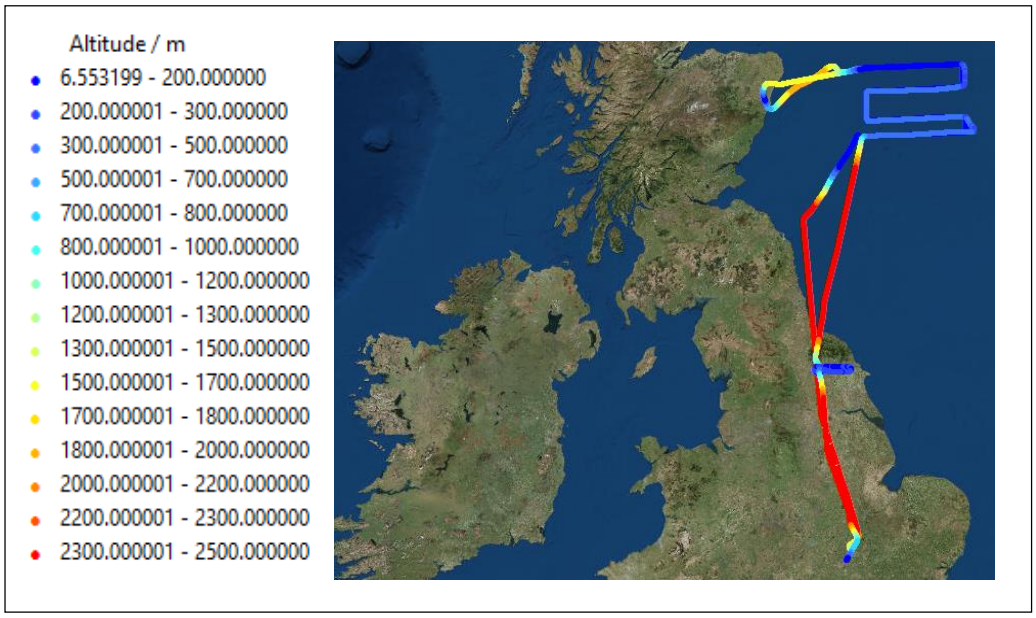

Figure 4.6: Route flown during flight B913

Flight B918: 23rd July 2015

The objective of this survey flight differed from the others in the campaign. In this case, a specific set of rigs in the northern sector of the North Sea were selected, namely the Forties and Nelson rigs (circled in **Figure 4.8**). The aim of the flight was to sample gas plumes from these rigs. This would be achieved by first sampling upwind, followed by conducting multi altitude cross wind legs downwind, thus flying through the gas plumes of each of the targeted rigs several times. The emissions from each rig could then be calculated using the

direct integration method (section 4.4). Flying altitudes ranged from 31 metres to 457 metres. This would give an indication as to the vertical extent of the gas plume. The flight also involved a circuit around the Vale of Pickering to repeat earlier flights.

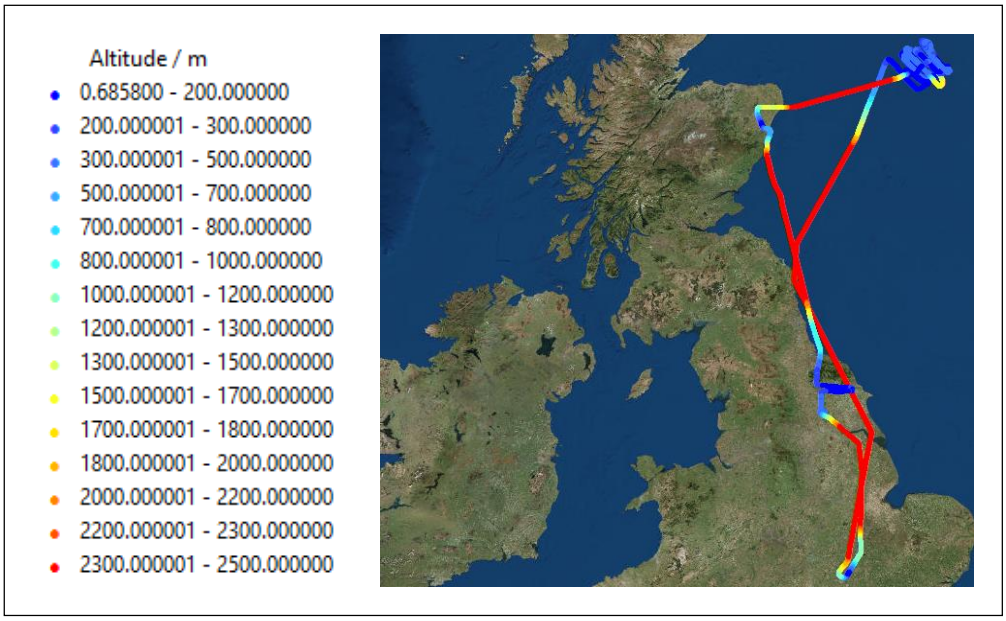

Figure 4.7: Route flown during flight B918

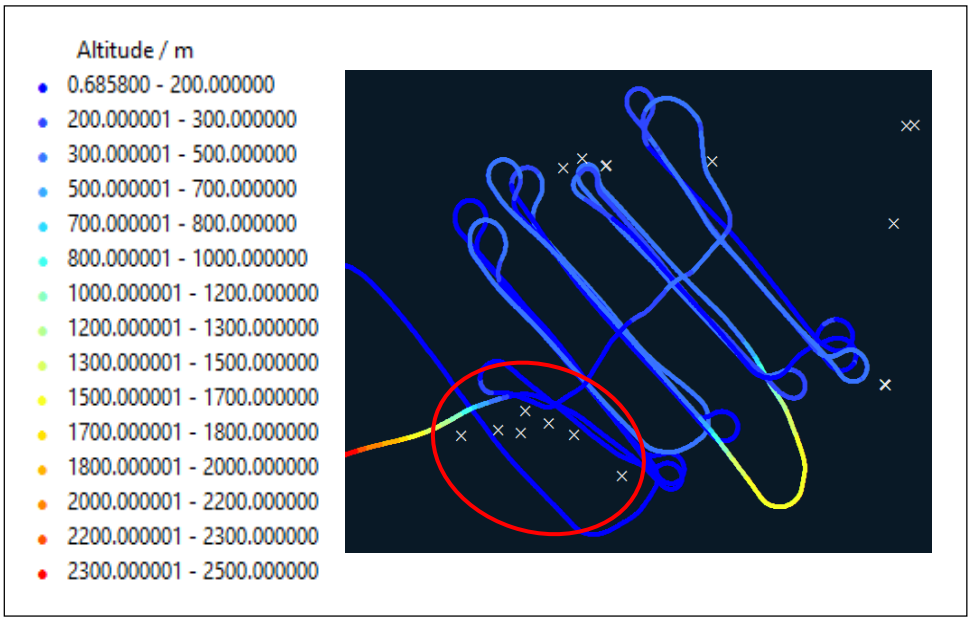

Figure 4.8: Location of Forties and Nelson rigs

4.2.2 NO_x Emissions from North Sea Rigs

Determination of Surface Layer Height

As previously discussed, a substantial amount of NO_x is emitted from oil and gas platforms, predominantly from power generation processes (namely gas or diesel consumption). In order to quantify these emissions as accurately as possible, it is first necessary to determine the altitude below which the emissions are trapped. In most cases, this is what is known as the boundary layer height. This boundary layer is the lower part of the atmosphere, and is between 1 and 2 kilometres deep. It is characterised by large amounts of turbulence, which, in turn means that the air within this layer is well mixed. Within the boundary layer, a normal temperature profile is observed, with warm air rising into cooler air. A common result of such a convective layer is cloud formation, with condensation occurring as the warm air rises and cools. However, the layer at the very top of the boundary layer is what is known as an inversion, or "capping" layer, where the normal temperature profile is reversed, and the dense, cold air now sits below the warm air. As a result of this inversion, cloud formation is capped, thus forming a barrier and trapping air and pollution below it to within the boundary layer.

However, the boundary layer height was not considered to be particularly important when sampling very close to the oil and gas platforms. This would only be relevant if the flights had been much further downwind of the rigs, the NO_x would have been well mixed in the boundary layer. Instead, the surface layer height was used. The surface layer is the lowest part of the boundary layer (typically the bottom 10%). As a result, the composition of this layer, along with its turbulence characteristics, are directly influenced by contact with the earth's surface. As with the top of the boundary layer, the upper limit of the surface layer is characterised by a temperature, or "capping" inversion, thus often resulting in cloud formation and trapping of pollutants below this height. During the campaign, therefore, the cloud layer base was assumed to be the upper limit of the surface layer, as this would be where the gas plume close to the rigs would be trapped. The surface layer height was estimated from the potential temperature, dew point temperature and relative humidity vertical profiles associated with each flight. These profiles indicated a relatively consistent surface layer height of around 300 metres. The NO_x data was therefore filtered for a surface layer height of 300 metres and below, thus ensuring that the NO_x mixing ratios would be confined to this altitude. A detailed explanation as to how the surface layer height is inferred

from the potential temperature and humidity profiles is given in section 4.4, whereby this height is used to derive NO_x emissions in the direct integration method.

NO_x Plumes from Rigs in the Southern Sector of the North Sea

Flight B907

As with all southern sector flights, flight B907 involved conducting cross wind legs at altitudes of 152 metres and 305 metres, downwind of operational rigs. It should be noted that the flights were planned on days when either southerly or northerly winds dominated. This would then make it possible to measure direct emissions from rigs, as these would travel downwind, towards the flight path.

The surface layer NO_x mixing ratios measured during these flight legs are illustrated using flight track plots which are shown below. White crosses are used to indicate the location of the operational rigs with respect to the flight track. The orange lines coming from the flight track are also shown on the map. These represent the dominant wind direction measured during the flight. As can be seen on the flight track plots (**Figure 4.9** and **Figure 4.10**), the wind came predominantly from the north-west, with an averaged direction of 330° and speed of 4 metres per second over the course of the flight, making it possible to measure the gas plumes from the oil and gas rigs.

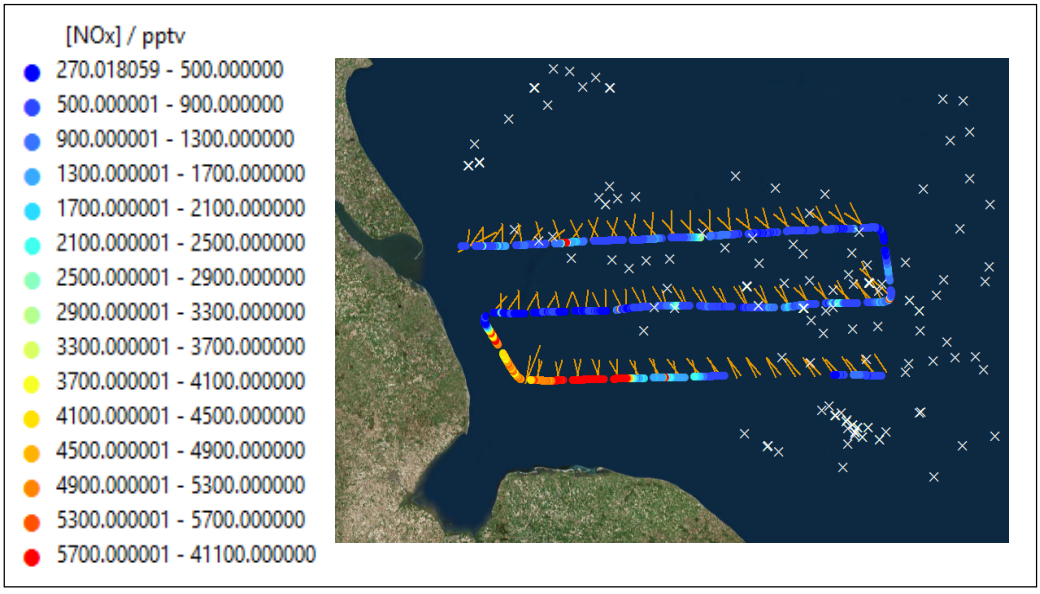

Figure 4.9: B907 NO_x mixing ratios during the flight legs conducted at 152 metres

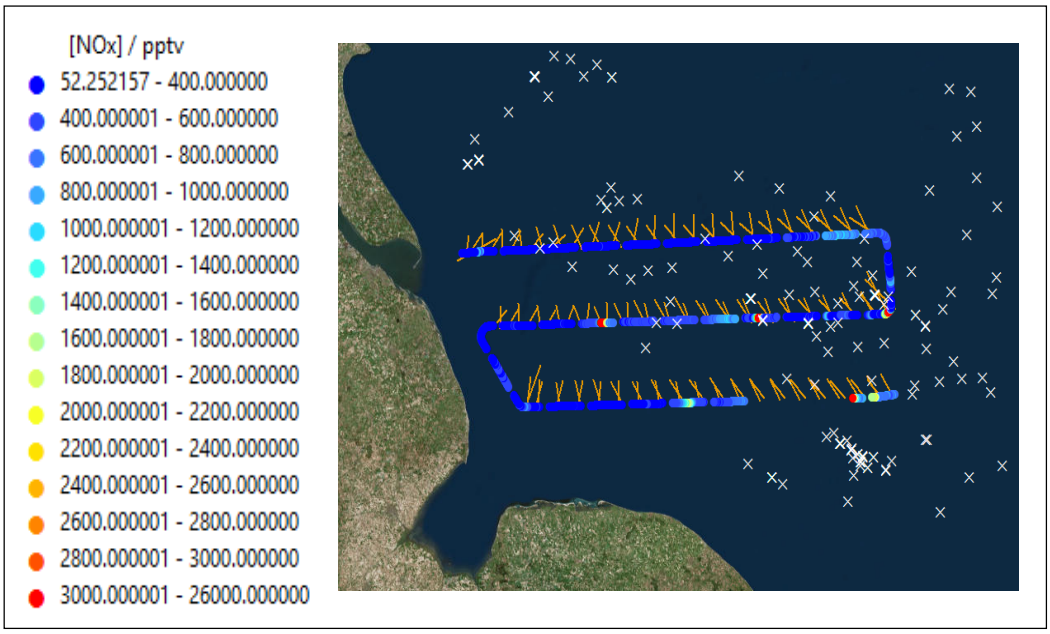

Figure 4.10: B907 NO_x mixing ratios during the flight legs conducted at 305 metres

A time series spanning the entirety of the flight is shown in **Figure 4.11**. This plot was used to relate the elevations in NO_x with the location of the plane using the flight track plots (**Figures 4.9 and 4.10**).

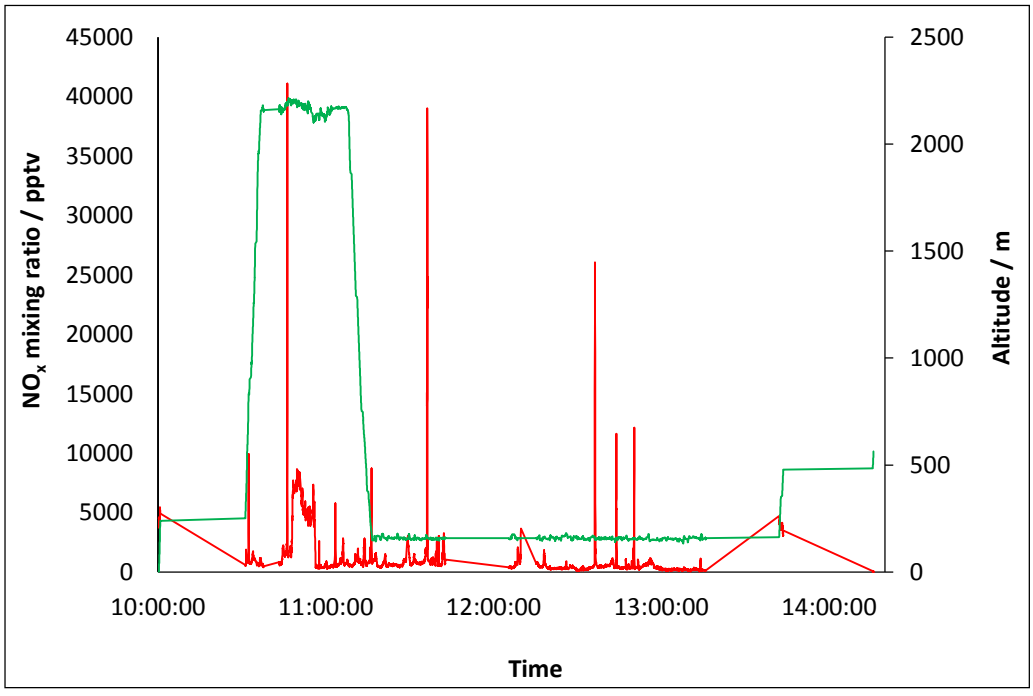

Figure 4.11: B907 surface layer NO_x mixing ratios (red) and flight altitudes (green)

Several distinct plume peaks were observed during the flight, ranging in intensity, as seen in the time series plot for the flight (**Figure 4.11**). The smallest peaks observed were between approximately 4,000 and 8,000 pptv. However, much larger peaks were also detected during the flight, ranging from approximately 26,000 up to 39,000 and 41,000 pptv. As can be seen on the flight track plots, the majority of these peaks were seen when the wind was coming directly from one, if not many, of the nearby oil and gas rigs in the area. Thus making it highly likely that these peaks were part of the rigs' gas plumes. However, due to the sheer density of rigs around the flight track, and uncertainties associated with wind direction variations, it is extremely difficult to assign peaks to individual rigs. It should be noted however, that an interesting sustained increase in NO_x mixing ratios was seen, approximately 8 nautical miles off the east coast of the UK (see **Figure 4.9**). The NO_x mixing ratios here increased to between approximately 4,000 and 7,500 pptv. In this case, there are no rigs nearby which could have caused this increase. Instead, this is more likely to be due to NO_x influences from the Humber estuary and Lincolnshire coastline, namely sources such as road transport, shipping and power plants. This changes the marine boundary layer signature, thus meaning that once travelled downwind, into the North Sea, this increased NO_x mixing ratio detected by the instrument during the survey flight.

Flight B908

The NO_x mixing ratios measured in the surface layer for the cross wind legs at 152 metres and 305 metres are given in **Figure 4.12** and **Figure 4.13**. As with flight B907, the lines on the flight tracks below show that the wind during flight B908 was north-westerly, with an average direction of 315° and an average speed of 8 metres per second. It was therefore possible to detect emissions from the oil and gas rigs in the surrounding area, as per the objective of the campaign.

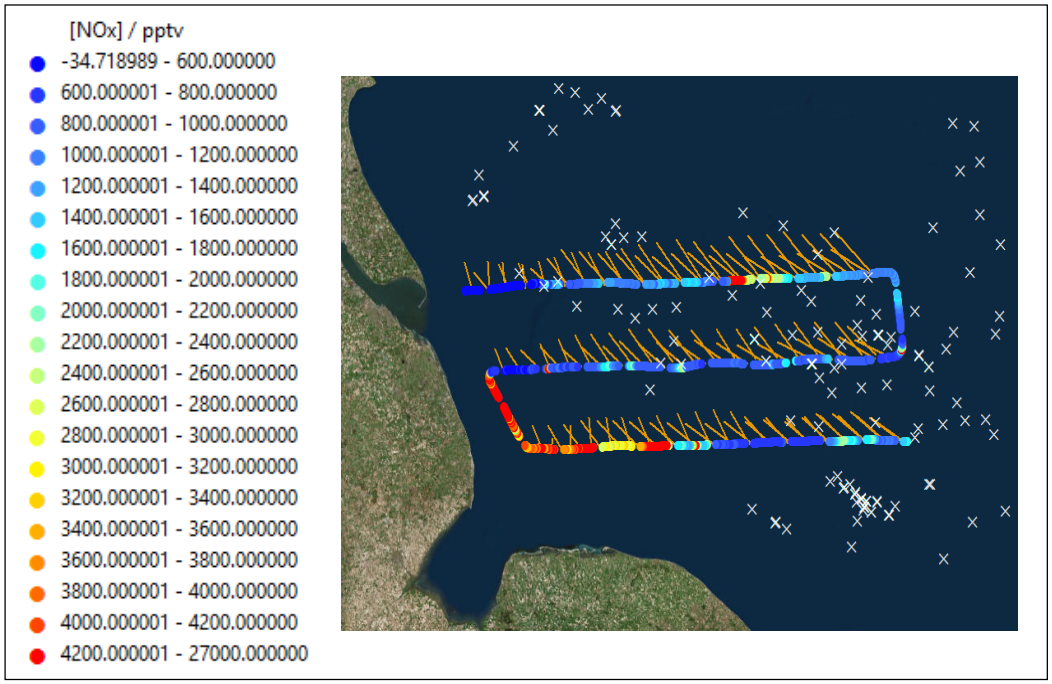

Figure 4.12: B908 NO_x mixing ratios during the flight legs conducted at 152 metres

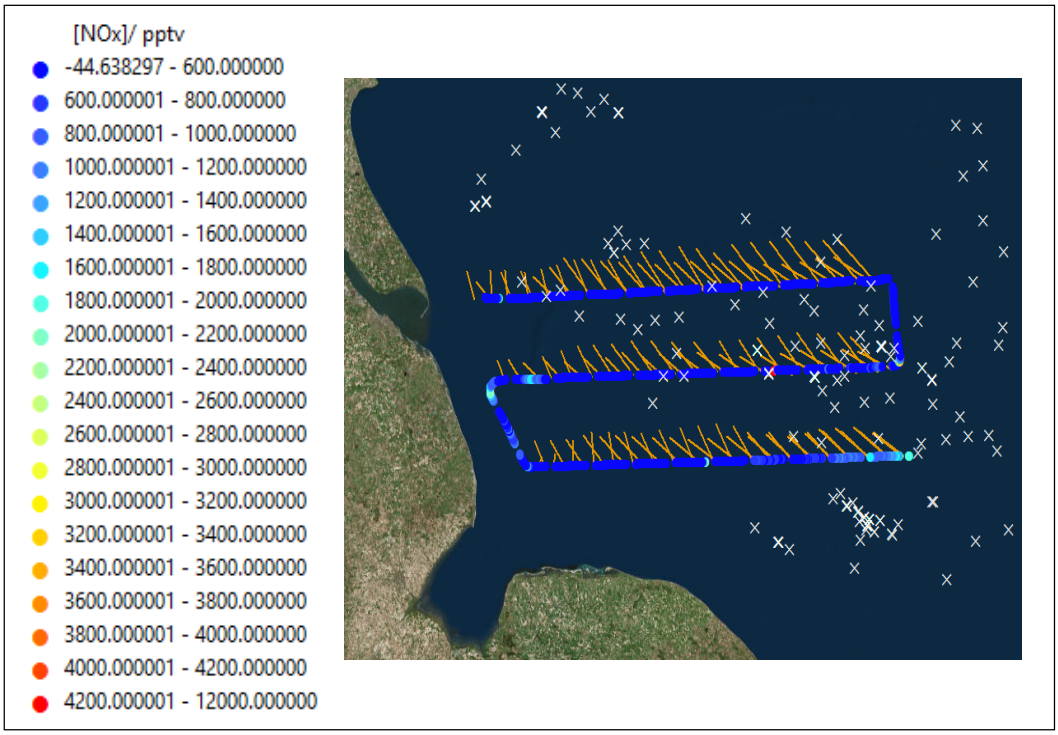

Figure 4.13: B908 NO_x mixing ratios during the flight legs conducted at 305 metres

The time series displaying all surface layer NO_x mixing ratios for flight B908 is shown in **Figure 4.14** below.

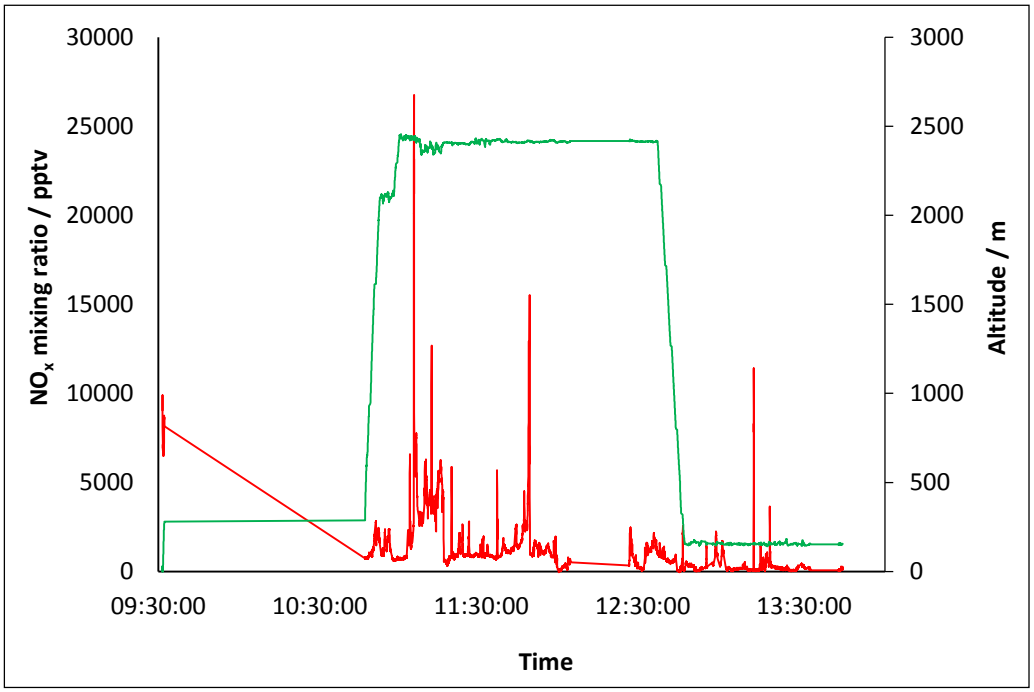

Figure 4.14: B908 surface layer NO_x mixing ratios (red) and flight altitudes (green)

Several notable gas plumes were observed during the flight, showing maximum mixing ratios of approximately 27,000 pptv. Smaller plumes were also detected, though these were still shown to contain around 4,000 to 5,000 pptv of NO_x. As can be seen in the flight track plots, these plumes were measured in close proximity to a number of operational oil and gas rigs in the area, thus highlighting the fact that these are the sources of these increased mixing ratios.

Flight B910

The NO_x mixing ratios measured in the surface layer for the cross wind legs at 152 metres and 305 metres are shown in **Figure 4.15** and **Figure 4.16**. The lines on the flight tracks below illustrate the north-westerly wind experienced during this flight (as with the previous two flights), averaging at 316°, with an average wind speed of 5 metres per second.

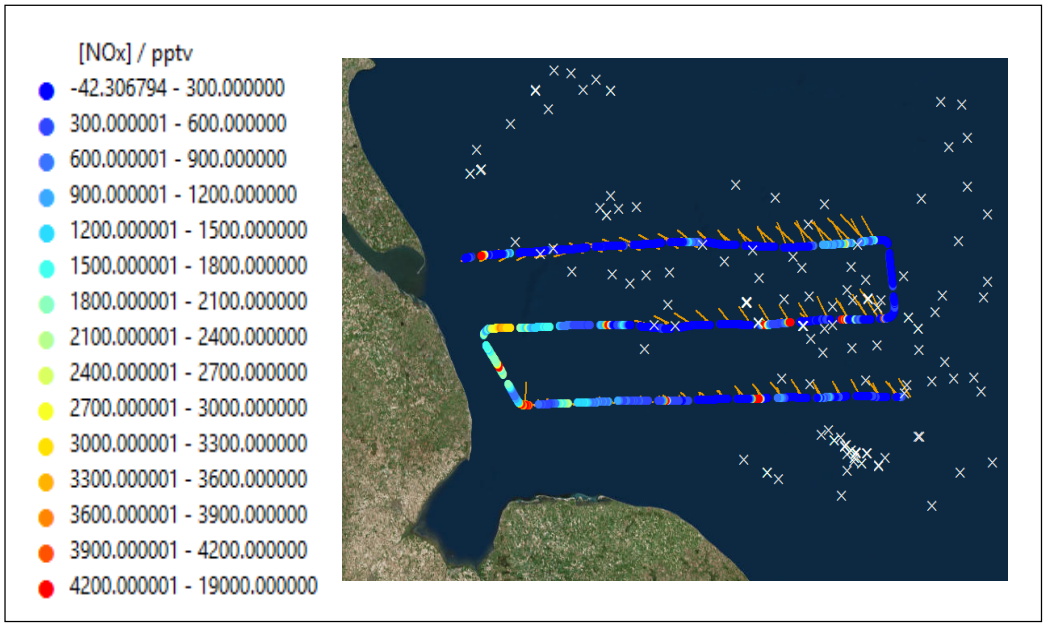

Figure 4.15: B910 NO_x mixing ratios during the flight legs conducted at 152 metres

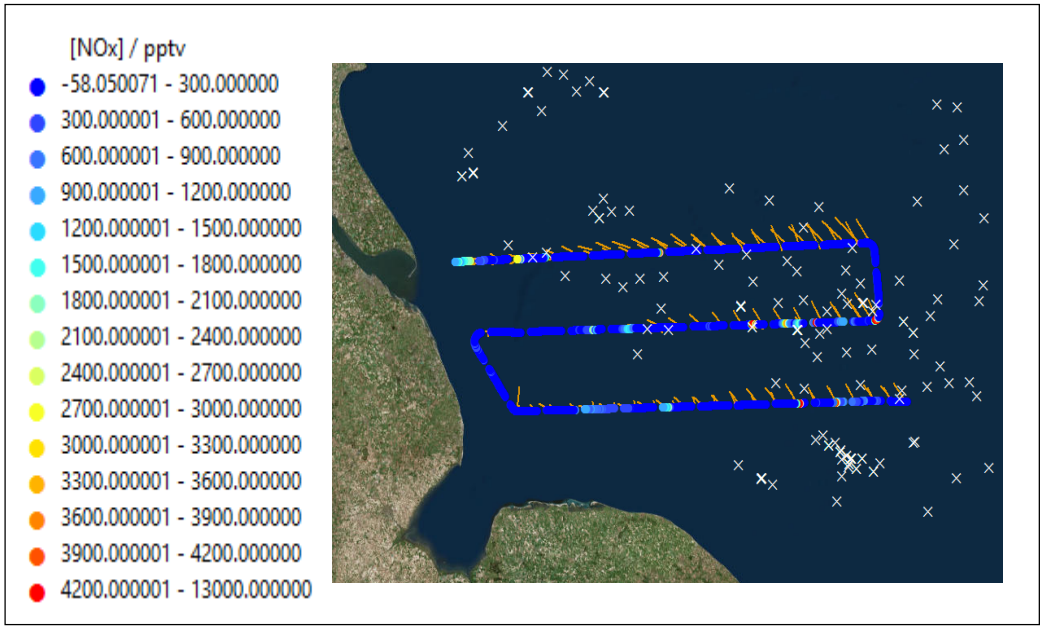

Figure 4.16: B910 NO_x mixing ratios during the flight legs conducted at 305 metres

The time series displaying all surface layer NO_x mixing ratios for flight B910 is shown in **Figure 4.17** below.

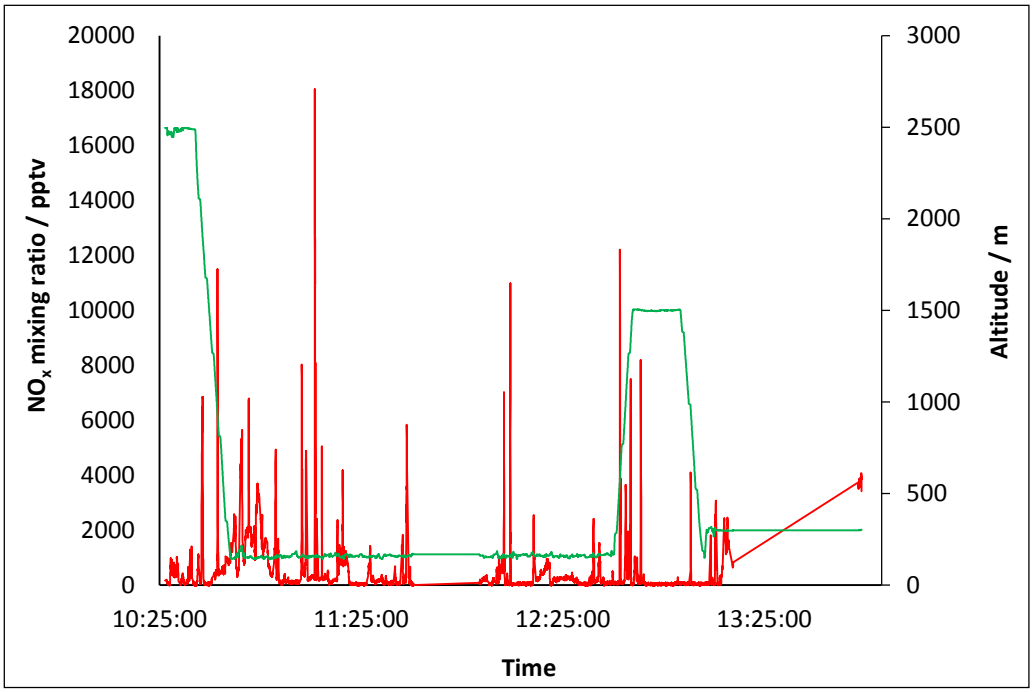

Figure 4.17: B910 surface layer NO_x mixing ratios (red) and flight altitudes (green)

The flight track plots (**Figure 4.15** and **Figure 4.16**) show that many gas plumes originating from the oil and gas rigs were detected during the flight. As can be seen in the time series plot for the flight (**Figure 4.17**), there were a number of plumes containing between approximately 3,000 and 8,000 pptv of NO_x, which are substantial amounts in themselves. However, as with the previous flights, there were several plumes which showed higher mixing ratios, ranging from around 10,000 to a maximum of 18,000 pptv. Although extremely high compared to the rest of the flight, these mixing ratios are lower than those observed during flights B907 and B908, which showed plumes of approximately 41,000 and 23,000 pptv, respectively. The reasoning behind this difference is likely to be a combination of factors associated with the wind experienced by each flight. The wind speed experienced by flight B910 (5.04 metres per second) was much lower than that experienced by flight B908 (7.86 metres per second), thus explaining the lower observed mixing ratios between those two flights. However, flight B907 saw a slower average wind speed (4.2 metres per second) than flight B910, but still showed much higher mixing ratios. The reason for this is therefore likely to be due to the wind direction, which could have varied a lot more in one of these flights, thus affecting the detection of the direct emissions coming from the rigs. However,

without further investigation into other parameters, it is extremely difficult to justify these as the reasons behind the differences observed.

The sustained increase in NO_x running up the east coast of the UK, observed during flights B907 and B908 was also seen in this flight (see **Figure 4.15**). However, in this case, the mixing ratios rarely exceeded 2,000 pptv, which was lower than those measured during the analogous runs of flights B907 and B908, where mixing ratios of 3,500 pptv and above were seen. This is again likely to be a result of the different wind speeds and directions associated with each of the flights.

Flight B912

The NO_x mixing ratios measured in the surface layer for the cross wind legs at 152 metres and 305 metres are shown in the flight track plots (**Figure 4.18** and **Figure 4.19**). The wind direction for the flight was north-easterly, averaging at 37°, which is represented by the orange lines shown on the flight track plots. The average wind speed during the flight was 9 metres per second.

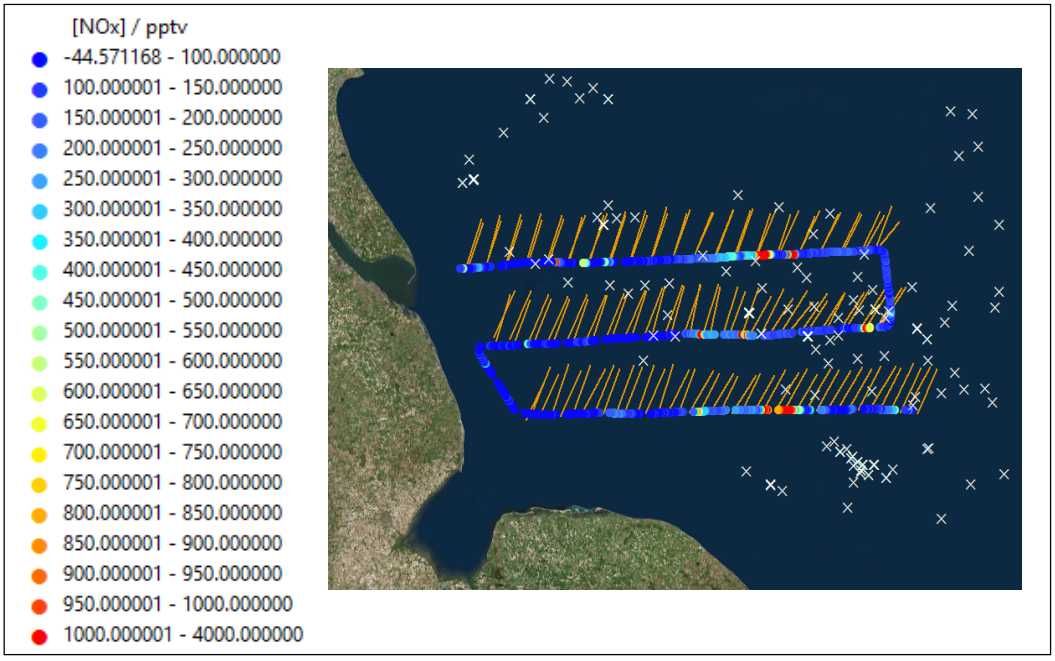

Figure 4.18: B912 NO_x mixing ratios during the flight legs conducted at 152 metres

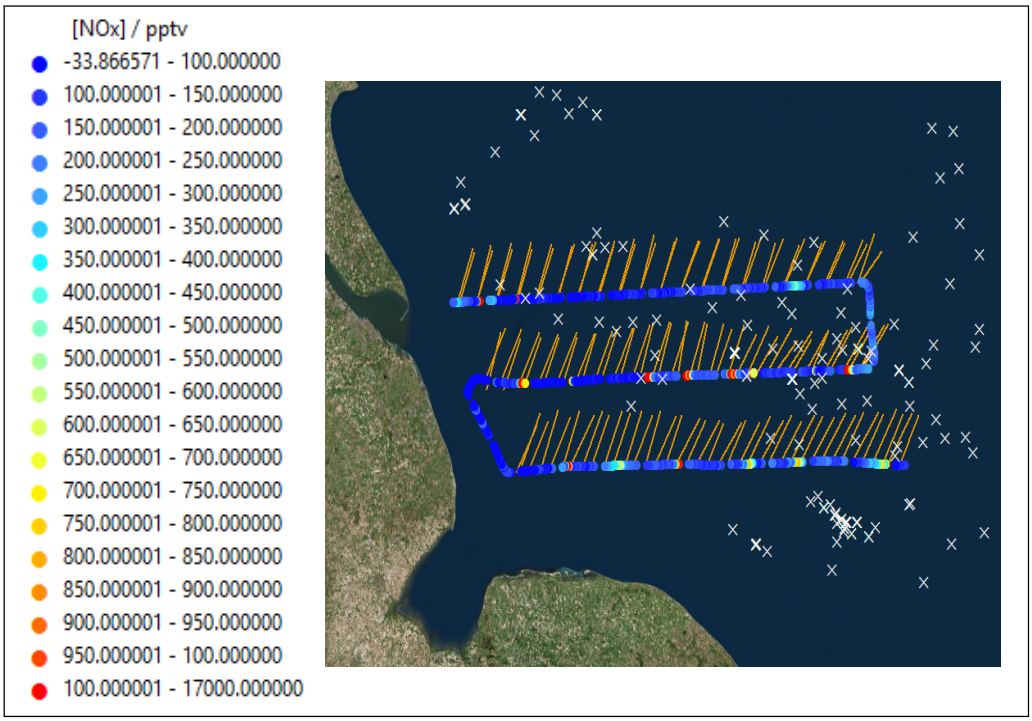

Figure 4.19: B912 NO_x mixing ratios during the flight legs conducted at 305 metres

The time series displaying all surface layer NO_x mixing ratios for flight B912 is shown in **Figure 4.20**.

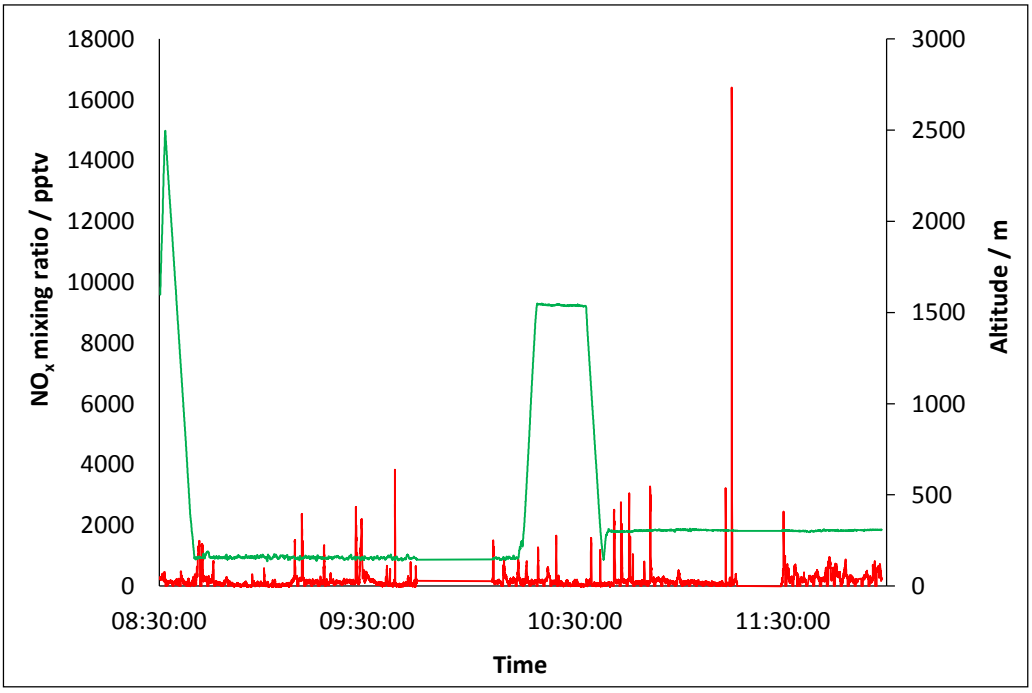

Figure 4.20: Flight B912 surface layer NO_x mixing ratios (red) and flight altitudes (green)

The gas plumes from the many oil and gas rigs in the surrounding area of the North Sea were detected during the flight. It is possible to deduce this by looking at the flight track plots, which show the average wind direction of 37° (**Figure 4.18** and **Figure 4.19**). These show that the elevated NO_x mixing ratios were often observed when the plane was directly downwind of one, or several of the rigs.

Compared to the other flights in the southern sector of the North Sea, the majority of gas plumes observed in flight B912 were a lot smaller, ranging from around 1,000 to 4,000 pptv, as can be seen on the time series plot for the flight (**Figure 4.20**). However, the largest gas plume detected during this flight contained approximately 16,000 pptv of NO_x. The reasons for the lower mixing ratios in flight B912 compared to other flights are as yet unclear. One possible reason could be the fact the wind, rather coming from a NNW direction (as in flights B907, B908 and B910), instead comes from a NNE direction. This therefore could have meant that plumes from particular rigs that were detected by the earlier three flights, were not seen during B912, as the wind was coming from a slightly different direction. However, as discussed earlier, it is very difficult to link plume peaks to particular rigs, so it is hard to say whether this is, in fact, the reason behind the lower plume mixing ratios.

Flight B913

As with the southern sector flights, flight B913 involved conducting cross wind legs at altitudes of 152 metres and 305 metres. The NO_x mixing ratios measured in the surface layer for these legs are shown in **Figure 4.21** and **Figure 4.22**. As with the southern sector flights, the flight tracks demonstrate that the average wind direction over the course of the flight was north-westerly, at 335°, with an average speed of 8 metres per second. Many of the gas plumes were detected when flying directly downwind of some of these rigs, meaning it was possible to count the majority of them as direct rig emissions.

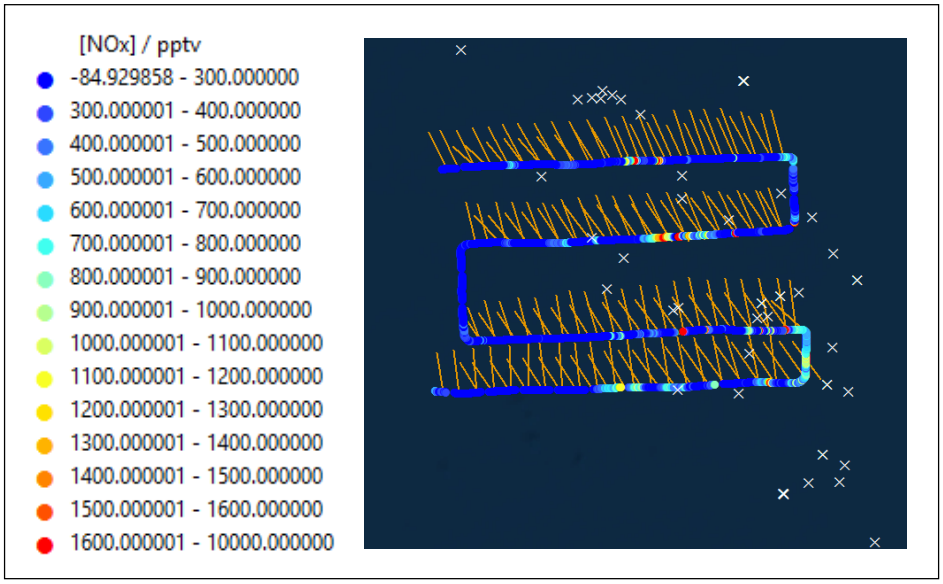

Figure 4.21: B913 NO_x mixing ratios during the flight legs conducted at 152 metres

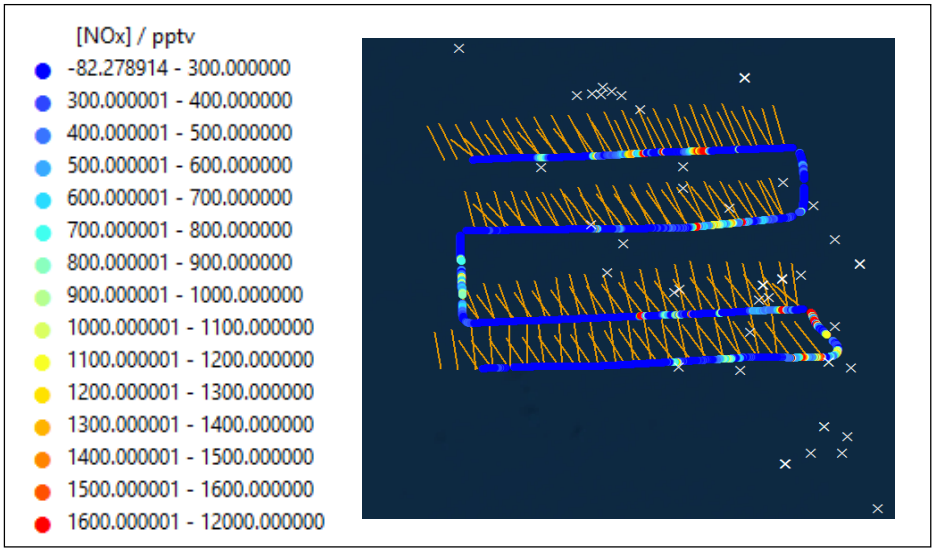

Figure 4.22: B913 NO_x mixing ratios during the flight legs conducted at 305 metres

The time series displaying all surface layer NO_x mixing ratios for flight B913 is shown in **Figure 4.23** below.

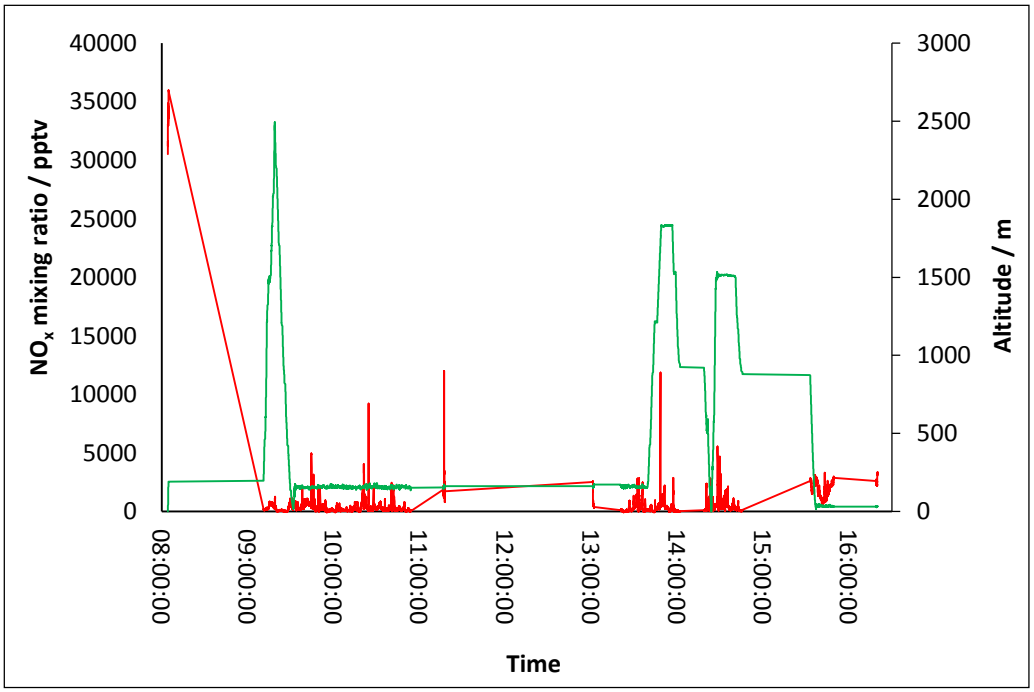

Figure 4.23: Flight B913 surface layer NO_x mixing ratios (red) and flight altitudes (green)

As with all previous flights in the southern sector of the North Sea, flight B913, based in the northern sector of the North Sea, also measured plumes which contained quite a wide range of NO_x mixing ratios. The majority of the plumes seen on the flight showed NO_x mixing ratios of around 2,000 to 5,000 pptv. There were two larger gas plumes detected during the flight, containing NO_x mixing ratios of approximately 9,000 and 11,000 pptv. These are considerable amounts of NO_x which are being emitted into an otherwise "clean" atmospheric environment. So it important that these peaks can be linked directly to the rigs. This can be done by looking at the background NO_x mixing ratios.

Flight B918

The time series displaying all surface layer NO_x mixing ratios for flight B918 is shown in **Figure 4.24** below.

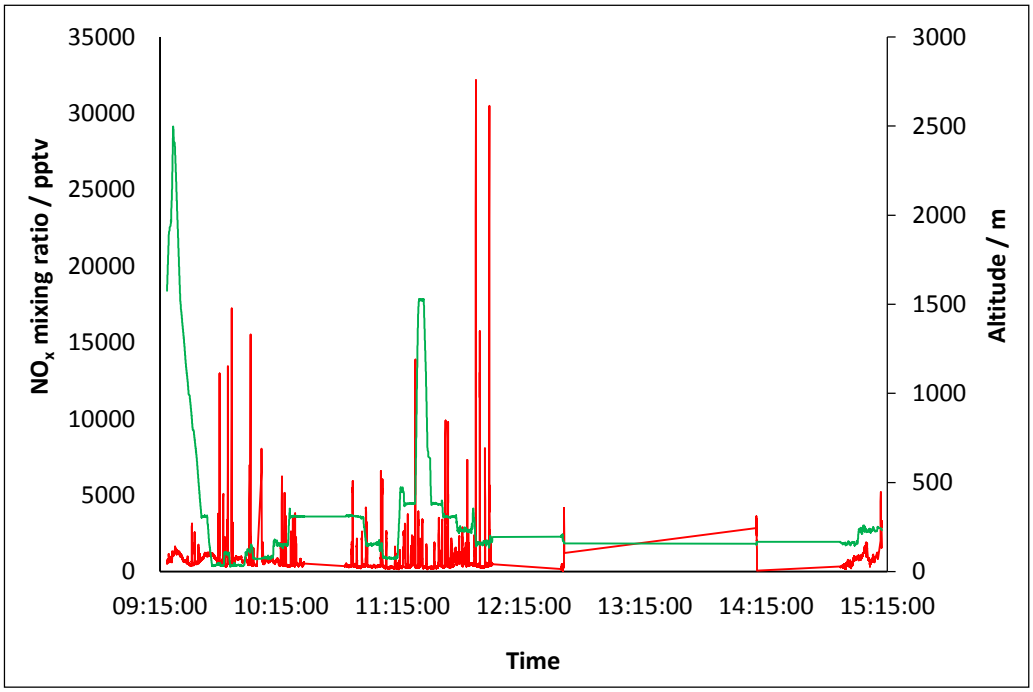

Figure 4.24: Flight B918 surface layer NO_x mixing ratios (red) and flight altitudes (green)

Two runs of this flight, runs 10 and 11, were conducted at 381 metres and 457 metres, respectively. The plane was therefore flying above the surface layer at these altitudes, meaning that it would be unlikely that NO_x mixing ratios measured during these runs would been part of the gas plume from the rigs. As a result, there are no surface layer NO_x mixing ratios to analyse for these two runs. The NO_x mixing ratios measured during runs conducted

in the surface layer are shown in **Figures 4.25-4.40**. The flight experienced a south-westerly wind, with an average direction of 247° over the course of the flight. This is shown on the plots, signifying where emissions from the rigs are likely to be detected on the flight path. **Figure 4.25** shows that the NO_x mixing ratios were much lower when the plane was flying directly upwind of the rigs, with a maximum of around 850 pptv being observed. This indicated that any enhancement in NO_x observed in the subsequent downwind runs must be coming from the rigs. **Figure 4.25** also shows that higher mixing ratios of up to around 1400 pptv were observed. These enhancements were therefore likely to have been a result of gas plumes from other rigs downwind of the flight track.

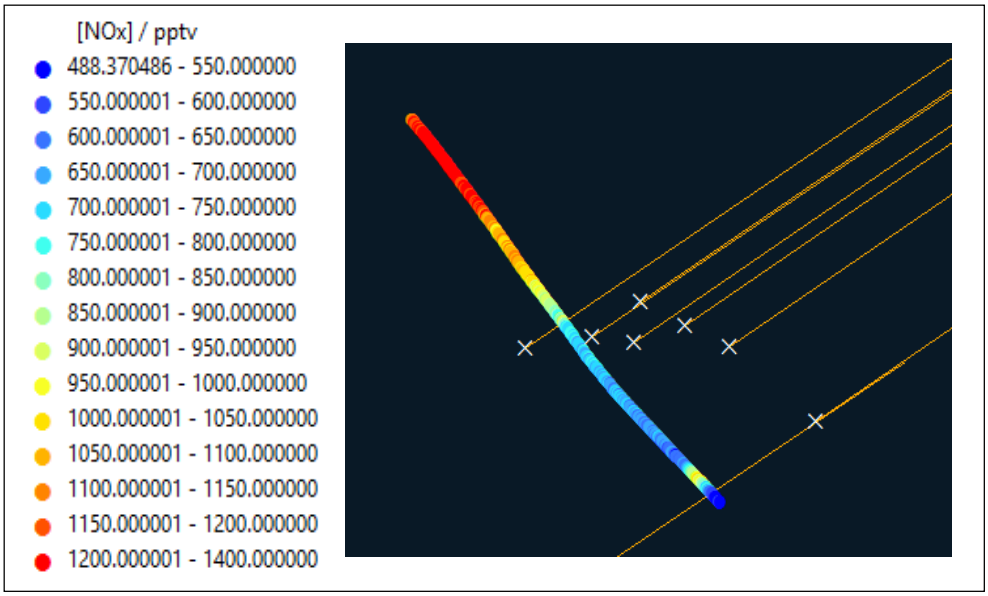

Figure 4.25: B918 NO_x mixing ratios upwind of Forties and Nelson rigs (Run 2: 31 metres)

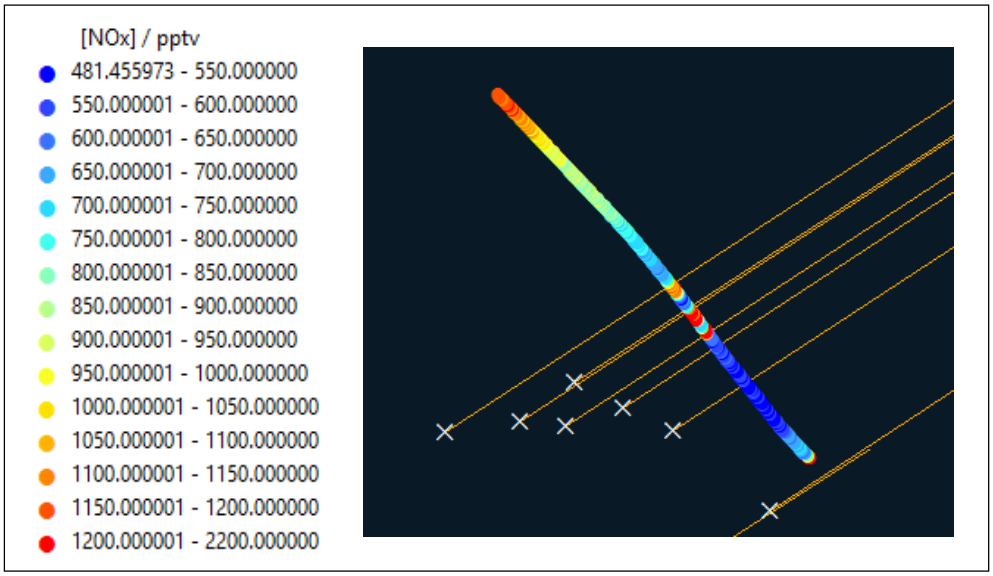

Figure 4.26: B918 NO_x mixing ratios on Run 3
(31 metres, 5 nautical miles downwind of Forties and Nelson rigs)

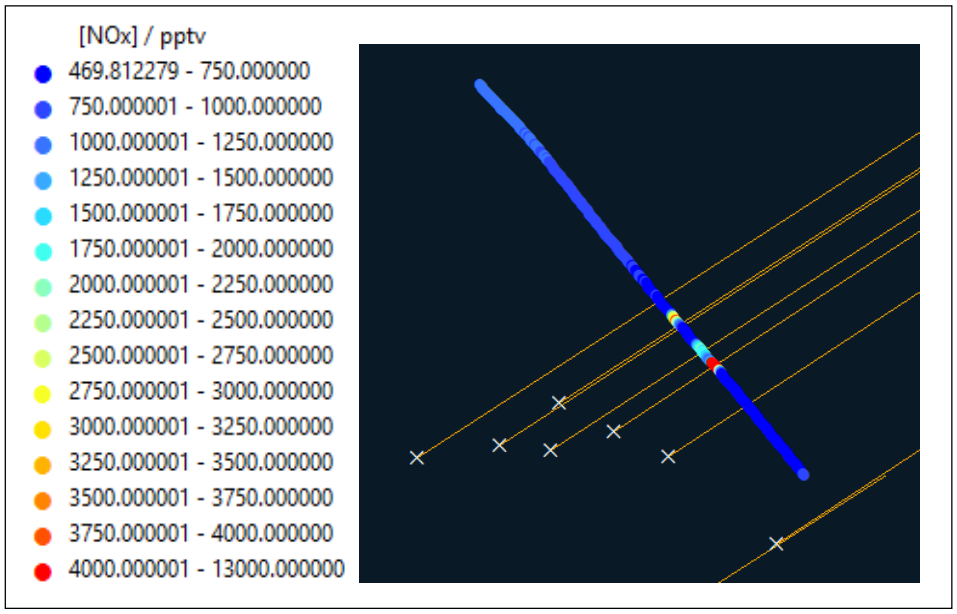

Figure 4.27: B918 NO_x mixing ratios on Run 4
(76 metres, 5 nautical miles downwind of Forties and Nelson rigs)

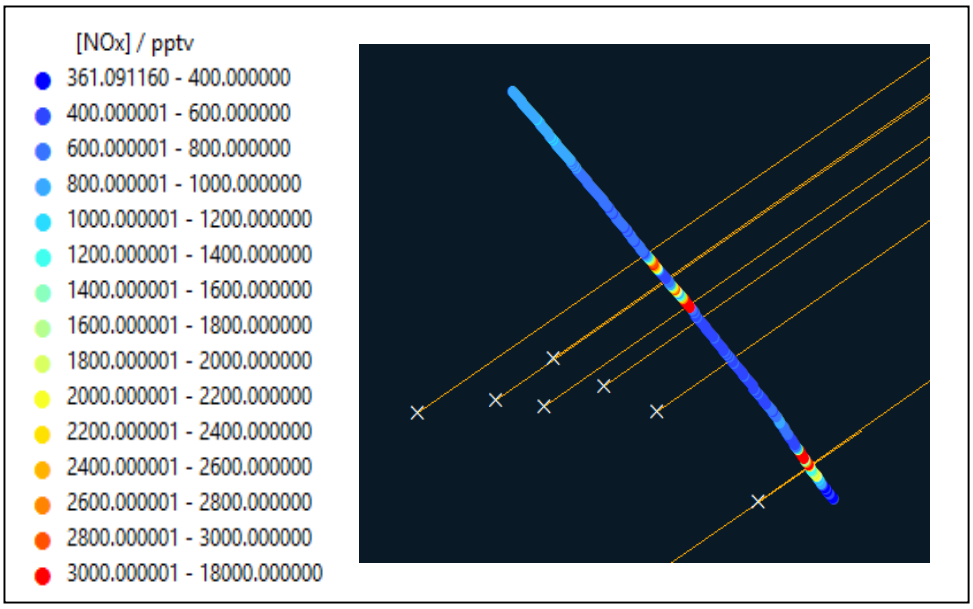

Figure 4.28: B918 NO_x mixing ratios on Run 5
(152 metres, 5 nautical miles downwind of Forties and Nelson rigs)

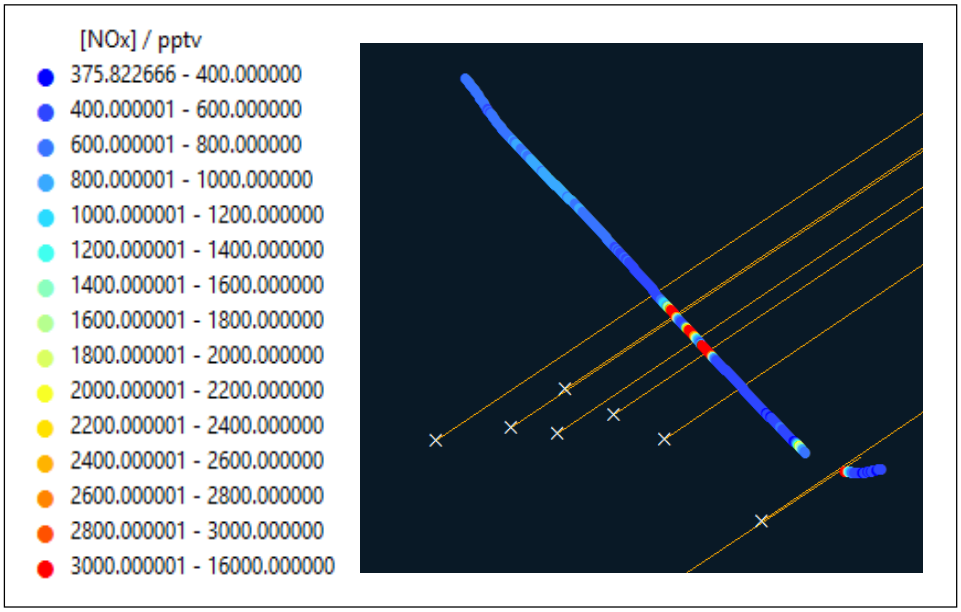

Figure 4.29: B918 NO_x mixing ratios on Run 6
(305 metres, 5 nautical miles downwind of Forties and Nelson rigs

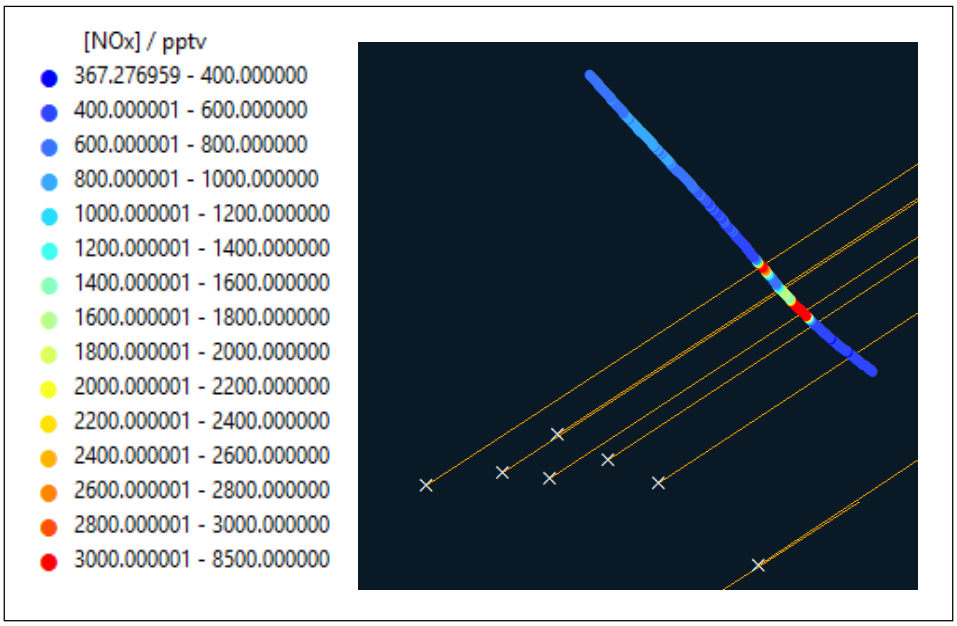

Figure 4.30: B918 NO_x mixing ratios on Run 7
(305 metres, 10 nautical miles downwind of Forties and Nelson rigs)

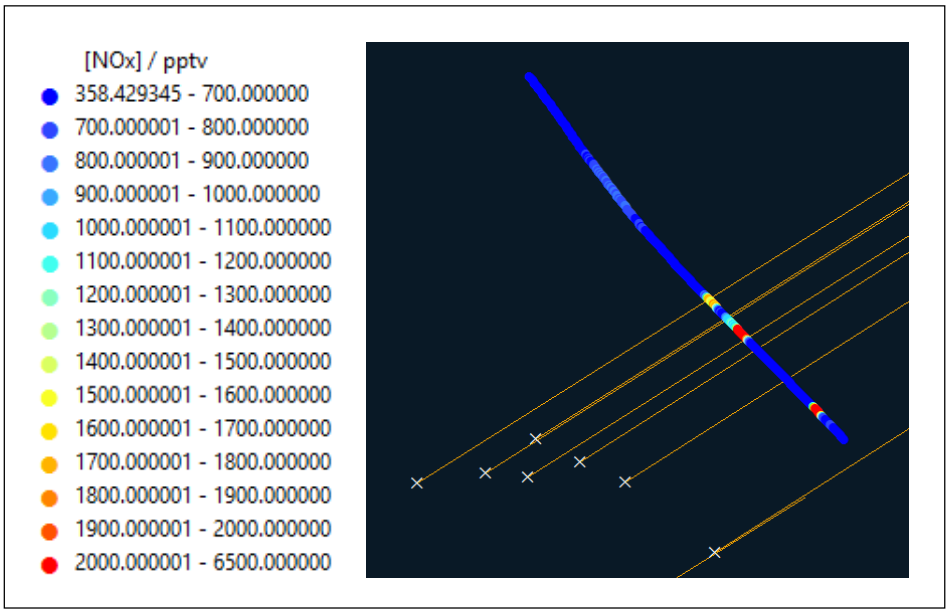

Figure 4.31: B918 NO_x mixing ratios on Run 8
(152 metres, 10 nautical miles downwind of Forties and Nelson rigs)

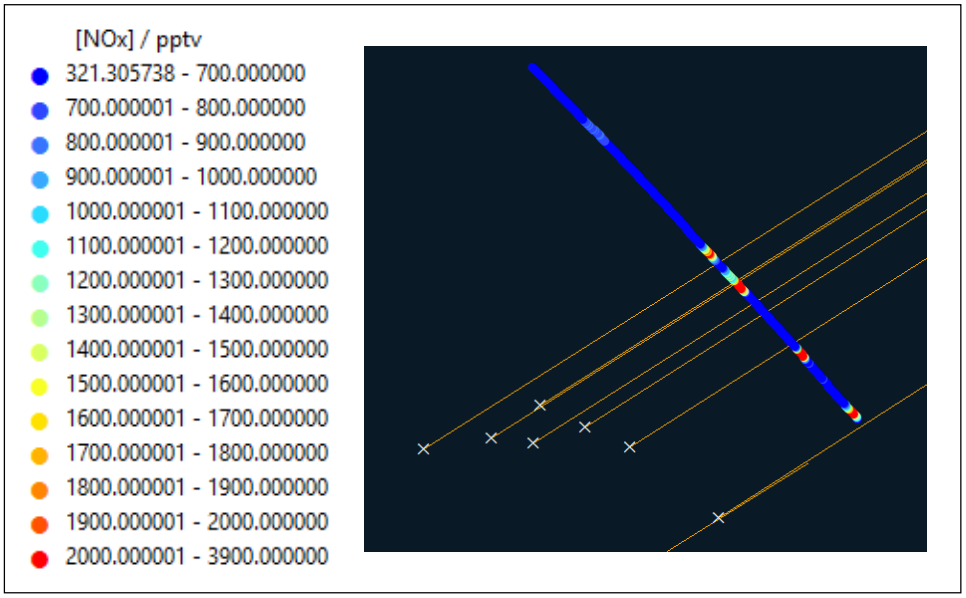

Figure 4.32: B918 NO_x mixing ratios on Run 9
(76 metres, 10 nautical miles downwind of Forties and Nelson rigs)

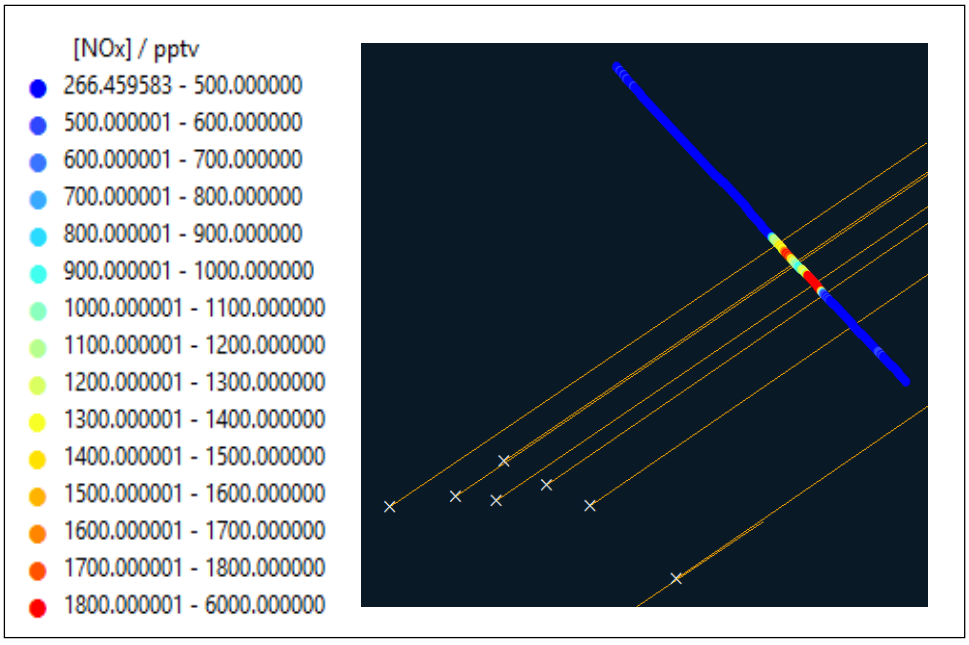

Figure 4.33: B918 NO_x mixing ratios on Run 12
(305 metres, 15 nautical miles downwind of Forties and Nelson rigs)

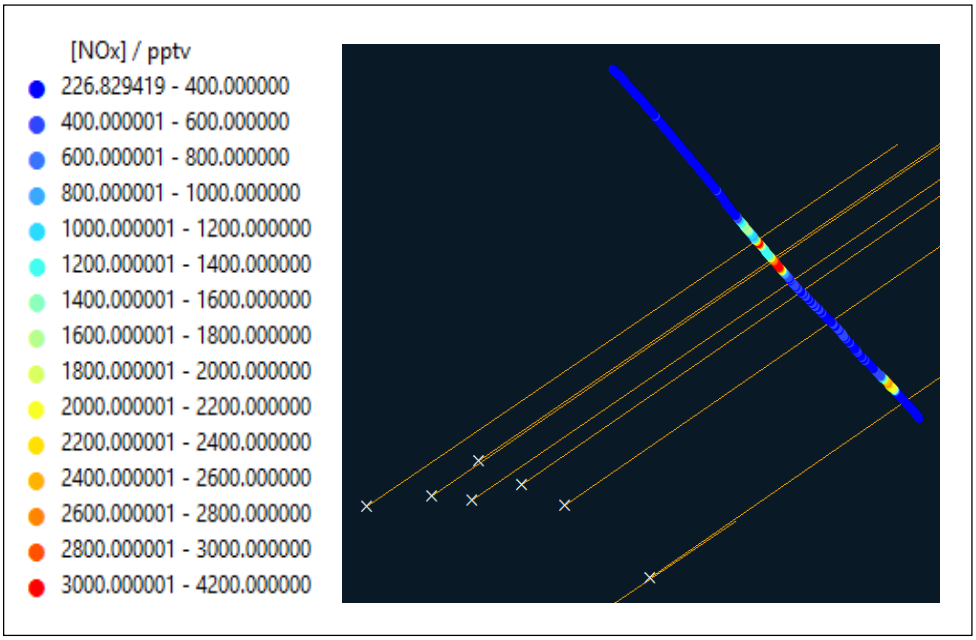

Figure 4.34: B918 NO_x mixing ratios on Run 13
(229 metres, 15 nautical miles downwind of Forties and Nelson rigs)

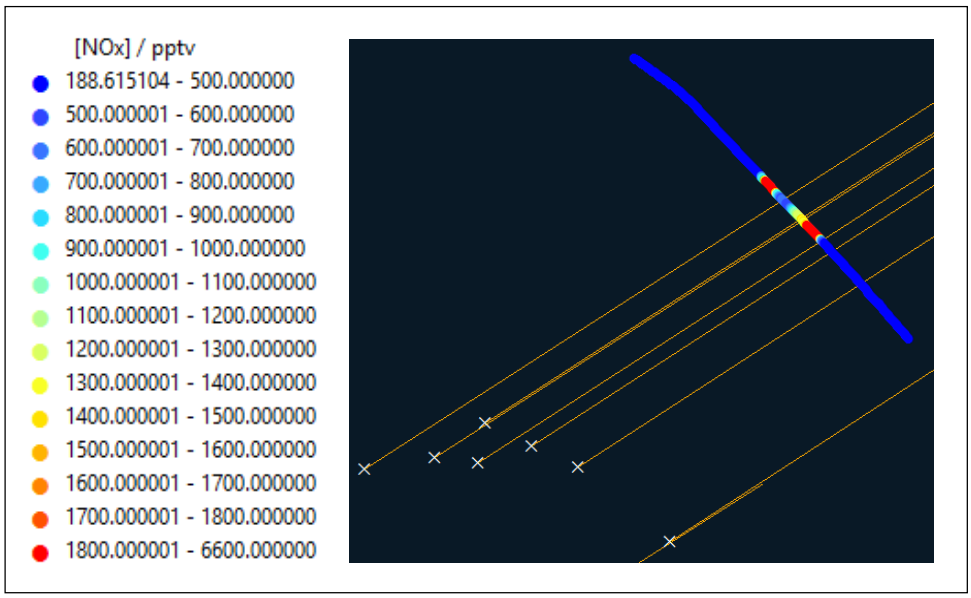

Figure 4.35: B918 NO_x mixing ratios on Run 14
(152 metres, 15 nautical miles downwind of Forties and Nelson rigs)

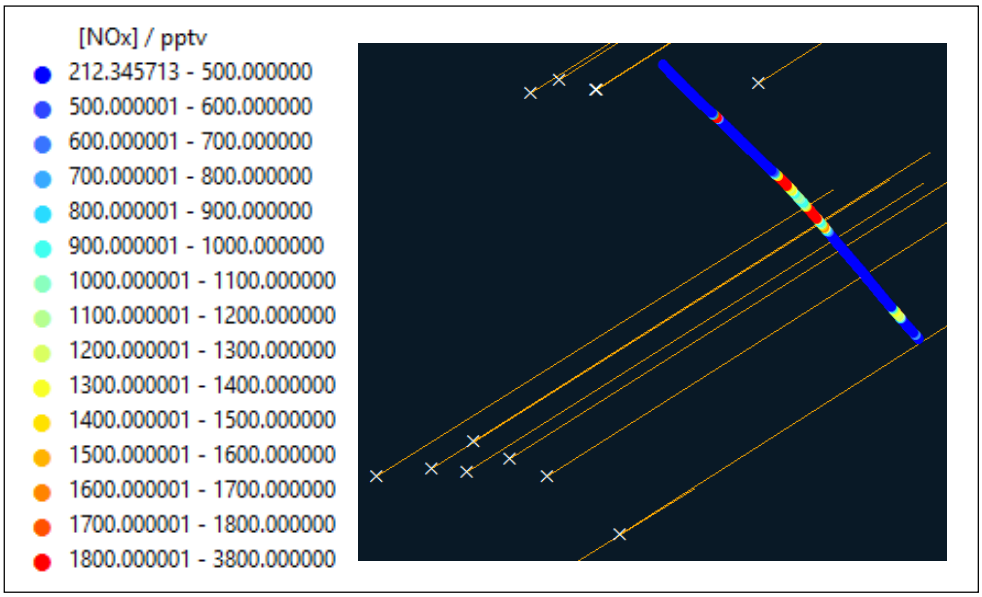

Figure 4.36: B918 NO_x mixing ratios on Run 15
(152 metres, 20 nautical miles downwind of Forties and Nelson rigs

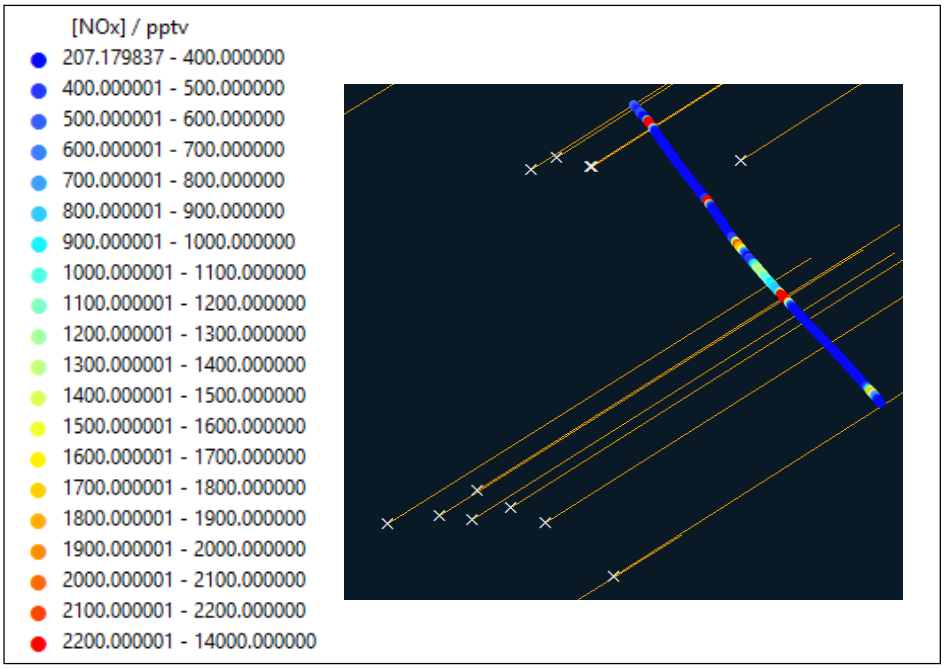

Figure 4.37: B918 NO_x mixing ratios on Run 16
(229 metres, 20 nautical miles downwind of Forties and Nelson rigs)

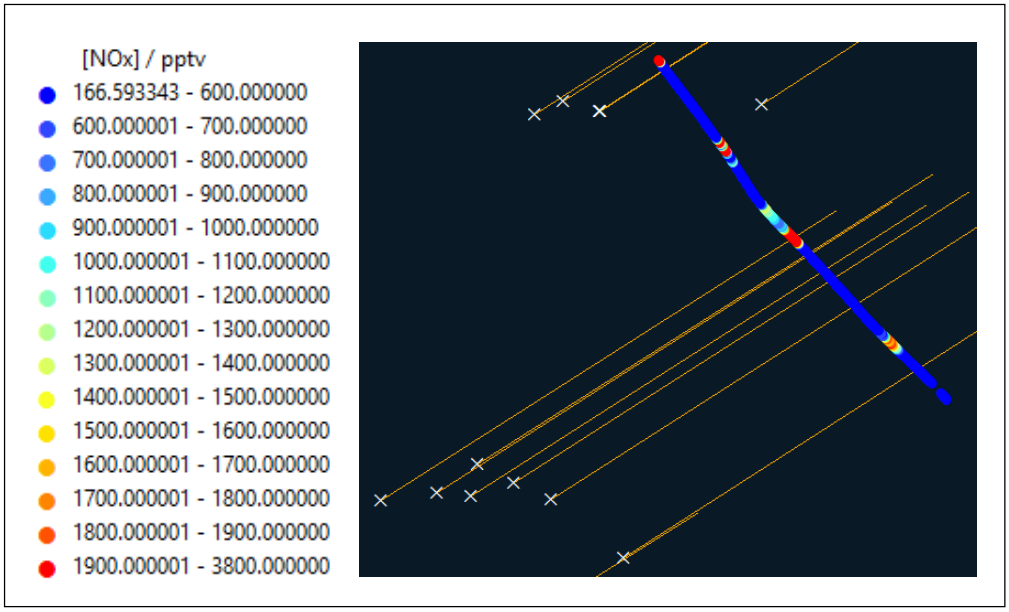

Figure 4.38: B918 NO_x mixing ratios on Run 17
(305 metres, 20 nautical miles downwind of Forties and Nelson rigs)

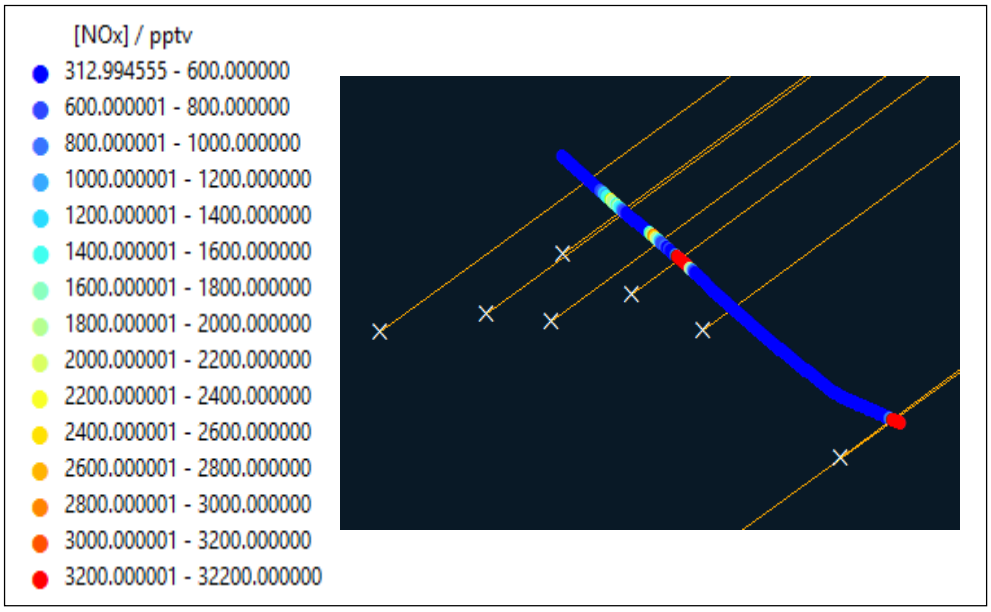

Figure 4.39: B918 NO_x mixing ratios on Run 19
(91 metres, 1 nautical mile downwind of Forties and Nelson rigs)

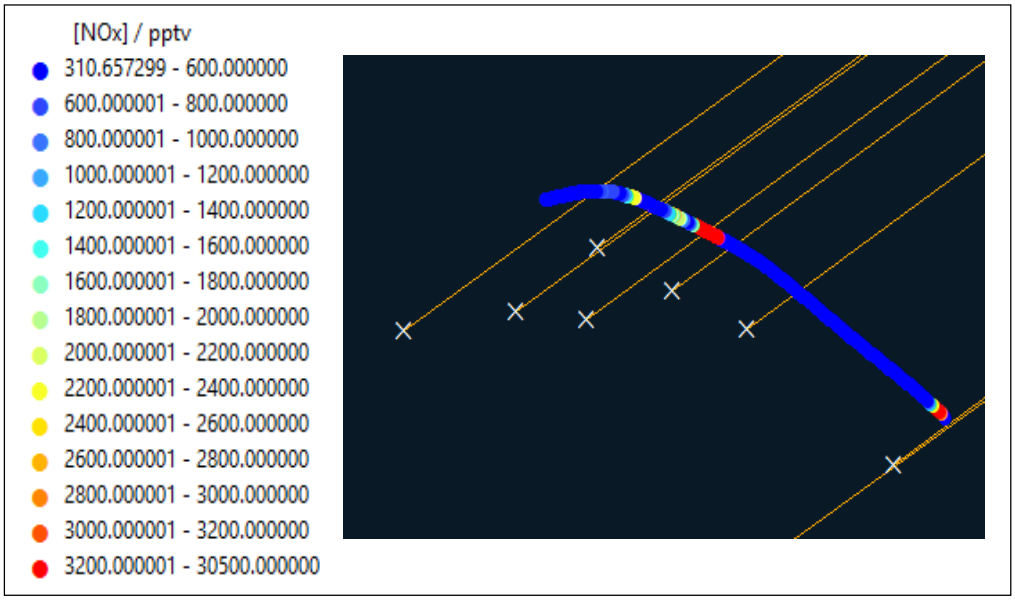

Figure 4.40: B918 NO_x mixing ratios on Run 20
(61 metres, 1 nautical mile downwind of Forties and Nelson rigs)

As described in section 4.2.1, the objective of flight B918 was to target a specific group of rigs (i.e. the Forties and Nelson rigs). The flight then involved conducting multi-altitude cross wind legs at a range of distances downwind of these rigs. It would then be possible to look at the gas plumes observed during the flight in greater detail. The lower density of rigs in this area of the North Sea meant it would be possible to focus in on NO_x emissions coming directly from the gas plumes of these specific rigs. However, it should be noted that, although not many, there were other operational rigs in this area of the North Sea, thus meaning that some of the peaks observed were likely to have been a result of diffusion of gas plumes from several rigs.

As can be seen in the flight track plots, a large number of gas plumes were detected during the flight, most of which were seen when flying directly downwind of the rigs. Some of which were seen at a range of altitudes and distances from the rigs, thus highlighting the sheer vertical and horizontal boundaries of the rig emissions. The NO_x mixing ratios within these plumes was found to vary, as with the other North Sea flights. The smallest plumes observed during the flights contained between around 5,000 and 10,000 pptv (as can be seen in both the flight track plots (**Figures 4.26– 4.40**) and the times series plot (**Figure 4.24**)). However, much larger plumes were also detected during the flight, particularly the closer the plane was to the rigs. As can be seen in **Figures 4.26-4.29**, when the plane was only approximately 5 nautical miles away from the Forties and Nelson rigs, NO_x mixing ratios of between 12,000

and 18,000 pptv were observed. The mixing ratios increased further when the plane was even closer to the Forties and Nelson rigs, with gas plumes containing around 30,000 pptv being measured when the plane was only approximately 1 nautical mile downwind (see **Figure 4.39** and **Figure 4.40**).

NO_x Plume Mixing Ratios from Rigs in the North Sea: a Summary

As discussed throughout section 4.2, the NO_x plume mixing ratios measured in each flight showed a large amount of variation, despite many of them taking place in similar areas of the North Sea. A summary table listing all flights, along with their associated wind speeds and maximum plume mixing ratios is shown below.

Table 4.3: summary of NO_x plume mixing ratios measured during the "Oil and Gas" campaign

Flight Number (sector of the North Sea)	Average Wind Speed / m s^{-1}	Maximum NO_x Plume Mixing Ratio / pptv
B907 (Southern)	4.18	41,083
B908 (Southern)	7.86	26,757
B910 (Southern)	5.04	18,056
B912 (Southern)	8.93	16,402
B913 (Northern)	8.31	11,873
B918 (Northern)	8.32	32,177

The table above indicates that generally, the highest plume mixing ratios were observed when the wind speeds were lower, as a result of minimal dilution. For example, flight B907 observed both the highest mixing ratio and the lowest wind speed of all the flights, whilst flight B908 observed both higher wind speeds and lower plume mixing ratios.

However, there are other factors which are likely to have contributed to the variability of the plume sizes. One of these is the distance of the flight track from the rigs. This is particularly evident when looking at the mixing ratios measured during flight B918, which saw very high mixing ratios of NO_x despite the wind speed also being relatively high (**Table 4.3**). This flight involved transects at multiple distances downwind of the rigs and the maximum mixing ratio of 32,177 pptv was measured during a run less than 1 nautical mile downwind of the rigs.

The mixing ratios measured in the gas plumes during each flight were also likely to be influenced by the emission rates of the rigs, as they may have been operating at different capacities when each flight took place, thus resulting in the variable NO_x emissions. The boundary layer height would also have affected the mixing ratios measured during each flight, as this dictates the area into which the gases are emitted into and thus, affects how diluted the emissions are.

In summary, it is likely that the plume sizes observed across all flights in the "Oil and Gas" campaign are a combination of emission rate, wind speed, distance from the rigs and the boundary layer height. Each of these variables would need to be investigated more extensively to determine their exact influence on the mixing ratios observed.

4.3 Background NO_x Mixing Ratios

Although the primary aim of the campaign was to look at the direct NO_x emissions coming from the oil and gas platforms, it is also important to consider the "background" atmosphere onto which these emissions are being added to. This background acts a baseline for atmospheric composition in the surrounding area, i.e. it provides information about the levels in the area that are not necessarily from specific sources. For example, background NO_x mixing ratios could result from the rigs, but they could also be from shipping or the UK itself.

In order to understand the origins of the background NO_x, and to confirm that most of the elevated mixing ratios were coming from the oil and gas rigs, it is first necessary to look at the data from the flights and determine what the average background mixing ratios were during each flight. This would provide information regarding NO_x which is not due to one particular local influence (e.g. rigs).This was done by plotting a histogram, in order to show the distribution of the NO_x data obtained during each flight. The data was first filtered to the surface layer altitude and below, as this is where the emissions would be confined to (and hence would be well mixed). An example of such a histogram, constructed for flight B907, is shown in **Figure 4.41**.

The distribution was constructed using all NO_x data below the surface layer height. The data was binned in 10 pptv bins, for mixing ratios up to 10 ppbv (10,000 pptv). A Gaussian fit was then least square fitted to the background data to derive a mean background and 1σ

standard deviation, both of which are in units of pptv. Plotting a histogram in this way makes it possible to statistically derive the background NO_x, as the mean of the Gaussian fit takes out the influence of the higher mixing ratios associated with the plume interferences, which are binned into the higher bins of the histogram (hence why the majority of the data lies in the low-level regions). Histograms like this could therefore be used to derive the background levels of NO_x observed outside of the gas plumes during each flight.

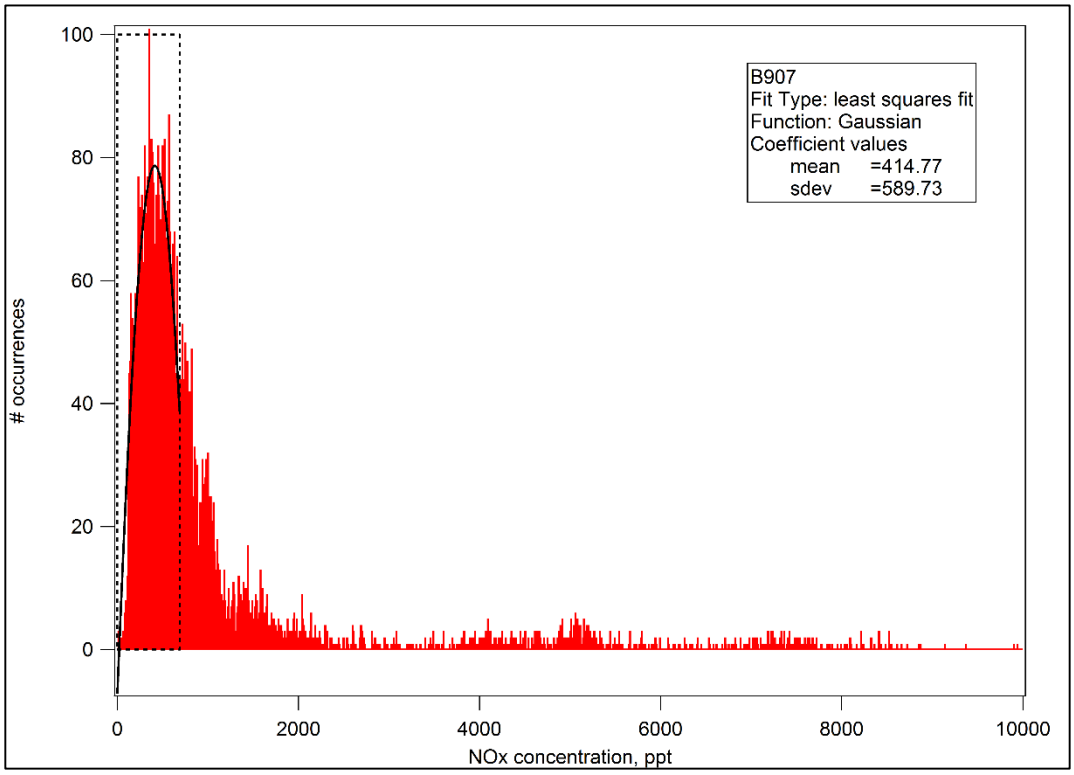

Figure 4.41: Histogram showing the distribution of NO_x data from flight B907. The dashed box represents the data used for the Gaussian fit

Flight B907

As can be seen in **Figure 4.41**, the mean background NO_x mixing ratio during flight B907 was found to be 414.77 pptv, with a standard deviation of 589.73 pptv. It is unclear as to why the standard deviation for the NO_x background was so high for this flight. One possible explanation involves the stability of the air mass, though this cannot be confirmed without further investigation.

The mean background mixing ratio was found to be 414.77 pptv, which is relatively high. This can be explained by looking at where the air sampled during the flight originated, that is by constructing back trajectories. The Hybrid Single-Particle Lagrangian Integrated Trajectory

(HYSPLIT) model[93] was used to produce 5-day back trajectories for each of the flights. Typically, four trajectories were produced for each flight; two during the 152.4 metre legs, followed by two during the 304.8 metre legs. This was done in order to monitor the origins and paths of the air parcels that were sampled over the course of the flights. Any changes in these would therefore mean that different air masses with different chemical compositions may have been sampled, thus affecting the background mixing ratios measured during the flights. The back trajectories for flight B907 are shown in **Figure 4.42**, with each triangle on the plots representing the position of the air parcel at every 12 hour interval.

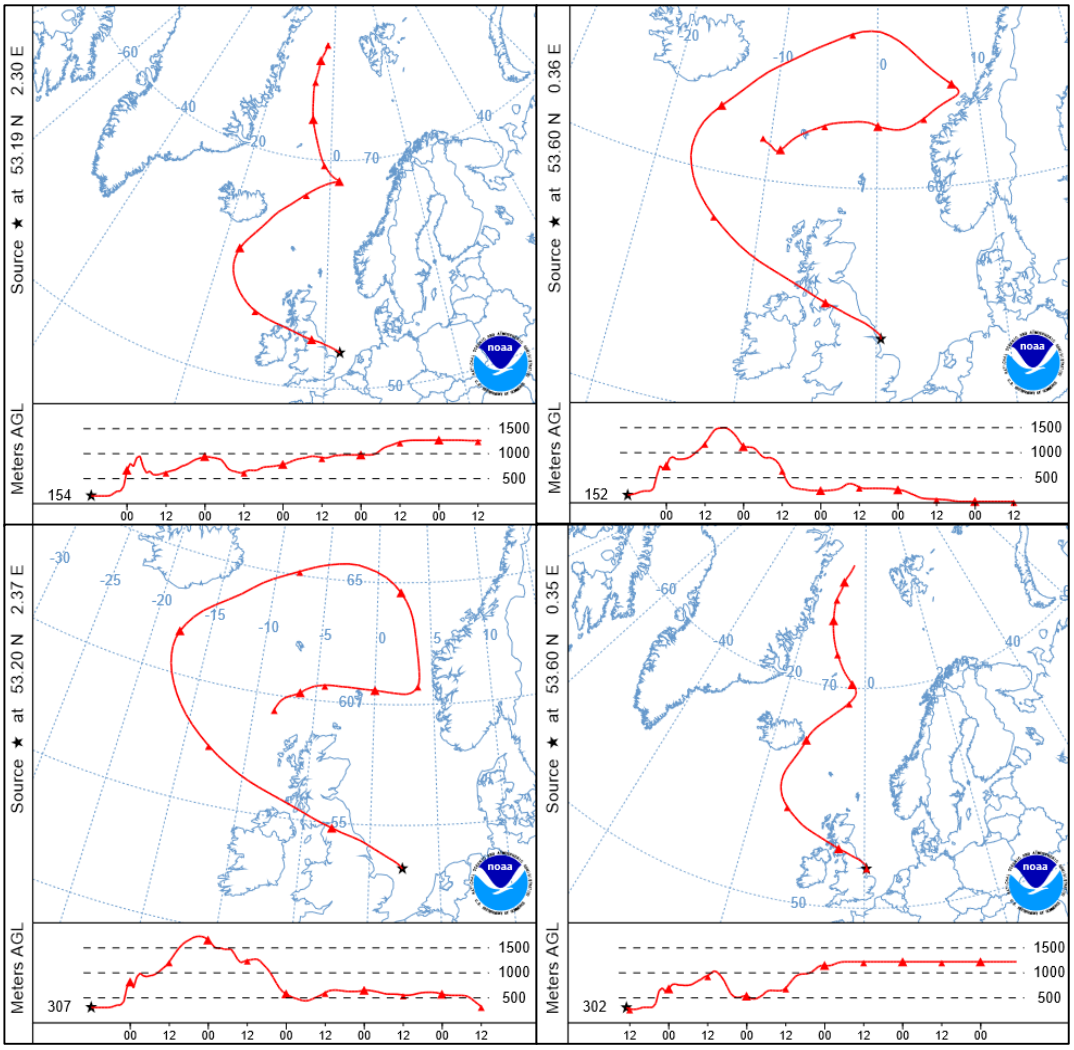

Figure 4.42: 5-day back trajectories for flight B907

The back trajectories above all show relatively similar origins and routes for the background air sampled during flight B907. In all cases, the air travelled from the low- NO_x are of the Arctic Circle and North Atlantic. However, the air parcel then travelled over the UK at

altitudes of around 700 metres, meaning that it was likely to be in the boundary layer at this time. This therefore increased the mixing ratio of NO_x in the air parcel, through accumulation of pollution from the surface, via the extensive number of transport and industry-based sources in the UK. By the time the air parcel reached the North Sea, it would have had substantial amounts of NO_x incorporated into it, prior to any influences of the oil and gas rigs being detected. This, therefore, provides an explanation as to why the background NO_x mixing ratio was particularly high for flight B907.

Flight B908

The histogram showing the background NO_x mixing ratios measured during the flight is shown below, with very few occurrences of spikes in NO_x mixing ratio, as expected for background air. The mean background NO_x mixing ratio was found to vary at different times during this flight. As seen in the histogram (**Figure 4.43**), two Gaussian curves could be fitted to the data, giving two mean background mixing ratios of 127 and 872 pptv, with 1σ standard deviations of 83 and 70 pptv, respectively. These small standard deviations support the fact that these are the true average background mixing ratios, showing that the majority of the background mixing ratios were distributed very closely around these values.

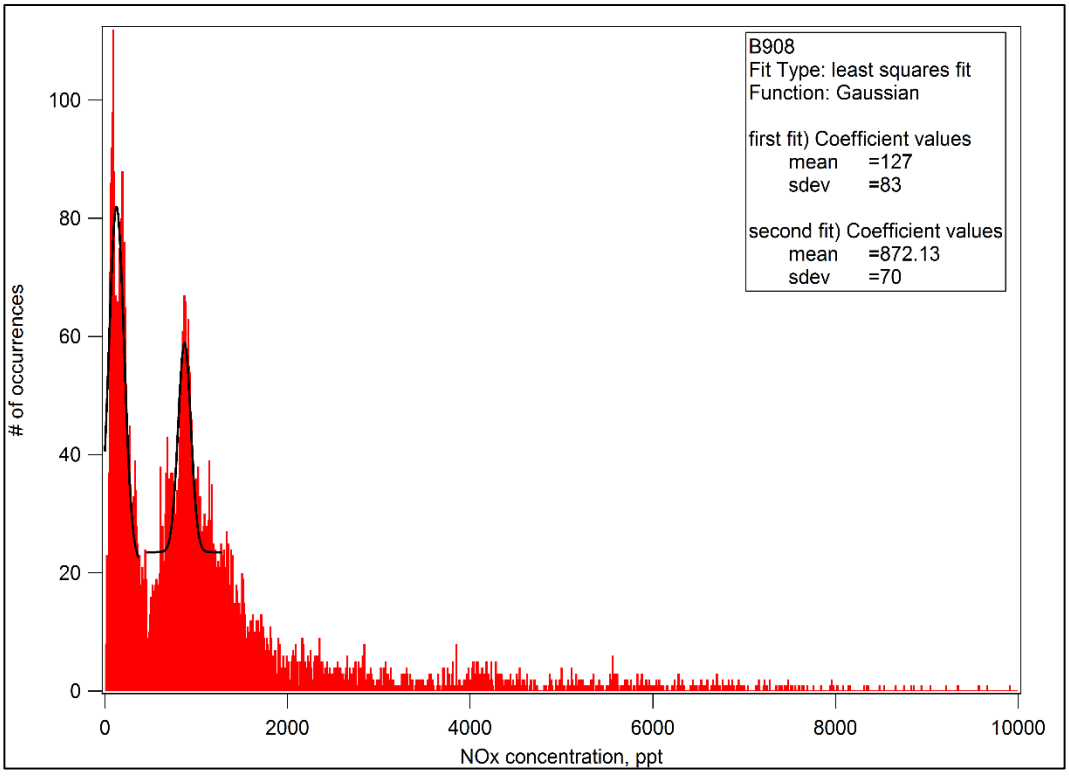

Figure 4.43: Histogram showing the distribution of NO_x data from flight B908

A possible reason for this variation in background is that two different air masses were being sampled over the course of the flight, each having different chemical compositions. The back trajectories constructed for the flight (**Figure 4.44**), can be used to give an indication as to whether this was, in fact, the case.

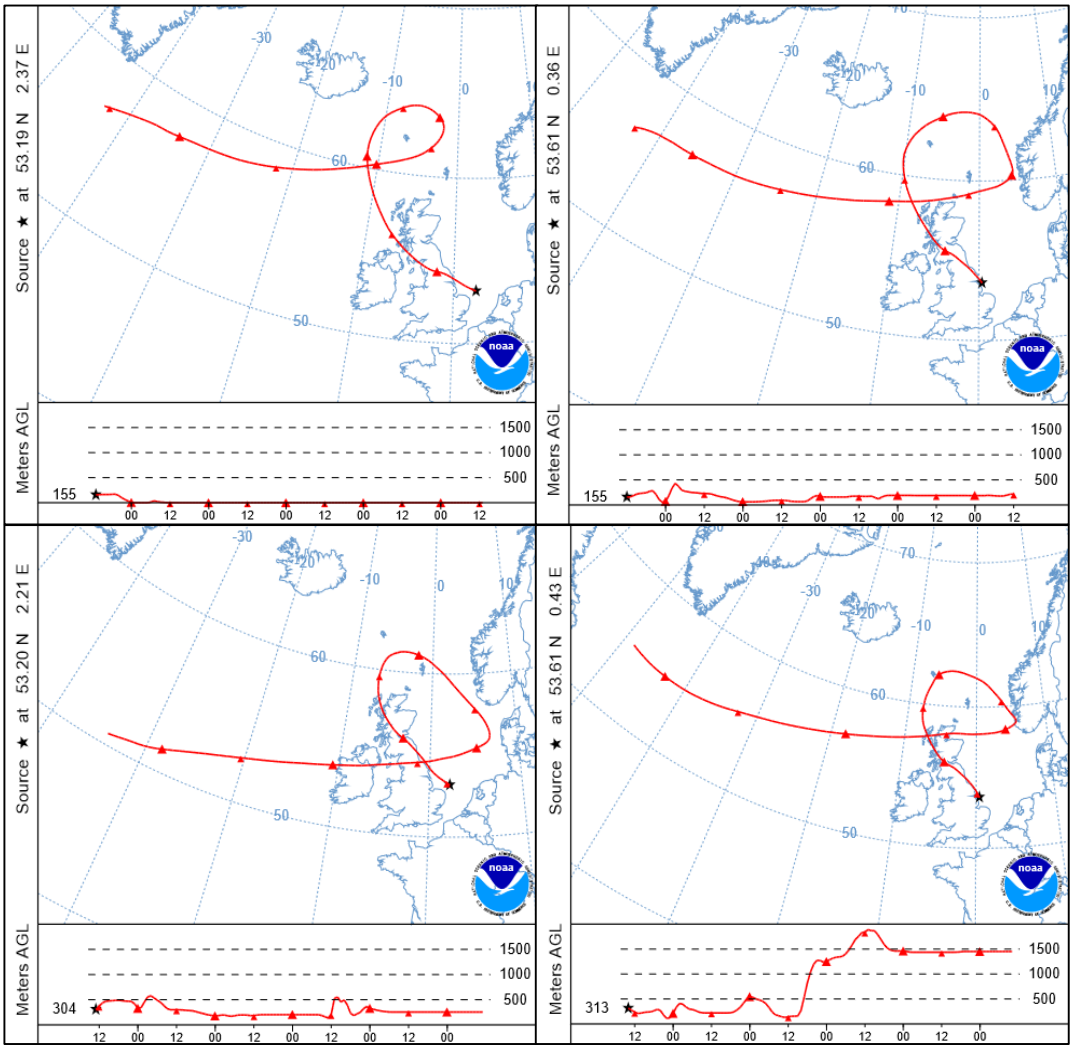

Figure 4.44: 5-day back trajectories for flight B908

As can be seen in **Figure 4.44** above, the air remained at altitudes of 600 metres and below over the course of its trajectory, thus meaning it would be greatly influenced by pollution from the surface. The trajectories of the air parcel sampled, particularly at the start and end of the flight, did not show a great amount of difference, i.e. the air mass sampled during the flight was likely to have the same, if not, very similar chemical composition. They all suggest

that the air parcel initially came from a “clean” maritime atmosphere, with very few, if any, NO_x sources around. However, the air parcel then travelled over the UK, thus increasing the mixing ratio of NO_x present. As a result, these changes in background mixing ratios were most likely a consequence of local NO_x sources, namely nearby rigs and ships, which could have contributed additional NO_x to the air parcel during the flight.

Flight B910

As with flight B908, the mean background NO_x mixing ratio was found to fluctuate during the B910 flight. As can be seen in the histogram (**Figure 4.45**), two Gaussian curves give two mean background mixing ratios of 43 and 198 pptv, with small 1σ standard deviations of 31 and 61 pptv, respectively.

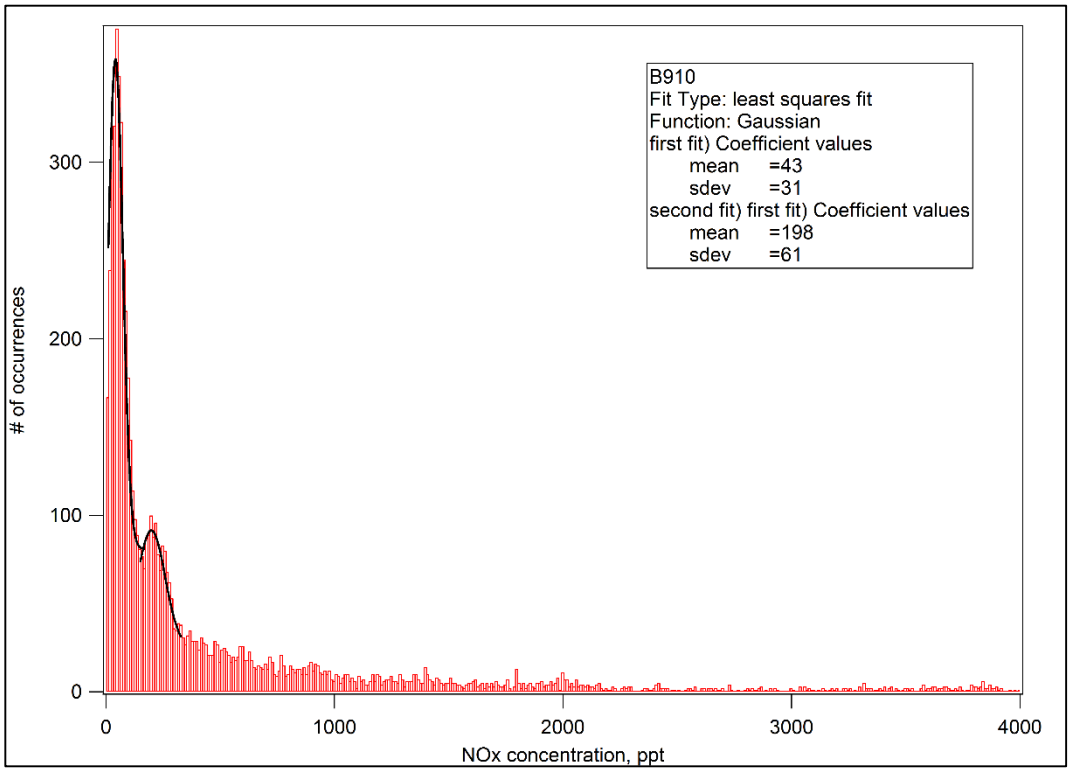

Figure 4.45: Histogram showing the distribution of NO_x data from flight B910

As with flight B908, the back trajectories of the air sampled during flight B910 can provide an insight into the reasons behind the variability in the background mixing ratios. These are shown in **Figure 4.46**.

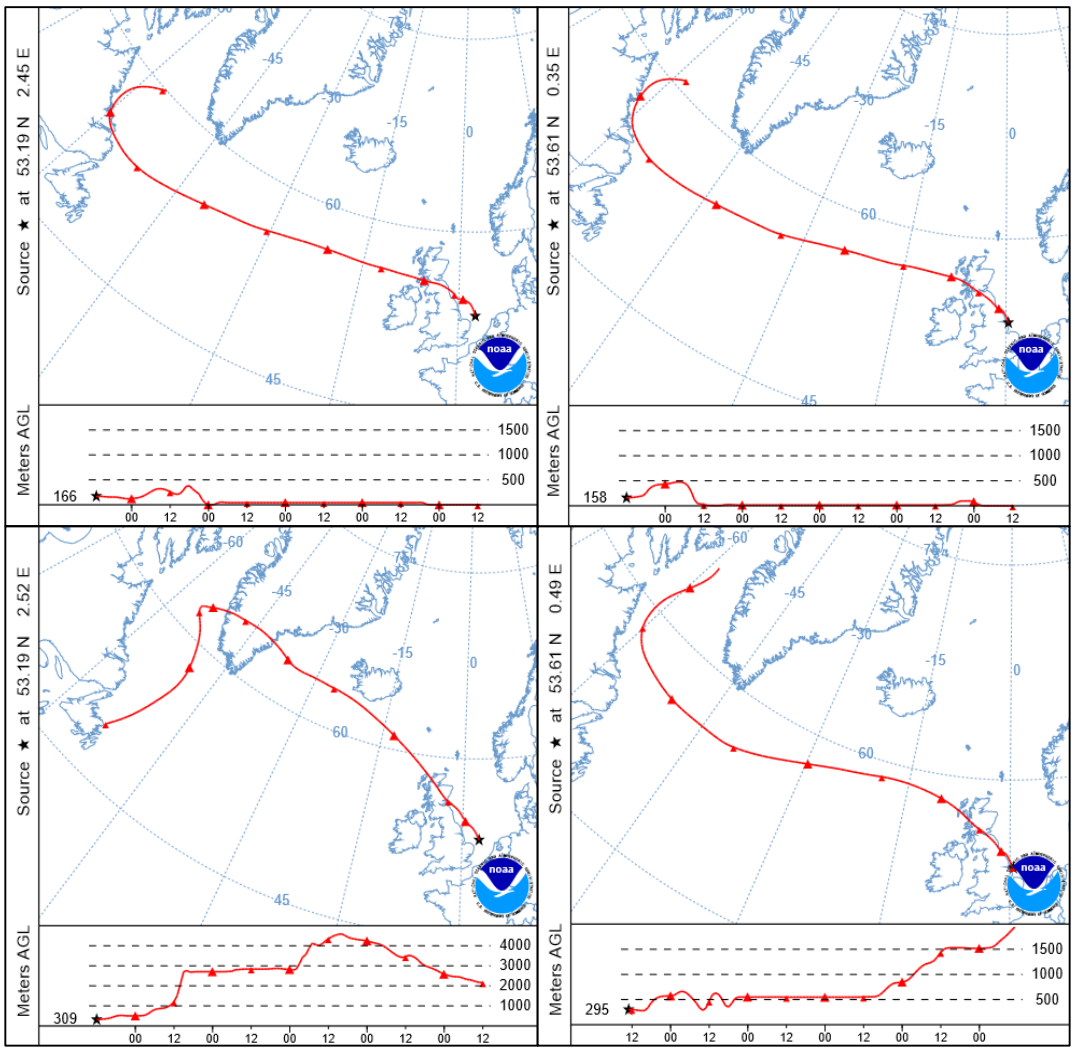

Figure 4.46: 5-day back trajectories for flight B910

The trajectories associated with flight B910 show that the air masses sampled over the course of the flight were likely to have been the same or extremely similar in terms of background NO_x mixing ratios. All four trajectories indicate that the air parcel was initially part of the typical marine boundary layer, containing minimal amounts of NO_x. This boundary layer signature would then have been altered, however, as the air crossed over the UK at altitudes of around 1000 metres and below, i.e. in the boundary layer, thus accumulating NO_x emissions from the surface. As with B908, this therefore does not explain why variations in background mixing ratios were observed. It does, however, support the findings regarding the background mixing ratios themselves. Similar trajectories were found for flight B908, meaning similar background mixing ratios may have been expected for B910. However, the wind speed was much lower for this flight (as discussed earlier), thus meaning that it is likely that reduced amounts of NO_x reached the flight track (and were subsequently detected),

compared with flight B908. The changes in background mixing ratios observed during flight B910 were therefore most likely a thought to be a result of emissions from local NO_x sources, namely nearby rigs and ships, as was found for flight B908.

Flight B912

The histogram of the background NO_x data from the entire flight (**Figure 4.47**), gave a mean background NO_x mixing ratio of 110 pptv, with a small 1σ standard deviation of 60 pptv.

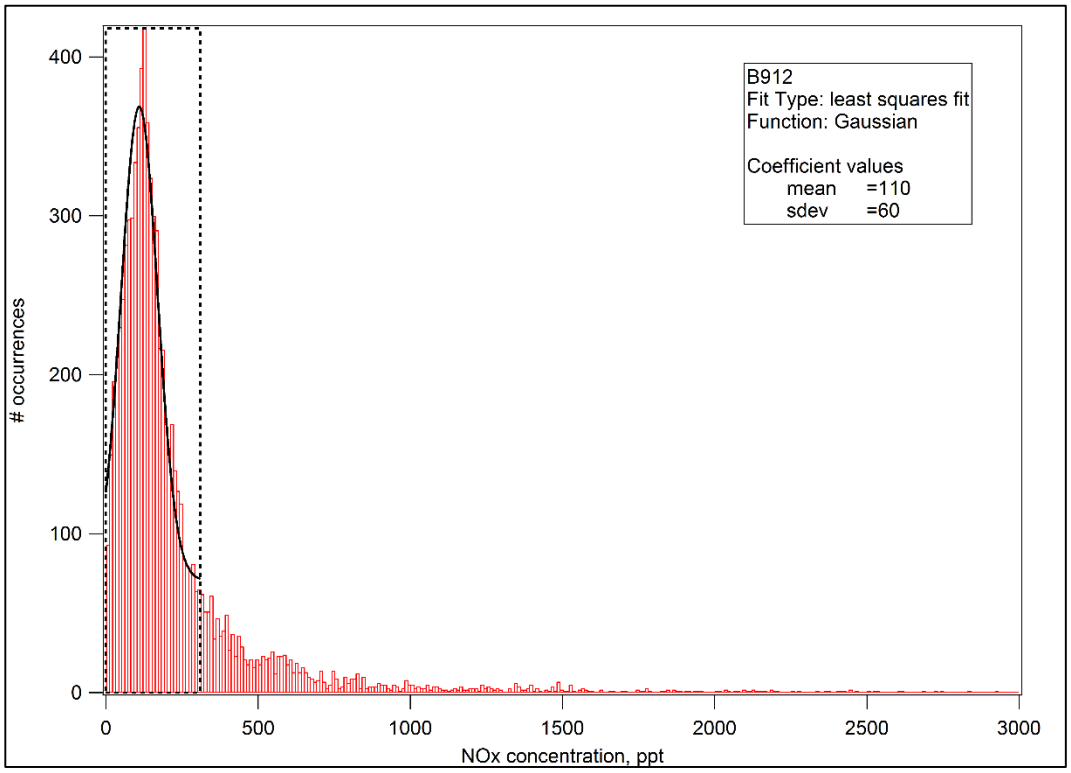

Figure 4.47: Histogram showing the distribution of NO_x data from flight B912. The dashed box represents the data used for the Gaussian fit

Such a small standard deviation gives assurance that the data is in fact, representative of the background atmosphere, as the data is tightly clustered around the lower levels, with minimal occurrences of high NO_x mixing ratios. This therefore shows that the majority of the peaks measured during the flight were likely from oil and gas rigs, as there are no plume peaks present in the background data shown in the histogram.

The mean background mixing ratio itself is much lower than most of those seen in other flights in this region of the North Sea. The back trajectories associated with the air mass sampled during this flight look quite different compared to those of flights B907 and B908. These are shown in **Figure 4.48**.

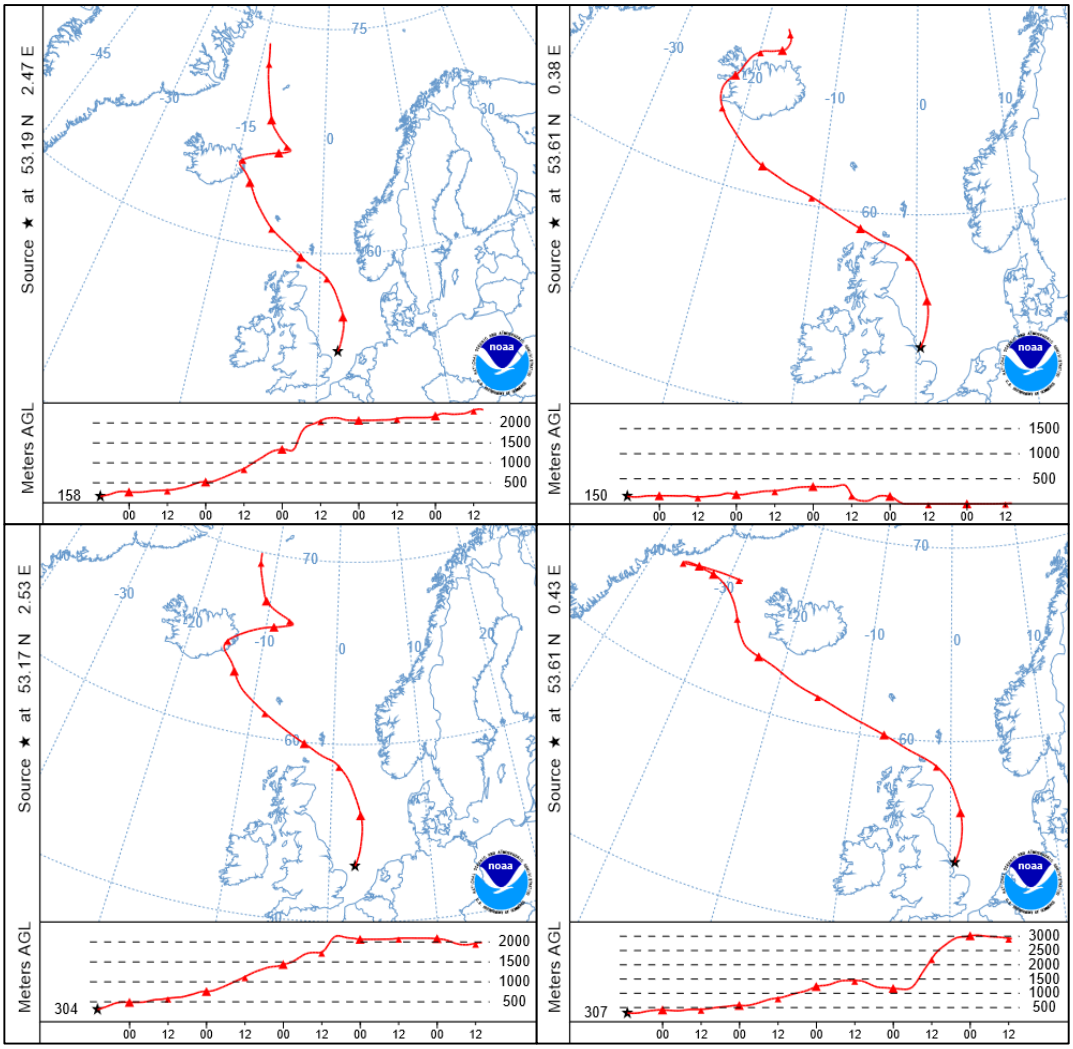

Figure 4.48: 5-day back trajectories for flight B912

All of the trajectories show that the air sampled during flight B912 was representative of the marine boundary layer, with minimal influence from the UK. This is due to the fact that, rather than crossing over the UK, the air mass instead travelled southwards over the North Sea, which meant that minimal amounts of NO_x would be introduced into this background air. This is confirmed by the low mixing ratio of background NO_x (110 pptv) that was measured during the flight. This background measurement was similar to that measured in flight B910 (**Figure 4.45**). This flight sampled air which had travelled over the UK in the

boundary layer before reaching the North Sea, meaning that the background NO_x measurements should have been much higher than those measured during flight B912. The similarity of the background measurements in these two flights is therefore likely to be a result of ships and rigs raising the NO_x levels in flight B912, but could also simply be due to the air in flight B910 passing over a non-polluted area of the UK, resulting in lower background NO_x levels than expected.

Flight B913

The histogram of the NO_x data from the entire flight (**Figure 4.49** below) gave a mean background NO_x mixing ratio of 95 pptv, with a 1σ standard deviation of 52 pptv.

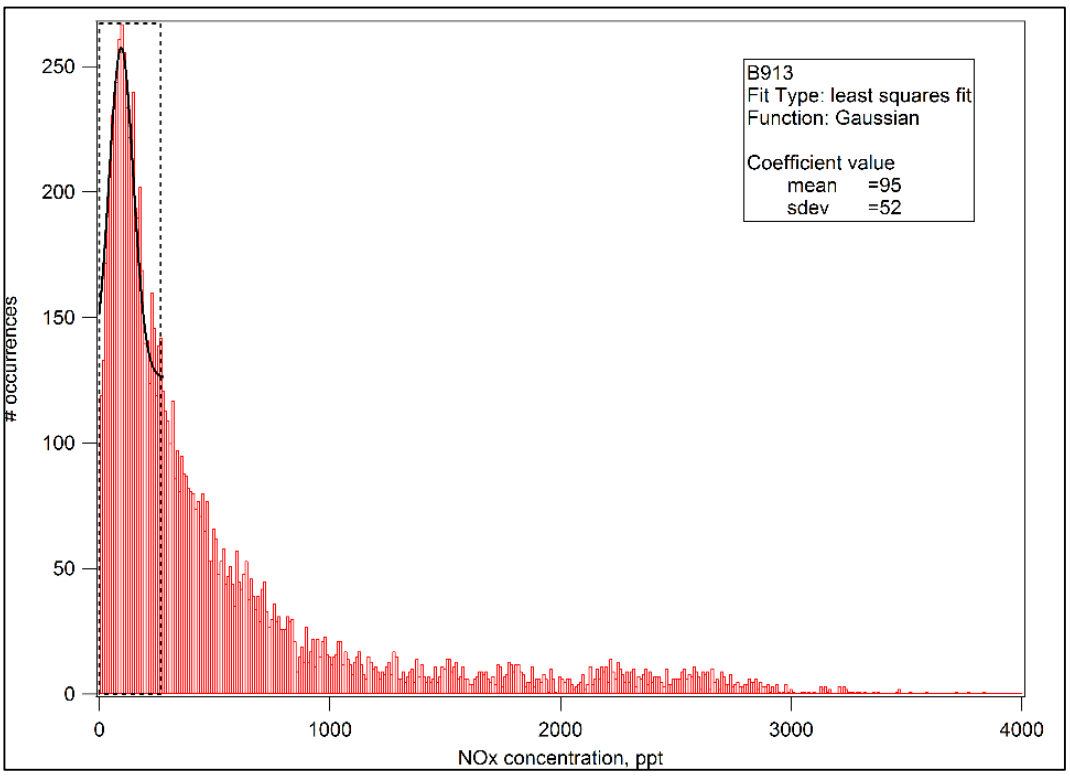

Figure 4.49: Histogram showing the distribution of NO_x data from flight B913. The dashed box represents the data used for the Gaussian fit

As can be seen in the histogram, the majority of the data is confined to lower level, with very few incidents of elevated NO_x mixing ratios. This provides assurance that the data shown is representative of the background atmosphere, whilst the distinct lack of high NO_x mixing

ratios proves that the majority of the peaks observed during the flight were coming from the oil and gas rigs.

The average mixing ratio of NO_x in this background air was found to very low, at 95 pptv. The reasons for this can be related to the back trajectories of the air sampled during the flight, which are shown in **Figure 4.50**.

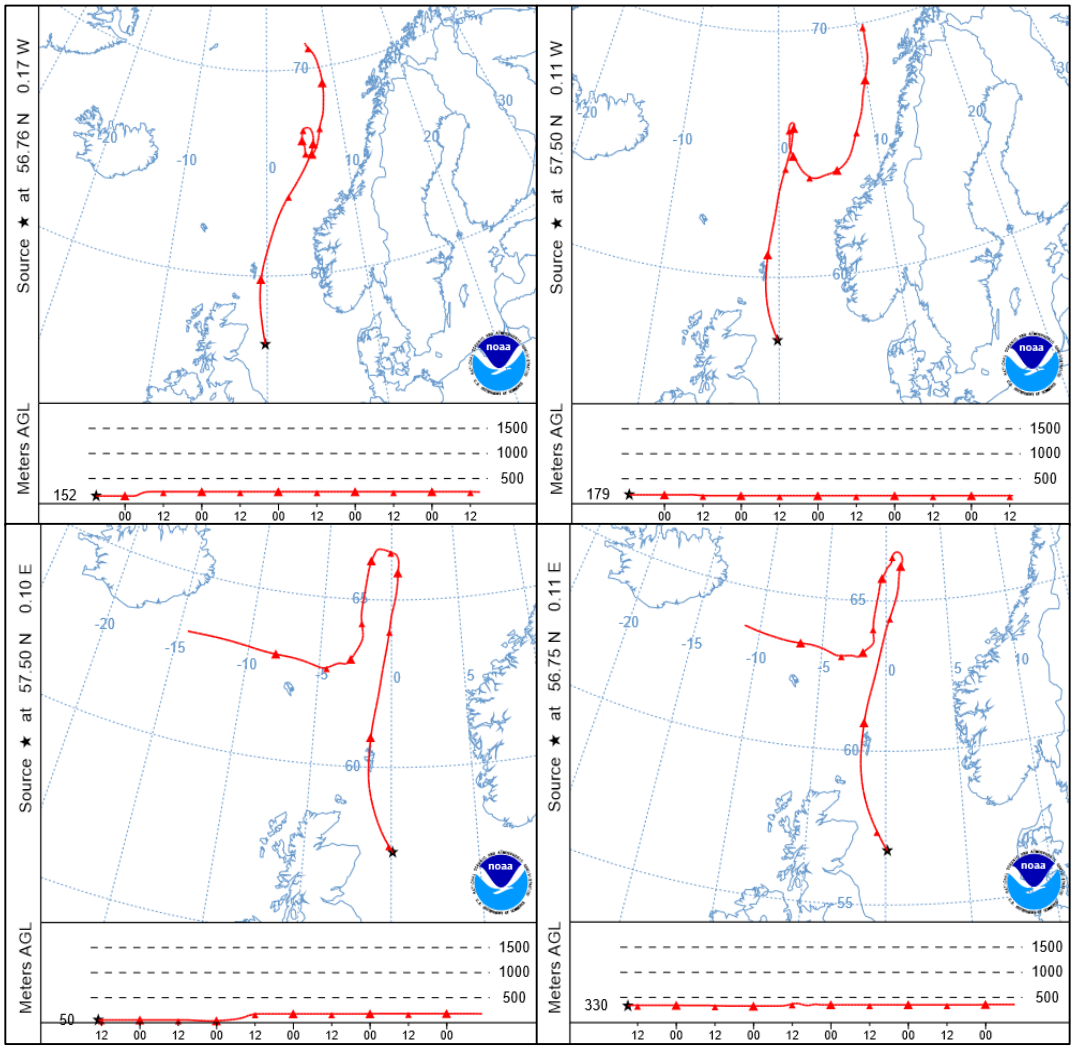

Figure 4.50: 5-day back trajectories for flight B913

The trajectories for the air mass sampled during flight B913 are all extremely similar, showing that the background mixing ratio measured was likely to be a good representation of the entire flight. The trajectories indicate very minimal influences from high areas such as the UK, with the air parcel therefore likely to have the typical low NO_x mixing ratios associated with marine boundary layer air, remaining at altitudes of around 500 metres and below over the course of the flight. This was indeed found to be the case, as, when sampled in the northern sector of the North Sea, the background air was found to only contain very low mixing ratios of NO_x (96 pptv).

Flight B918

The mean background NO_x mixing ratio over the course of flight B918 was found to be 367 pptv, through plotting of the histogram shown below. The standard deviation of the data was calculated to be 67 pptv.

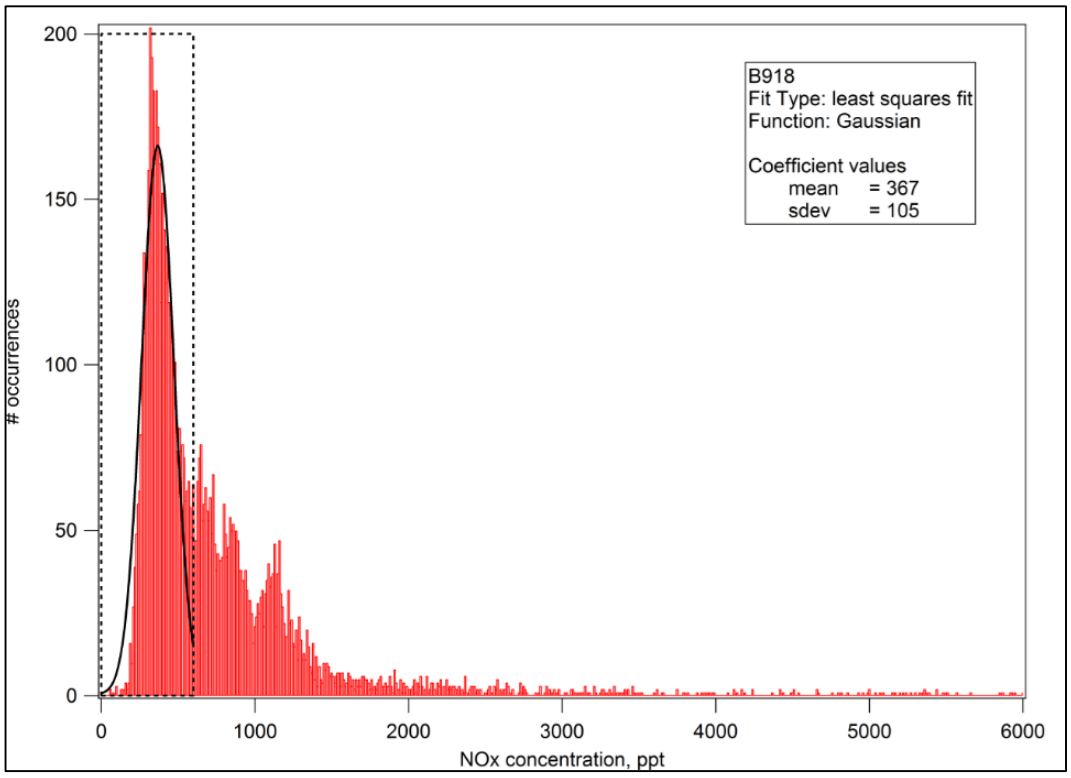

Figure 4.51: Histogram showing the distribution of NO_x data from flight B918. The dashed box represents the data used for the Gaussian fit

Although in a very similar location to flight B913, in the northern sector of the North Sea, the background NO_x mixing ratios measured in the two flights are considerably different. Flight B913 saw an average background mixing ratio of 95 pptv, whereas, for flight B918, this was found to be almost 300 pptv higher, at 367 pptv. This may be a result of different air masses sampled in the two flights, this being a consequence of the back trajectories. The trajectories associated with the air mass sampled during flight B918 can be seen in **Figure 4.52**.

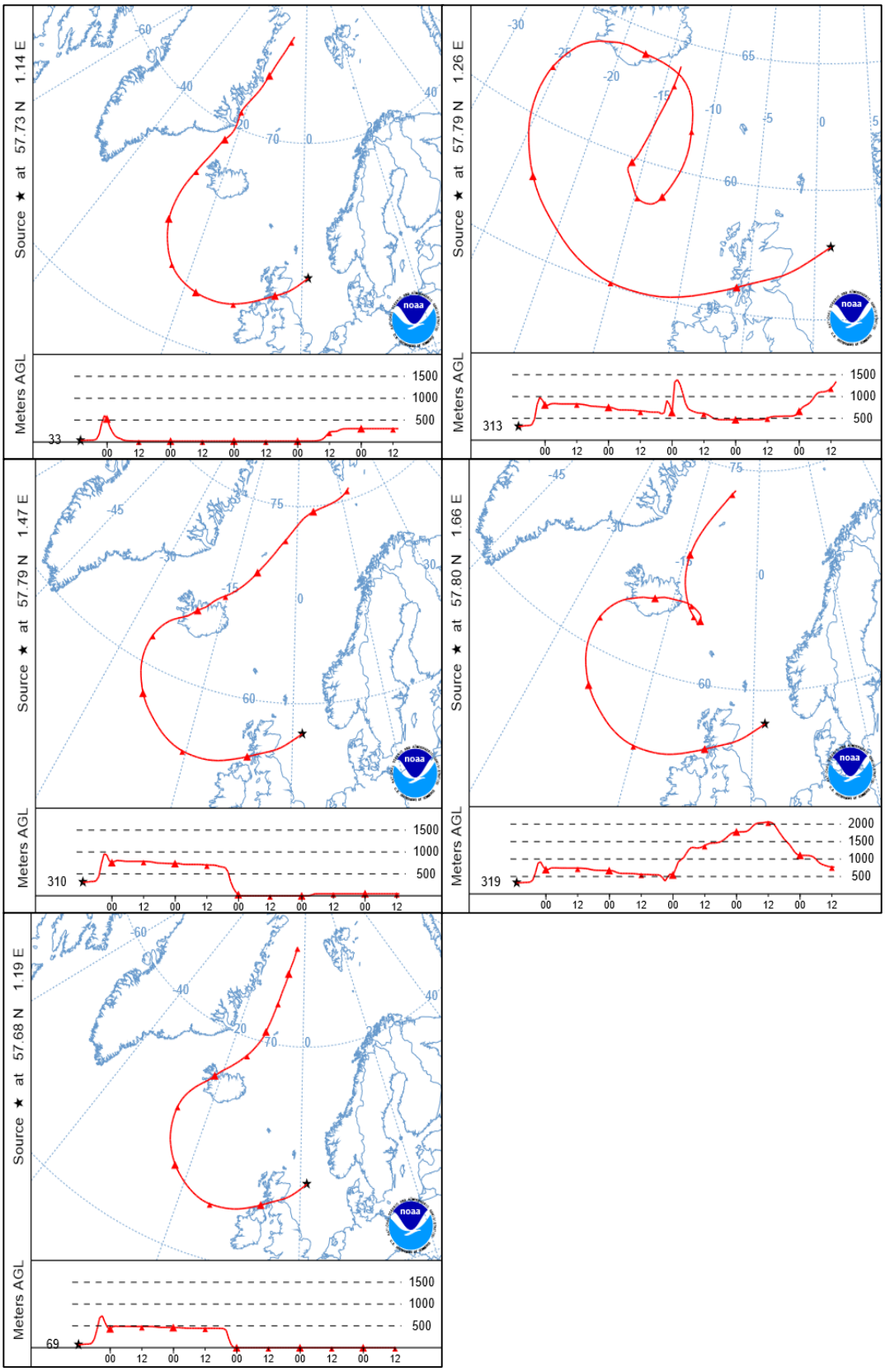

Figure 4.52: 5-day back trajectories for flight B918

The trajectory plots associated with flight B918 show a distinct difference to those constructed for flight B913 (**Figure 4.50**). Both air masses begin in the North Atlantic Ocean, in low- NO_x conditions which are typical of the marine boundary layer. However, the key difference is that the air sampled during flight B918 passes over the northern UK at altitudes of between 500 and 1,000 metres (i.e. within the boundary layer), thus accumulating NO_x emissions from UK-based sources such as road transport and industry. This consequently means that this additional NO_x is then transported in the forward trajectory of the air parcel, thus resulting in the observed higher background NO_x mixing ratios by the time it reaches the North Sea.

Summary of Background NO_x Mixing Ratios

The average background NO_x mixing ratios measured for each of the flights, along with the respective 5-day back trajectories are shown in **Table 4.4** below.

Table 4.4: Summary of background NO_x mixing ratios and back trajectories for all "Oil and Gas" flights

Flight Number	North Sea Sector	Mean background NO_x mixing ratio / pptv	1σ Standard deviation / pptv	5-day Back trajectory
B907	Southern	414.77	589.73	Originates in the north Atlantic Ocean, with passage over the northern UK.
B908	Southern	127 872	83 70	Originates in the mid-Atlantic Ocean, then travels over the northern UK.
B910	Southern	43 198	31 61	Originates in western Atlantic Ocean, with passage over the northern UK.
B912	Southern	110	60	Originates in the northern Atlantic Ocean, then travels southwards over the North Sea. No passage over the UK.
B913	Northern	95	52	Originates in the northern Atlantic Ocean, then travels southwards over the North Sea. No passage over the UK.
B918	Northern	367	105	Originates in the northern Atlantic Ocean, with passage over the northern UK.

The background NO_x mixing ratios measured over the course of the “Oil and Gas” campaign could generally be explained by their respective back trajectories. The lowest mixing ratios were observed for the two survey flights in which the air mass sampled had not been influenced by UK-based NO_x emissions. These two flights were B912 and B913 and, as seen in **Table 4.4**, although the flights took place in different sectors of the North Sea, both showed very similar, low background NO_x mixing ratios as a result of their similar back trajectories.

Higher background mixing ratios were measured during the remaining survey flights, all of which measured in air masses which had experienced some influence from the UK. For example, the average background NO_x mixing ratio measured in flight B908 was 872 pptv. The air sampled during this flight had travelled over the UK before reaching the North Sea. This explains why the average background mixing ratio was over 700 pptv higher than flight B912, despite both flights taking place in the same sector of the North Sea.

These background mixing ratio measurements were necessary as they show a lot of variation depending on the back trajectory of the air mass. Measuring the background mixing ratios was also needed in order to measure any NO_x enhancements coming from the rigs.

4.4 Evaluation of NAEI Estimates for Oil & Gas NO_x Emissions in the North Sea: The Direct Integration Method

4.4.1 Background to the NAEI

The inventory used for emissions estimates in the UK is the NAEI. As discussed earlier in the chapter, the inventory compiles estimates of atmospheric emissions from UK sources, such as vehicles, power stations and on- and off-shore oil and gas platforms. Research campaigns have been conducted in the past to assess the accuracy of the inventories by comparing the point source estimates to their measured emissions, with a notable discrepancy observed for NO_x emissions from traffic sources.[94] This has emphasised the need for continued measurements in and around the UK in order to assess the inventory estimates, as these provide a basis for reducing the impact of human activities on the environment and our health.

4.4.2 Calculation of Emissions: Direct Integration Method

The direct integration method is a useful analytical approach which is used to quantify the mass flux of a particular species in a gas plume. This method was used by Ryerson et al. (1998)[95] in order to investigate the emissions lifetimes of species within power plant plumes. The flux of a species can be calculated across a theoretical plane which is perpendicular to the wind direction and is defined by the transect of the aircraft. The flux, in units of kilograms per second (kg s^{-1}), is therefore derived, according to the equation:

$$\text{flux} = \nu \cos(\alpha) \int_0^z n(z)\, \partial z \int_{-y}^{y} X_m\,(y)\, \partial y \qquad \textit{Equation 4.1}$$

Where:

ν = a constant, uniform wind speed

α = the angle between the aircraft track and the direction normal to wind direction

n = atmospheric number density

X_m = measured mixing ratio enhancement for species, m, integrated over the observed plume

z = vertical coordinate

y = cross-wind coordinate

The direct integration method assumes that the plume is well mixed in the vertical within the marine boundary layer. The study by Ryerson et al. (1998)[95] involved integrating the transects of the plumes over successive distances downwind of the source (i.e. the power plant), which accounted for this vertical mixing of the plume within the marine boundary layer. This was done by measuring the total amount of a particular species in the boundary layer at each transect, the value of which would have been a result of the gas plume being present.[96]

The surface layer height is therefore an extremely important parameter when using the direct integration method. As part of the vertical dimension (i.e. the "z" term in **Equation 4.1**), this defines the area in which the emissions from the rigs are confined. As discussed earlier in the chapter, this height can be derived using the vertical profiles of potential temperature, dew point temperature and relative humidity.

Potential Temperature

Potential temperature is a parameter which is more dynamically important than temperature, particularly when looking at the atmospheric vertical profile. It is not affected by processes such as evaporation, condensation, heating or cooling, as temperature is. For example, as a parcel of air moves over an obstacle (a small mountain, for example), it will expand and cool on ascension. Then, as it descends the other side of the mountain, it will then compress and warm again. Potential temperature accounts for the impact of air pressure, thus making it possible to compare potential temperatures at different altitudes. It is defined as the temperature that a parcel of air would acquire should it be adiabatically brought to a standard reference pressure, p_0, (usually 1,000 millibar). It is calculated using **Equation 4.2**. The equation involves the Poisson constant, κ. This refers to the ratio of the gas constant to the specific heat capacity at constant pressure. For air, the value typically used for this constant is 0.285.[97]

$$\text{Potential Temperature } (\theta) = T \times \left(\frac{p_0}{p}\right)^{\kappa}$$ ***Equation 4.2***

Where:

T = current absolute temperature of the air parcel (K)

P_0 = standard reference pressure (1000 mbar)

P = original pressure of parcel before raising or lowering the parcel to standard pressure (mbar)

κ = Poisson constant

The potential temperature can be used as an indicator of the stability of the unsaturated atmosphere. Under normal conditions, potential temperature typically increases with altitude, thus suppressing vertical motion. However, the atmosphere can become unstable with respect to vertical motions, thus causing convection. In this case, the potential temperature decreases with altitude. This convection can cause cloud formation, as discussed earlier in the chapter. Hence, it is possible to use the vertical profile to infer where the cloud base is, as this will be the point at which the vertical motion (i.e. the turbulence), is inhibited due to the temperature inversion at the top of the surface layer. The vertical profile of potential temperature for flight B918 is shown in **Figure 4.53**.

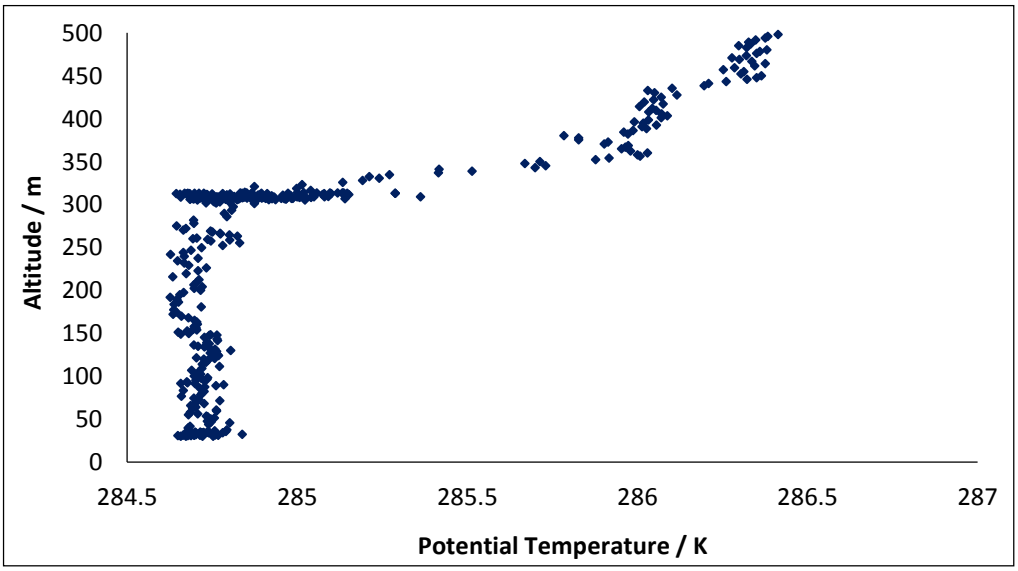

Figure 4.53: Potential temperature vertical profile for flight B918

Figure 4.53 shows a distinct "layer" at an altitude of approximately 310 metres. This is likely to be the altitude at which a temperature inversion is occurring, thus causing convection and cloud formation. This plot therefore infers a cloud base, and therein, a surface layer height of approximately 300 metres. However, the vertical profiles of other parameters, namely dew point temperature and the humidity, need to be considered for one to be confident in the inferred surface layer height.

Dew Point Temperature & Specific Humidity

The dew point temperature and the specific humidity of the air can provide a great amount of insight into the cloud base height, due to their direct link to cloud formation.

The dew point temperature is a measure of the moisture in the atmosphere. It is defined as the temperature at which water vapour condenses at the same rate at which it evaporates, in a sample of air at constant pressure, i.e. the point at which the air reaches saturation. Typically, saturation is reached via the vertical movement of air from the surface into the atmosphere. Cloud formation occurs when the air is cooled below this point of saturation. Once the air parcel has risen through the atmosphere and has reached saturation temperature (i.e. the air is at 100% relative humidity), condensation of the water vapour onto cloud condensation nuclei occurs. This leads to cloud droplet formation. More droplets form, and hence the cloud forms and grows when more condensation than evaporation is occurring. During the flights, the dew point temperature was measured using the General Eastern GE 1011B Chilled Mirror Hygrometer, details of which can be found on the "Science Instruments" page on the FAAM website (http://www.faam.ac.uk/index.php/faam-documents/science-instruments/).

The specific humidity is the ratio of water vapour mass to an air parcel's total (including dry air) mass. The formation of a cloud only occurs once the air has become saturated with water vapour, and has then been cooled, resulting in condensation. This was measured using the Total Water Content (TWC) probe. The principle of operation for this instrument is described by S. Nicholls et al. (1990).[98]

Hence, the cloud base height can be inferred as the altitude at which there is a distinct increase in both the dew point temperature and in the water specific humidity of the air.

Figure 4.54 and **Figure 4.55** show the vertical profiles of the dew point temperature and total water specific humidity from flight B918.

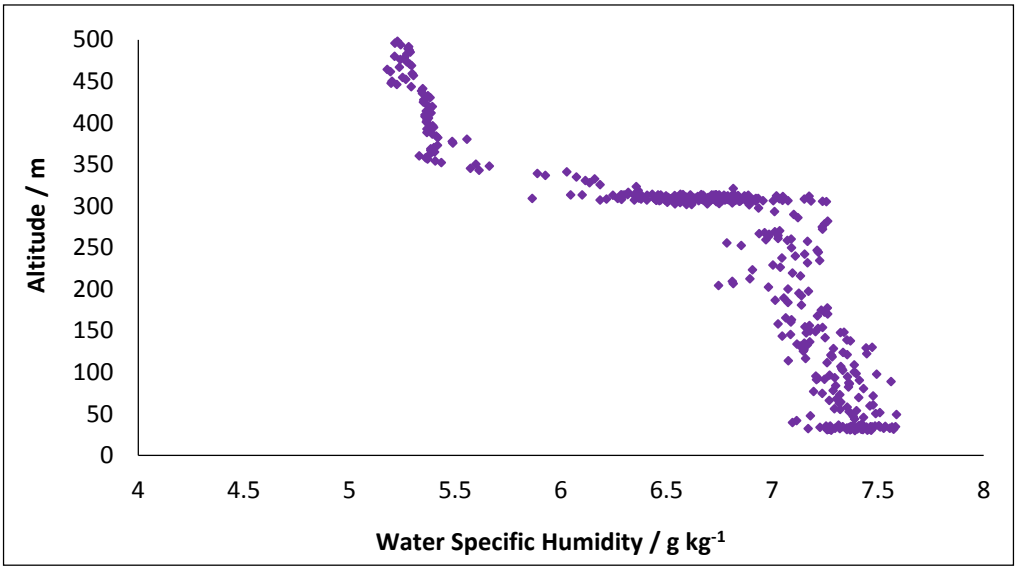

Figure 4.54: Total water specific humidity vertical profile for flight B918

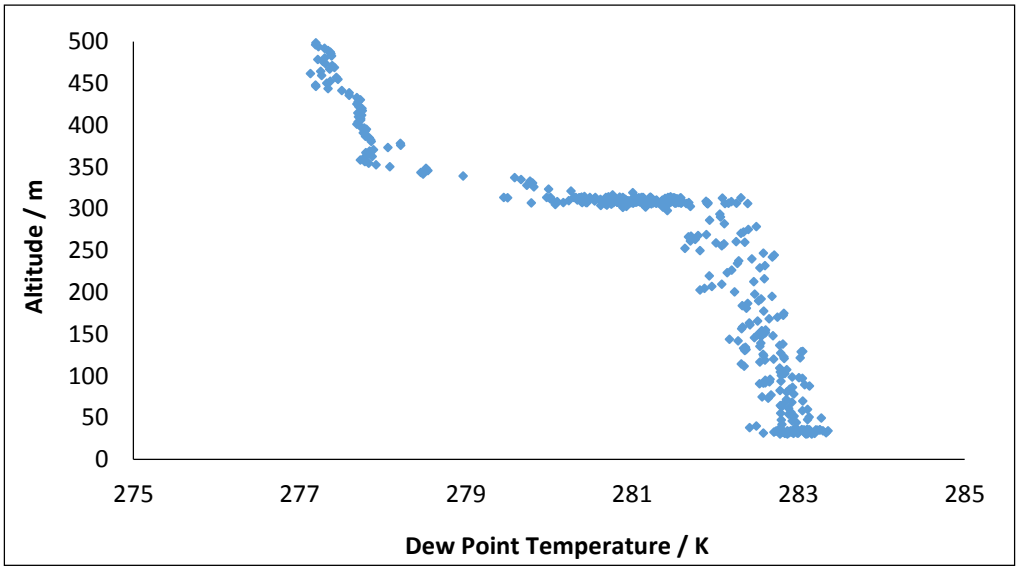

Figure 4.55: Dew point temperature vertical profile for flight B918

As can be seen above, the potential temperature, dew point temperature and humidity all support a proposed surface layer height of around 310 metres for flight B918. The number was then applied to **Equation 4.1** and used to calculate NO_x emissions via the direct integration method.

4.4.3 Using the Direct Integration Method to Calculate NO_x Emissions from the Forties and Nelson Rigs in the North Sea

The direct integration method was used to calculate the NO_x emissions from a specific set of rigs in the northern sector of the North Sea. Although many flights had taken place around the active drilling areas of the North Sea, it was extremely difficult to link plume peaks to specific rigs. This was due to the fact that the sheer number of rigs surrounding the flight track meant that it was likely that many of the plumes were accumulations of emissions from several rigs. Flight B918, however, was used to focus in on a specific set of rigs, namely the Forties and Nelson rigs in the northern sector of the North Sea. Inventory data from 2014[99] indicated that no emissions were coming from the Forties Bravo or the Forties Echo rigs, suggesting that they were not active. As a result, only emissions from the Forties Alpha, Forties Charlie, Forties Delta and Nelson rigs were calculated using this technique.

As discussed previously, the direct integration method can only be applied to plumes which are well-mixed in the vertical. As with Ryerson et al. (1998)[95], the plumes measured during flight B918 were integrated over successive distances downwind of the rigs. Multiple transects comprising of multi-altitude runs were conducted over the course of the flight, thus accounting for the vertical mixing. These runs, along with their respective altitudes are shown in **Table 4.5.** Many peaks were observed in similar locations along each run within a particular transect. The integrated areas of these peaks were often very similar, despite being detected when flying at different altitudes. This was observed up to the surface layer height, thus demonstrating that the plumes were well mixed in the vertical. Examples of such peaks from flight B918, with their respective altitudes and integrated areas, are shown in **Table 4.5** to demonstrate this.

It was then possible to use the flight track plots to attribute certain plume peaks to a particular rig, using the average mean wind direction measured during the flight (246.488°). It should be noted, however, that runs 10 and 11 were not incorporated into the calculations,

as these flight legs occurred at altitudes above the surface layer height, meaning that any peaks observed were unlikely to be from the rigs.

Table 4.5: Flight runs and integrated plume peak areas measured during flight B918. Integrated areas were not available for the corresponding peaks observed in runs 3, 6 and 14 as these peaks were not sufficiently discernible to provide accurate results.

Transect	Run	Altitude / m	Integrated Area of Peak / pptv-secs
1	3	30.5	Not available
	4	76.2	11.27
	5	152.4	9.39
	6	304.8	Not available
2	7	304.8	88.07
	8	152.4	52.39
	9	76.2	33.94
3	12	304.8	101.05
	13	228.6	83.19
	14	152.4	Not available
4	15	152.4	13.40
	16	228.6	14.80
	17	304.8	14.27
5	19	91.4	150.31
	20	61.0	166.37

The plume peaks seen in the transects, with respect to the rig positions and wind direction are shown in **Figure 4.56** below.

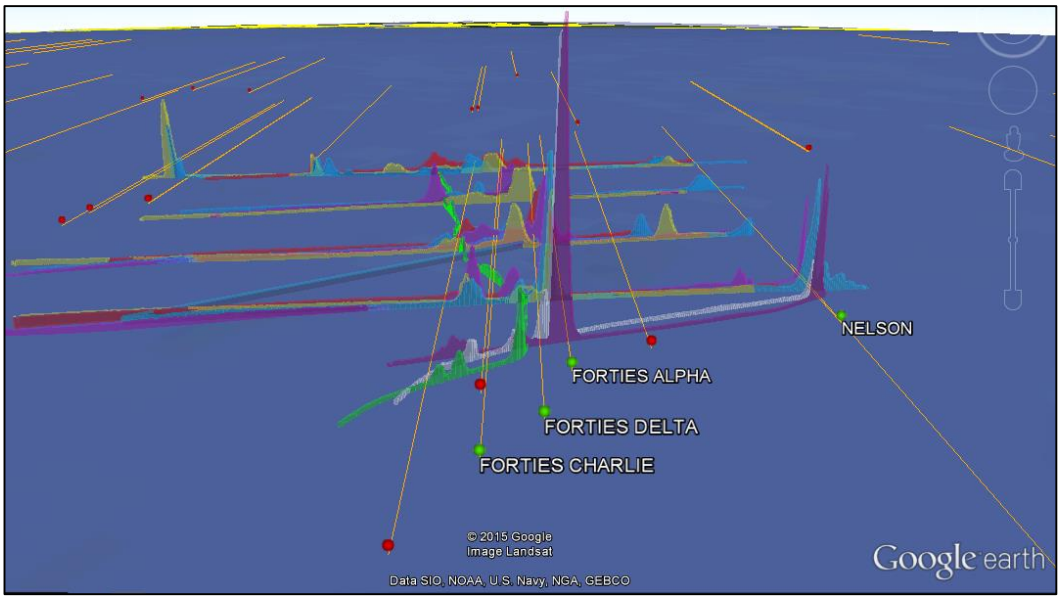

Figure 4.56: NO_x plume peaks measured during flight B918. The vertical lines represent the wind direction (247°). Credit for this figure goes to Axel Wellpott at the Facility for Airborne Atmospheric Measurements (FAAM) in Cranfield, UK

Although a large number of plume peaks were observed during the flight, a few of them were not not very well characterised, i.e. they could be due to several rigs. Only the peaks which could be directly attributed to one of the four rigs in particular could be integrated to derive an average flux. For example, the large peak in the run nearest to the rigs was seen when the plane was directly downwind of the Forties Alpha rig. The plume peaks were then grouped according to their source (i.e. one of the four rigs), and were using the "OriginPro 8" software to derive the peak areas. A flux was then calculated for each plume peak, by pooling together all of the required respective parameters shown in **Equation 4.1**. It should be noted that the background mixing ratios used to measure "X_m" (i.e. the mass molar ratio enhancement) were those measured outside each plume, thus accounting for the variability of the background mixing ratios during the flight. The averaged fluxes for each rig were then calculated by averaging the fluxes associated with each plume peak. The units associated with the derived flux were in kilograms per second. These were converted into units of tonnes per year, in order to enable direct comparison with NAEI emissions estimates.

It was then possible to compare the average measured NO_x emissions associated with each rig to the respective NAEI estimates, through extraction of the emissions data extracted from the NAEI website.[99] As describing in the introduction to this chapter, there are many

processes taking place on oil and gas rigs which emit NO_x into the surrounding atmosphere. The NAEI takes this into account by listing the emissions estimates not only in terms of total NO_x, but it also breaks them down into the different source sectors, namely fuel consumption and gas flaring. These can then be compared to the averaged measured NO_x emissions for each rig, and scaled up in order to assess to accuracies of the estimates for NO_x emissions in the entire North Sea. The relationship between the estimated and measured NO_x emissions for the Forties and Nelson rigs targeted during the flight are shown in **Table 4.6** and **Figure 4.57** below.

Table 4.6: Comparison of estimated and measured NO_x emissions from the Forties and Nelson rigs

	Forties Alpha	**Forties Charlie**	**Forties Delta**	**Nelson**	**Total**
Estimated NO_x emissions / tons per year	570.85	613.66	242.75	341.00	1768.26
Average measured NO_x emissions / tons per year	1414.48	437.78	427.20	912.60	3912.06

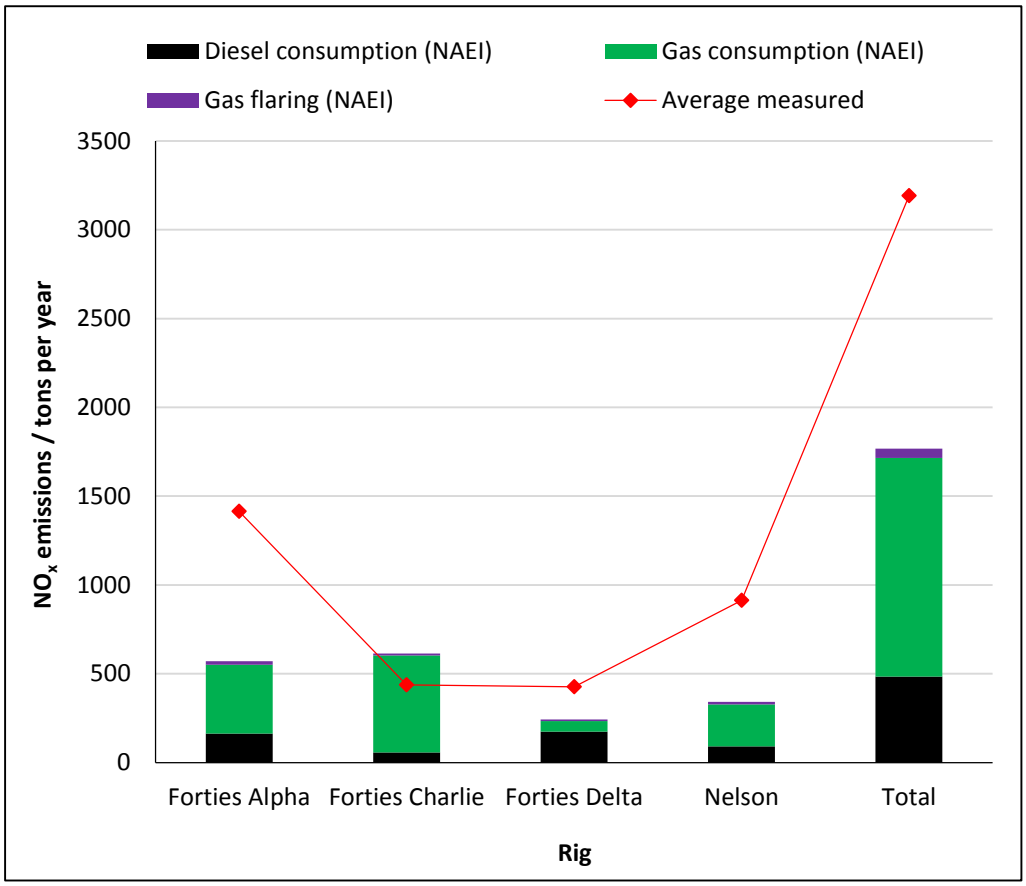

Figure 4.57: Comparison of estimated and measured NO_x emissions from the Forties and Nelson rigs

As can be seen in **Figure 4.57** and **Table 4.6**, there is no uniform relationship between the NAEI emissions estimates and the measured emissions that is seen for all four rigs. However, one feature which is common to all four of the rigs is that the majority of their NO_x emissions come from fuel consumption, whether it be diesel or gas, which is required to run the turbines. Although some is produced from gas flaring, it can be seen on **Figure 4.57** that this is minimal in comparison to diesel and gas consumption.

Several observations can be made regarding each individual rig. For example, where the emission measurements for the majority of the rigs are much higher than the NAEI estimates, the relationship is reversed when looking at the data from the Forties Charlie rig. Measurements from this rig were found to be around 40% lower than the NAEI estimates, as shown in **Figure 4.57**, and also showed the best agreement between measured and estimated NO_x emission data. The reasoning behind this observation could be to do with the source of the majority of the NO_x for this rig. Inventory data for the Forties Alpha, Forties Charlie and Nelson rigs shows that the highest proportion of NO_x is emitted from gas consumption, which occurs through the running of the gas turbines on the rigs. However, this proportion is the highest for the Forties Charlie rig, at 89.02% (compared to 67.92 and

69.53% for the Forties Alpha and Nelson rigs, respectively). This is also significant when looking at the Forties Alpha and Nelson rig measurements, and their comparisons to NAEI estimates. The source contributions of these two rigs are relatively similar, each predominantly emitting NO_x through the operation of gas turbines. Another similarity between the Forties Alpha and Nelson rigs is that their average measured NO_x emissions both greatly exceed the inventory estimates, being 2.5 and 2.7 times higher, respectively.

All of these observations regarding the Forties Alpha, Forties Charlie and Nelson rigs appear to be under-pinned by the proportion of NO_x emitted through the operation of gas turbines. As can be seen in Figure and Table, all of the rigs except Forties Charlie have underestimated the NO_x emissions. This could be because this rigs has a larger proportion of its NO_x coming from gas turbines, compared to the Forties Alpha and Nelson rigs, which also run on gas turbines. This may be due to these turbines being better represented by the NAEI, thus resulting in a better agreement between measured and inventory data. It also suggests that there may be some differences in the operation of these turbines on each of these rigs, i.e. there may be more turbines, or they may be running at higher power on this rig, compared to the other two.

The Forties Delta rig, according to the NAEI data, should emit the least amount of NO_x out of the four rigs used for this study (see **Figure 4.57**). This inventory prediction was corroborated by the average emissions measured during the flight. The operation of this rig appears to be slightly different, compared to the other three, particularly in the type of turbines used. According to the inventory data, the majority of the NO_x emitted by the Forties Delta rig comes from diesel consumption through the operation of the turbines, whereas, on the other three rigs, the turbines are predominantly powered by gas. The lower total NO_x emissions from the Forties Delta rig can therefore be attributed to the use of diesel, as opposed to gas turbines. This could therefore lead to further speculation surrounding oil and gas rigs in general, suggesting that NO_x emissions from these sources could be reduced through alteration of the rig infrastructure. However, the type of turbine does not make a difference when comparing the inventory estimates to the average measured emissions from the Forties Delta rig. As with the Forties Alpha and Nelson rigs, the measured NO_x emissions greatly exceeded the inventory estimates, being approximately 1.8 times higher.

In summary, although a relatively good relationship was observed for the Forties Charlie rig, the majority of the data obtained suggest that the NAEI is severely under-estimating the NO_x emissions from the Forties and Nelson rigs in the North Sea. Both **Figure 4.57** and **Table 4.6**

show a large difference between the summed inventory estimates and measured data for the four rigs. The total measured data suggests that 1,423 tons of extra NO_x is being emitted into the atmosphere by these four rigs alone, compared to what the NAEI is predicting.

Limitations of the Study

There are errors and limitations with this type of study which must be considered. This study only involved analysis of data from a single flight, meaning that diurnal or seasonal changes in emissions were not taken into account. For example, the increased amount of fuel burning in colder winter months would mean that the demand for oil and gas would be higher, thus requiring an increase in activity (and subsequent increase in emissions) by the rigs compared to the milder times of year. It was also assumed that not only were all rigs in the North Sea operational, but that they were operating 365 days a year. This means that it is highly likely that the majority of rigs were misrepresented in the study, i.e. it was assumed that NO_x emissions are uniform across all North Sea rigs. Not all rigs in the North Sea operate in exactly the same manner as each other, meaning that their NO_x emissions are likely to differ.

In order to get a better understanding of emissions from North Sea rigs in the future, this direct integration method could be applied, by conducting regular, year-round survey flights around all oil and gas fields in the active drilling regions. Ensuring that all criteria for the direct integration are met (for example, the air being well mixed in the vertical), the method could then be used to calculate average emissions of all species by the rigs, and investigated further in terms of their seasonal variations and comparison to NAEI estimates. As discussed previously, the NAEI breaks down the emissions estimates into different source sectors. Comparison of the measured and estimated emissions could then be used to investigate how well each source sector is being represented by the NAEI. This, in turn, would help to improve the understanding of the reasons behind any discrepancies between measured and estimated rig emissions in the North Sea, whilst also giving a more accurate representation of emissions coming from North Sea rigs.

4.3.4 NO_x Emissions from North Sea Oil and Gas Platforms: A Wider Perspective

As discussed previously, the North Sea is now considered one of the world's most active drilling areas. Therefore, these findings must be scaled up and applied to all of the operational rigs in the North Sea, in order to fully understand the extent and potential impacts of NO_x emissions from oil and gas platforms.

One way of doing this is to take the percentage extra NO_x produced according to the measured Forties and Nelson rig data and apply it to the rest of the operational rigs in the North Sea. This percentage is calculated by dividing the total measured NO_x emissions by the total NO_x emissions according to the inventory. Doing so shows that the measured NO_x emissions from the Forties and Nelson rigs are 1.805 times higher than the respective NAEI estimates. The most recent NAEI data[99] indicates that there are 272 rigs emitting NO_x in the North Sea, with total annual emissions of 52,705 tons, according to the inventory. Assuming the extra NO_x measured from the Forties and Nelson rigs is duplicated across all rigs in the North Sea, an extra 42,438 tons of NO_x, is being emitted, which is not being accounted for by the NAEI.

Using the NAEI mapping tool,[100] it was found that this surplus NO_x from the oil and gas rigs in the North Sea (42,438 tons per year) is roughly equivalent to the annual NO_x emissions coming from a circle of 50 km diameter around London (45,851 tons per year). London is an extremely large, industrialised city, with a population of approximately 8.6 million. This urban environment brings with it high NO_x mixing ratios, due to the large number of vehicles travelling in and around the city and all hours of the day. This can be seen on **Figure 4.58**, whereby the large density of high NO_x areas, predominantly roads, can be easily distinguished. The fact that the North Sea oil and gas rigs could possibly be emitting around the same amount of NO_x as a busy city like London is a good indication that the rigs are a significant point source of NO_x, and that the inventory data is severly underestimating their contribution to the UK's NO_x budget.

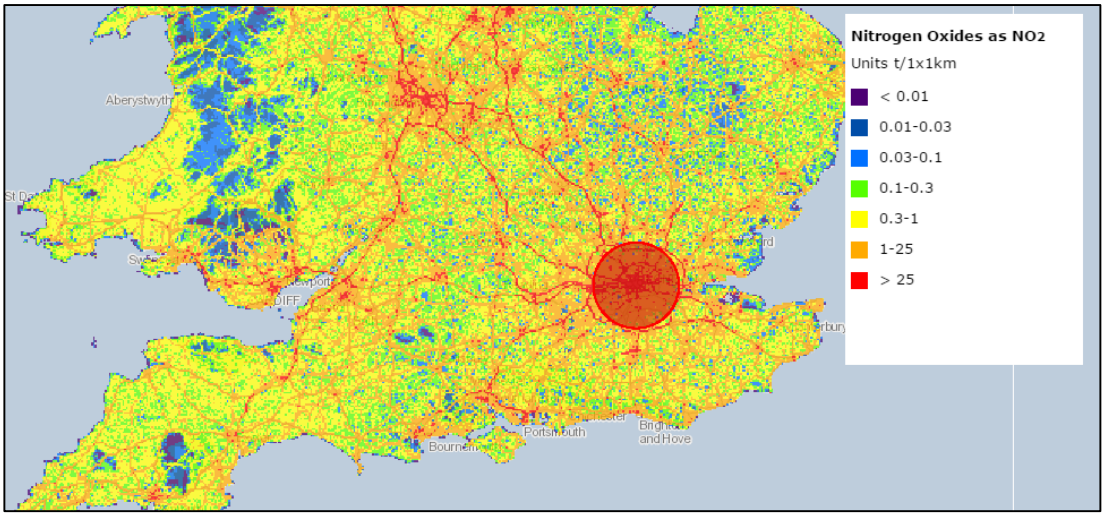

Figure 4.58: NAEI map of total NO_x emissions from the south of the UK in 2012.[100] The highlighted area represents a 50 km diameter around London

Transboundary air pollution is a big problem for European countries in particular. It is defined as pollution which remains in the atmosphere long enough for it to be transported thousands of kilometres away from its original source. This means that otherwise "clean" countries have their air quality worsened by long-range transport of various air pollutants. This can have a number of detrimental effects, including the acification and eutrophication of soils and waters and the formation of summer smog (caused by tropospheric ozone).

Such substantial amounts of NO_x coming from the North Sea are therefore likely to cause serious problems for countries like Norway, particularly in terms of ground-level O_3 formation. The main source of precursor emissions (i.e. NO_x and VOCs) is long-range transport from other European countries, such as the UK, with the predominant source of NO_x being the combustion of nitrogen-containing fuels. South-westerly winds dominate in the North Sea, thus transporting emissions from oil and rigs in the area to other countries like Norway. The natural background mixing ratio of ground-level O_3 in Norway ranges between 40 and 80 µg m^{-3}.[101] However, the hourly mean value recommended by the European Agency (100 µg m^{-3}) is regularly exceeded. This is predominantly believed to be a result of surplus NO_x emissions from other European countries. This indicates that Norway is already seeing notable alterations in their national air quality, so these NO_x emissions from the North Sea oil and gas rigs may already be contributing to this.

The NO_x emissions coming from the North Sea oil and gas rigs could also add to the high levels of NO_x that are already observed in the UK, particularly when an anticyclonic (high

pressure) system is dominating the regional meteorology. These systems have small pressure gradients, which bring about gentle winds. These winds generally blow from an easterly direction, thus bringing air from the North Sea to the UK. Such high pressure systems therefore result in the accumulation of high pollutant mixing ratios, brought about by limited mixing and dilution. A consequence of this "trapping" of pollutants, such as NO_x and VOCs, can result in increased amounts of ground-level O_3. This was observed during the "heat wave" over Western Europe in 2003, whereby a persistent anticyclone resulted in regular exceedances of 30°C in the UK. This high pressure system also caused significantly enhanced levels of pollutants such as NO_x and tropospheric O_3. A study by Lee et al. (2006)[102] suggested that these increased levels were likely to be a result of both local atmospheric processes and regional transport. Derwent and Jenkin (1991)[103] also emphasised the contribution that atmospheric transport makes to high O_3 events in the UK. Therefore, these additional NO_x emissions from the oil and gas rigs in the North Sea would only exacerbate the tropospheric O_3 production under these conditions. High mixing ratios of ground-level, or tropospheric O_3 can cause a range of health problems, including eye irritation and exacerbation of respiratory illnesses. It can also affect vegetation, reducing crops yields by slowing down processes like photosynthesis and growth, hence why it is of utmost important that its mixing ratios are minimised.

The road transport sector (predominantly diesel-fuelled vehicles), is a key NO_x source in the UK and is believed to be at least in part, the reason behind the UK not meeting EU standards for NO_2. Breaching these limits means that the UK would be fined by the EU. As well as these economic costs, NO_2 causes detrimental effects to human health, particular in terms of respiratory disease, whilst also being an element of tropospheric O_3 formation. It is therefore in the best interests of the UK to keep NO_x mixing ratios as low as possible, meaning any additional emissions from oil and gas platforms are only likely to make this a more difficult process.

CONCLUSION

A LIF instrument was evaluated as a direct method for tropospheric NO_2 quantification. The instrument was initially tested for NO_2 measurements in a polluted atmosphere at the University of York campus in the suburban village of Heslington, York. Ambient measurements of NO_2 made by the LIF instrument were directly compared with a standard P-CL analyser in the laboratory. The mixing ratios measured by both instruments compared well with each other, both measuring NO_2 levels that were consistent with the surrounding atmospheric environment (between around 3 and 6 ppbv). NO_2 data from an urban monitoring site in the centre of York was compared with the data measured in Heslington. The NO_2 mixing ratios from the city centre were significantly higher, peaking at approximately 66 ppbv, which could be attributed to the higher road traffic volume in the area. This provided a great amount of assurance as to the reliability of the NO_2 measurements made by the LIF instrument in Heslington. The LIF instrument was also characterised for NO measurements, through the installation an efficient GPT system, similar to those used in commercial chemiluminescence instruments. This involved the manipulation of various experimental conditions, to ultimately yield the highest conversion efficiency possible. A conversion efficiency of over 90% was achieved through the incorporation of an additional reaction volume, thus emphasising the importance of mixing time for efficient NO measurements.

However, the instrument proved not to perform as well for remote marine boundary layer measurements. Deployment at the CVAO saw the instrument significantly over-estimating the ambient NO_2 mixing ratios. The cause of such an over-estimation was deduced to be a result of a leak within the instrument, which meant that the instrument was sampling laboratory air, as well as the marine boundary layer air. Consumable restrictions meant that it was deemed unviable to use the LIF for NO measurements at the CVAO. Deployment at the observatory led to the conclusion that, although performing well in the polluted boundary layer, the instrument would not be suitable for long-term NO_2 measurements in the remote boundary layer in its current configuration.

Although the LIF technique has the distinct advantage over chemiluminescence instruments in terms of direct NO_2 measurements, this study has found that, for this instrument in particular, there is still scope to improve it. As discussed in section 2.1, there are a great number of factors which can influence of the sensitivity of LIF instruments, and it is these

factors in particular which must be taken into account to maximise the capability of the LIF technique in tropospheric measurements.

Oil and gas rigs are a point source of NO_x within the NAEI, though it has been as yet unclear as to how well the inventory represents these NO_x emissions. The operation of these rigs is also known to release vast amounts of other atmospheric species, such as CO_2 and CH_4 into the surrounding atmosphere every year, would could lead to dramatic impacts on the environment. The "Oil and Gas" campaign took place in summer 2015, with the objective of assessing the extent of these emissions coming from North Sea rigs (a highly active drilling region), whilst also using the direct integration method to assess the accuracy of NO_x estimates in the NAEI.

Survey flights took place around the active oil and gas fields in the southern and northern sectors of the North Sea. Substantial NO_x enhancements were regularly observed when flying directly downwind of the rigs, with the largest gas plumes containing between around 20,000 and 40,000 pptv. Analysis of the background mixing ratios, along with back trajectories were used to confirm that the majority of the plume mixing ratios observed were coming from the rigs. However, in some flights, there was a notable influence from UK-based NO_x sources, namely the Humberside and Lincolnshire coastline, which also contributed to some of the high level NO_x detected.

The nature of these survey flights, i.e. the high density of rigs in the surrounding area meant that it was very difficult to attribute each NO_x plume peak to a specific rig. Flight B918 was used to derive NO_x emissions coming from individual rigs using the direct integration method. The Forties and Nelson rigs in the North Sea were targeted and multiple-altitude transects were conducted at various distances downwind of them. Doing so would mean that it would be possible to ascertain which plume peaks were coming from which rig. Once this was done, the emissions coming from each of the rigs could be ascertained using the direct integration method. Averaging the measured emissions from the Forties and Nelson rigs and comparing them to the respective NAEI estimate indicated a significant discrepancy, with the NAEI under-estimating the annual NO_x emissions by around 2,000 tons. Further analysis of the NAEI data indicated that some source sectors were better represented than others, particularly in terms of the fuel used to operate the turbines. These findings were then scaled up to evaluate the NAEI estimates for the whole North Sea drilling region, showing that this poor representation of NO_x emissions from oil and gas rigs was leading to a (theoretical) under-estimation of around 40,000 tons per year. Such a substantial amount of surplus NO_x

in the atmosphere could have detrimental impacts on a large scale, highlighting the importance of the NAEI for accurate NO_x measurements.

However, there are errors and limitations with this type of study, meaning that important factors such as diurnal and seasonal variations were not taken into account. In order to get a more representative picture of NO_x emissions from North Sea rigs, it would therefore be necessary to conduct year-round survey flights around the operational drilling areas and use the direct integration method to compare their emissions with the respective inventory data. This would also provide more information as to how well the rigs are represented as point sources in the NAEI.

LIST OF ABBREVIATIONS

AN	alkyl nitrate
BLC	blue light converter
BOC	British Oxygen Company
c/s/ppbv	counts per second per ppbv
CAPS	cavity attenuated phase shift spectroscopy
CEAS	cavity enhanced absorption spectroscopy
CRDS	cavity ring down spectroscopy
CVAO	Cape Verde Atmospheric Observatory
DOAS	differential optical absorption spectroscopy
FAAM	Facility for Airborne Atmospheric Measurements
FAGE	fluorescence assay by gas expansion
GPT	gas phase titration
LED	light emitting diode
LIF	laser induced fluorescence
MFC	mass flow controller
NAEI	National Atmospheric Emissions Inventory
Nd:YAG	neodymium-doped yttrium aluminium garnet (crystal used as a lasing medium)
nm	nanometres
P-CL	photolytic chemiluminescence

PMT	photomultiplier tube
PN	peroxy nitrate
ppbv	parts per billion by volume (10^{-9})
pptv	parts per trillion by volume (10^{-12})
sccm	standard cubic centimetres
slpm	standard litres per minute
SNR	signal to noise ratio
TDLAS	tunable diode laser absorption spectroscopy
TD-LIF	thermal dissociation-laser induced fluorescence
µg/m^3	micrograms per cubic metre
ppmv	parts per million by volume (10^{-6})

REFERENCES

[1] R. Atkinson, *Atmos. Environ.*, 2000, **34**, 2063-2101

[2] G. –J. Roelofs and J. Lelieveld., *Tellus B*, 1997, **49**, 38-55

[3] J. A. Logan et al., *J. Geophys. Res.*, 1981, **86**, 7210-7254

[4] G. J. M. Velders et al., *J. Geophys. Res.*, 2001, **106**, 12643-12660

[5] J. A. Thornton et al., *Anal. Chem.*, 2000, **72**, 528-539

[6] G. Villena et al., *Atmos. Meas. Tech.*, 2011, **4**, 1663–1676

[7] K. Mannschreck et al., *Atmos. Chem. Phys.*, 2004, **4**, 1265–1277

[8] O. R. Cooper et al., *Elem. Sci. Anth*., 2014, **2**, doi: 10.12952/journal.elementa.000029

[9] R. Van Dingenen et al., *Atmos. Environ.*, 2009, **43**, 604-618

[10] J. D. Lee et al., *J. Geophys. Res.*, 2009, **14**, D21302

[11] H. Fuchs et al., *Atmos. Meas. Tech.*, 2010, **3**, 21-37

[12] S. E. Schwartz, *Science*, 1989, **243**, 753-763

[13] W. S. Tunnicliffe et al., *Lancet*, 1994, **344**, 1733-1736

[14] V. Strand et al., *Euro. Respir. J.*, 1998, **12**, 6-12

[15] L. K. Emmons et al., *Atmos. Environ.*, 1997, **31**, 1851-1904

[16] X. Tie et al., *J. Geophys. Res.*, 2001, **106**, 3167–3178.

[17] X. Tie et al., *J. Atmos. Chem.*, 2002, **43**, 61–74

[18] E. Aruffo et al., *Atmos. Environ.*, 2014, **94**, 479-488

[19] E. V. Fischer et al., *Atmos. Chem. Phys.*, 2014, **14**, 2679–2698

[20] R. K. Talukdar et al., *J. Geophys. Res.*, 1995, **100**, 14163-14173

[21] J. Matsumoto and Y. Kajii, *Atmos. Environ.*, 2003, **37**, 4847-4851

[22] J. A. Thornton et al., *J. Geophys. Res.*, 2003, **108**, D4496

[23] T. Gherman et al., *Environ. Sci. Technol.*, 2008, **42**, 890-895

[24] T. Wu et al., *Appl. Phys. B*, 2009, **94**, 85-94

[25] H. D. Osthoff et al., *J. Geophys. Res.*, 2006, **111**, D12305

[26] H. Fuchs et al., *Environ. Sci. Technol.*, 2009, **43**, 7831-7836

[27] P. L. Kebabian et al., *Anal. Chem.*, 2005, **77**, 724-728

[28] Y. Q. Li et al., *J. Geophys. Res.*, 2004, **109**, D16S08

[29] G. L. Gregory et al., *J. Geophys. Res.*, 1990, **95**, 10103-10127

[30] L. A. George and R. J. O'Brien, *J. Atmos. Chem.*, 1991, **12**, 195-209

[31] C. Fong and W. H. Brune, *Rev. Sci. Instrum.*, 1997, **68**, 4253-4262

[32] C. Dari-Salisburgo et al., *Atmos. Environ.*, 2009, **43**, 970-977

[33] Y. Matsumi et al., *Anal. Chem.*, 2001, **73**, 5485-5493

[34] P. A. Cleary et al., *Appl. Opt.*, 2002, **41**, 6950-6956

[35] J. G. Murphy et al., *Atmos. Chem. Phys.*, 2004, **4**, 377-384

[36] F. Taketani et al., *Appl. Opt.*, 2007, **46**, 907-915

[37] D. A. Day et al., *J. Geophys. Res.*, 2002, **107**, D64046

[38] P. Di Carlo et al., *Atmos. Meas. Tech.*, 2013, **6**, 971-980

[39] B. J. Finlayson-Pitts and J. N. Pitts, Jr., *Chemistry of the Upper and Lower Atmosphere*, Academic Press, San Diego, 2000

[40] E. J. Dunlea et al., *Atmos. Chem. Phys*., 2007, **7**, 2691-2704

[41] R. R. Dickerson et al., *Rev. Sci. Instrum.*, 1984, **55**, 1995-1998

[42] Y. Sadanaga et al., *Anal. Chem.*, 2010, **82**, 9234-9239

[43] D. Grosjean and J. Harrison, *Environ. Sci. Technol.*, 1985, **19**, 862-865

[44] A. M. Winer et al, *Environ. Sci. Technol.*, 1974, **8**, 1118-1121

[45] N. A. Marley et al., *Rev. Sci. Instrum.*, 2004, **75**, 4595-460

[46] D. D. Parrish et al., *J. Geophys. Res.*, 1990, **95**, 1817-1836

[47] T. B. Ryerson et al., *J. Geophys. Res.*, 2000, **105**, 26447-2646

[48] I. B. Pollack et al., *J. Atmos. Chem.*, 2010, **65**, 111-125

[49] M.D. Shaw et al., *Atmos. Chem. Phys*., 2015, **15**, 5083-5097

[50] C. Reed et al., *Atmos. Chem. Phys. Discuss.*, submitted 2015

[51] C. A. Biesheuvel et al., *J. Chem. Phys.*, 1998, **109**, 9701-9712

[52] J. Bradshaw et al., *Geophys. Res. Lett.*, 1999, **26**, 471

[53] K. K. Perkins et al., *J. Geophys. Res.*, 1999, **104**, 26687

[54] J. B. Burkholder and R. K. Talukdar, *Geophys. Res. Lett.*, 1994, **21**, 581

[55] L. S. Rothman et al., *J. Quant. Spectrosc. Radiat. Transfer*, 2005, **96**, 1394

[56] B. A. Bodhaine et al., *J. Atmos. Oceanic Technol.*, 1999, **16**, 1854

[57] A. Bucholtz, *Appl. Opt.*, 1995, **34**, 2765

[58] C. D. Salisburgo, PhD Thesis, University of L'Aquila, 2006-2007

[59] J. Drummond et al., *J. Atmos. Chem.*, 1985, **2**, 287–306

[60] M. C. Peterson and R. E. Honrath, *J. Geophys. Res.*, 1999, **104**, 11,695–11,707

[61] M. Val Martin et al., *J. Geophys. Res.*, 2008, **113**, D17307

[62] http://www.theicct.org/sites/default/files/ICCT_PEMS-study_diesel-cars_2014_factsheet_EN.pdf (accessed 4/8/15)

[63] D. C. Carslaw., *Atmos. Environ.*, 2005, **39**, 4793

[64] P. Anttila and J.-P. Tuovinen, *Atmos. Environ.*, 2010, **44**, 30

[65] R. Alvarez et al., *Atmos. Environ.*, 2008, **42**, 4699

[66]http://www.jorair.co.uk/reports/Further/Further%20Assessment%20for%20Fulford%20Main%20Street%20-%20April%202011.pdf (accessed 4/8/15)

[67] http://uk-air.defra.gov.uk/data/ (accessed 13/10/15)

[68] S. S. Brown et al., *J. Geophys. Res. Lett.*, 2004, **31**, doi:10.1029/2004GL019412

[69] N. Riemer et al., *J. Geophys. Res.*, 2003, **108**, 1-21

[70] L. J. Carpenter et al., *J. Atmos. Chem.*, 2010, **67**, 87–140

[71] P. J. Crutzen et al., *Tellus A*, 1999, **51**, 123–146

[72] B. A. Ridley et al., *J. Geophys. Res.*, 1988, **93**, 15803–15811

[73] P. C. Moonen et al., *J. Atmos. Chem.*, 1998, **29**, 299-314

[74] G. D. Edwards and P. S. Monks, *J. Geophys. Res.*, 2003, **108**, doi:10.1029/2002JD002844

[75] S. J. B. Bauguitte et al., *Atmos. Chem. Phys.*, 2012, **12**, 989–1002

[76] Z. Hosaynali Beygi et al., *Atmos. Chem. Phys.*, 2011, **11**, 8497–8513

[77] M. M. Frey et al., *Atmos. Chem. Phys.*, 2013, **13**, 3045–3062

[78] M. M. Frey et al., *Atmos. Chem. Phys.*, 2015, **15**, 7859–7875

[79] C. A. Cantrell et al., *J. Geophys. Res.*, 2003, **108**, doi:10.1029/2002JD002198

[80] http://oilandgasuk.co.uk/key-facts/energy-provider.cfm (accessed 12/09/15)

[81] http://oilandgasuk.co.uk/environment-report.cfm (accessed 12/09/15)

[82] http://cdiac.esd.ornl.gov/pns/current_ghg.html (accessed 12/09/15)

[83]I. S. A. Isaksen et al., *Atmos.*, 2014, **5**, 518-535

[84]G. L. Vaghjiani and A. R. Ravishankara, *Nature*, 1991, **350**, 406-409

[85] G. N. Petersen and I. A. Renfrew, *Q. J. R. Meteorol. Soc.*, 2009, **135**, 2030–2045

[86] J. R. Ström et al., *J. Atmos. Tech.*, 1994, **11**, 1392–1399

[87] *Probing the Atmospheric Boundary Layer*, ed. D. H. Lenschow, Americ. Met. Soc., Boston, Massachusetts, 1986

[88] C. Gerbig et al., *J. Geophys. Res.*, 1999, **104**, 1699–1704

[89] K. L. Wilson and J. W. Birks, *Env. Sci. Tech.*, 2006, **40**, 6361-6367

[90] S. J. O'Shea, et al., *Atmos. Meas. Tech.*, 2013, **6**, 1095-1109

[91] J. R. Hopkins et al., *J. Environ. Monit.*, 2003, **5**, 8-13

[92] P. D. Rosenberg et al., *Atmos. Meas. Tech.*, 2012, **5**, 1147-1163

[93] https://ready.arl.noaa.gov/HYSPLIT_traj.php (accessed 29/09/15 and 30/09/15)

[94] J. D. Lee et al., *Environ. Sci. Technol.*, 2015, **49**, 1025−1034

[95] T. B. Ryerson et al., *J. Geophys. Res.*, 1998, **103**, 22569-22583

[96] W. H. White et al., *Science*, 1976, **194**, 187-189

[97] http://glossary.ametsoc.org/wiki/Poisson_constant (accessed 25/9/15)

[98] S. Nicholls, J. Leighton and R. Barker, *J. Atmos. Ocean. Tech.*, 1990, **7**, 706-718

[99] http://naei.defra.gov.uk/ (accessed 21/9/15)

[100]http://naei.defra.gov.uk/data/gis-mapping (accessed 5/10/15)

[101] http://www.environment.no/Topics/Air-pollution/Ground-level-ozone-/ (accessed 5/10/15)

[102] J.D. Lee et al., *Atmos. Environ.*, 2006, **40**, 7598–7613

[103] R. G. Derwent and M. E. Jenkin., *Atmos. Environ. Part A*, 1991, **25**, 1661-1678